

Characterization of Negevirus and insect virome interactions during co-infection in cell culture

By  
Anneliese von Eicken, B. Sc.

A thesis submitted to the Centre for Biotechnology  
in partial fulfillment of the requirements for  
the degree of Master of Science

August 2023  
Brock University  
St. Catharines, ON  
L2S 3A1 Canada

© Anneliese von Eicken 2023

## Abstract

Negevirus are a newly described taxon of insect-specific viruses (ISVs) that show potential to be used as a virus-based pathogen control strategy through superinfection exclusion. Due to their recent discovery, little is known about the biology of these ISVs or how they interact with the insect's virome. It was recently demonstrated that both wild-type and genetically modified Negevirus can inhibit the replication of Alphaviruses in mosquito cell culture. For Negevirus to be used in wild mosquito populations they will have to compete with other viruses that infect mosquitoes, typically other wild-type Negevirus and ISVs. Thus, I performed co-infection assays in different cell types to observe homologous and heterologous exclusion during virus infection. The cell lines used were Aag2 cells derived from *Aedes aegypti*, and C7/10 cells derived from *Aedes albopictus*. C7/10 cells have a dysfunctional RNA interference response, while Aag2 cells have a functional RNA interference pathway and pre-existing chronic infections with two ISVs: CFAV and PCLV. Homologous exclusion will be tested through additional infectious clones of Negevirus that have fluorescent reporter genes inserted into their genome. Analyzing the growth trends of different Negevirus in these cell lines allow us to determine which Negevirus isolates can establish infection in the presence of existing or co-infections with other viruses. Results demonstrated the successful cloning of PIUV ORF3 mScarlet, but with concerns regarding insert stability. The variability in outcomes during co-infection experiments was attributed to cell type differences, mainly RNAi competency, and pre-existing infections. Fitness variations were observed among the viruses, with NEGV isolates and LORV demonstrating higher fitness. These findings contribute to our understanding of Negevirus biology and highlight the importance of further research to overcome the challenges encountered in cloning and characterization of the behavior of these viruses.

## **Acknowledgements**

I would like to thank my supervisor, Dr. Ian Patterson, for his guidance, expertise, and mentorship throughout this research. I am grateful I was welcomed into your lab with open arms and that you trusted me with this project, thanks for your continuous support. Additionally, I thank my committee members, Dr. Jeffrey Atkinson and Dr. Aleksandar Necakov for being supportive, kind and encouraging throughout my progress.

I would also like to express my gratitude and appreciation to Dr. Ana Sanchez. Your passion for knowledge, unwavering support, and insightful advice have played a pivotal role in shaping who I am today (and this thesis). I am truly fortunate to have found both a mentor and a friend in you.

Special thanks to my friends, who have provided me with encouragement, love, and laughter throughout this journey. To Rush, Breyer, Raissa, and Theo, thank you for lending an ear, and providing a much-needed distraction when the pressures of academia became overwhelming. Your belief in me has been a source of motivation, and I am deeply grateful. I would also like to thank the members of the Patterson and Hunter labs, and Dr. Candace Panagabko who showed me constant support and offered me advice during my degree.

Finally, I would like to express my heartfelt appreciation to my family. To my parents, your constant encouragement and sacrifices have been instrumental in my pursuit of knowledge. I am forever grateful for your love and support.

Table of Contents

**Abstract**

**Acknowledgements**

**List of Figures**

**List of Tables**

**List of Abbreviations**

**Chapter 1 – Literature Review ..... 1**

1.1 Introduction to arboviruses and insect-specific viruses ..... 1

1.2 Negevirus ..... 4

1.3 Co-infections ..... 7

1.4 Virus Infectious Clones, Reporter Genes, and their Stability in ISVs ..... 12

1.5 Mosquito Cell Lines ..... 16

**Research Purpose and Objectives ..... 18**

**Chapter 2 – Materials and Methods..... 20**

**Materials..... 20**

2.1 Cell culture and viruses ..... 20

2.2 Cloning NEGV and PIUV for exogenous gene expression ..... 21

2.3 Plaque assays..... 22

2.4 Virus growth curves using RT-qPCR..... 22

**Methods ..... 23**

2.5 Cell culture and viruses ..... 23

2.6 Cloning NEGV and PIUV for exogenous gene expression ..... 25

2.7 Virus Purification ..... 29

2.8 Plaque assays..... 29

2.9 Virus growth curves using RT-qPCR.....	30
2.10 Negevirus co-infections .....	32
2.11 Statistical analysis .....	34
<b>Chapter 3 – Cloning Results .....</b>	<b>35</b>
3.1 Construction of modified NEGV and PIUV infectious clones .....	35
3.1.1 Cloning of fluorescent reporters onto virus infectious clones: PIUV .....	35
3.1.2 Cloning of fluorescent reporters into infectious viral clones: NEGV .....	43
3.2 Plaque assay results for all virus stocks .....	48
<b>Chapter 4 – Growth Curve Results .....</b>	<b>49</b>
4.1 Virus growth curves in C7/10 cells using RT-qPCR.....	49
4.1.1 Plaque assays for growth curves samples using C7/10 cells .....	51
4.2 Virus growth curves in Aag2 cells using RT-qPCR.....	53
4.2.1 Plaque assays for growth curves samples using Aag2 cells .....	55
4.3 Genome copy vs titer comparison for single infections.....	57
<b>Chapter 5 – Co-infection Results.....</b>	<b>60</b>
5.1 C7/10 cell co-infection results using RT-qPCR .....	60
5.2 Aag2 cell co-infection results using RT-qPCR .....	62
5.3 Co-infection plaque assay: NEGV ORF3 GFP X PIUV ORF3 mScarlet.....	65
<b>Chapter 6 – Discussion.....</b>	<b>69</b>
Part I – Cloning Experiments.....	69
Part II – Single & Co-infection Experiments.....	72
Conclusions .....	77
<b>Appendix .....</b>	<b>87</b>
Part A – Cloning and sequencing.....	87
Part B – Titer: Plaque Assays .....	98
Part C – Growth Curve Raw Data.....	101

## List of Figures

Figure 1. Maximum likelihood analysis of Negevirus based on the RNA-dependent RNA polymerase region of the genome. ....	6
Figure 2. Co-infection scenarios that may occur from simultaneous or sequential arboviral infections. ....	8
Figure 3. Co-infection growth curves of CHIKV and paratransgenic NEGV on C7/10 cells. ....	15
Figure 4. Flow chart demonstrating all steps taken to clone mScarlet into ORF3 of PIUV. ....	28
Figure 5. Simulation of the cloning process for PIUV ORF3 mScarlet.....	36
Figure 6. Gel image for Q5 Hi-Fi PCR products used to clone PIUV ORF3 mScarlet.....	37
Figure 7. Sequencing data chromatograms for PIUV ORF3 mScarlet-fused infectious clone. ....	39
Figure 8. Plaque assay using C6/36 cells to determine titers of PIUV ORF3 mScarlet stocks.....	41
Figure 9. SDS-PAGE image for purified and concentrated Negevirus. ....	42
Figure 10. Gel image for PCR products for cloning reporter genes into infectious clones. ....	44
Figure 11. Sequencing results for NEGV modified infectious clones. ....	45
Figure 12. NEGV clone backbone switch experiment scheme and sequencing results.....	47
Figure 13. Growth curves of Negevirus by genome copy number in C7/10 cells. ....	50
Figure 14. Titers for Negevirus using C7/10 cells for the 48hpi sample of growth curves. ....	51
Figure 15. Growth curves of Negevirus by genome copy number in Aag2 cells. ....	54
Figure 16. Titers for Negevirus using Aag2 cells for the 48 hpi sample of growth curves. ....	55
Figure 17. Plot comparing genome copy numbers/mL vs. pfu/mL of Negevirus in C7/10 & Aag2 cells. ....	57
Figure 18. Plot depicting the ratio of genome copy numbers/mL vs pfu/mL for Negevirus in different cell types.....	58
Figure 19. Co-infection growth curves of Negevirus by genome copy number in C7/10 cells. ....	61

Figure 20. Co-infection growth curves of Negevirus by genome copy number in Aag2 cells. .63	
Figure 21. Fluorescent plaques formed from co-infection with NEGV ORF3 GFP and PIUV ORF3 mScarlet in C7/10 cells at 48hpi. ....67	67
Figure 22. Fluorescent plaques formed from co-infection with NEGV ORF3 GFP and PIUV ORF3 mScarlet in Aag2 cells at 48hpi. ....68	68
Figure 23. Sequencing data chromatograms for PIUV ORF3 ZsGreen-fused infectious clone....91	91
Figure 24. Sequencing data chromatograms for PIUV ORF3 mEmerald-fused infectious clone.95	95
Figure 25. Plaque assay using C6/36 cells to determine titers of NEGV and PIUV wild type virus stocks. ....98	98
Figure 26. Plaque assay using C6/36 cells to determine titers of PIUV ZsGreen. ....99	99

## List of Tables

Table 1. Cell cultures used in the present study. ....	18
Table 2. Wild type Negevirus described in the current study. ....	19
Table 3. Reagents used for cell culture maintenance and experiments.....	20
Table 4. Reagents used for <i>in vitro</i> transcription and electroporation. ....	20
Table 5. Reagents used for bacterial culture during cloning experiments. ....	21
Table 6. PCR mixes, enzymes, kits, and cells used for cloning experiments. ....	21
Table 7. Reagents used for gel electrophoresis and gel extraction. ....	22
Table 8. Reagents using for insect cell plaque assays.....	22
Table 9. RNA extraction and RT-qPCR kit used for growth curve experiments. ....	22
Table 10. Negevirus co-infection pairs used in the present study. ....	34
Table 11. Negevirus titers (PFU/mL) determined by plaque assay. ....	48
Table 12. Statistical results for Negevirus plaque assays at 48hpi in C7/10 cells. ....	52
Table 13. Statistical results for Negevirus plaque assays at 48 hpi in Aag2 cells. ....	56
Table 14. Average genome copy number vs plaque titer ratio for Negevirus at 48 hpi. ....	59
Table 15. Statistical results for Negevirus during co-infections in C7/10 cells. ....	62
Table 16. Statistical results for Negevirus during co-infections in Aag2 cells. ....	64
Table 17. Titers resulting from the co-infection of NEGV ORF3 GFP and PIUV ORF3 mScarlet at 48 hpi. ....	66
Table 18. Primer sets used for cloning of exogenous genes into NEGV and PIUV infectious clones.....	87
Table 19. Primer sets used for sequencing and growth curves of negevirus infectious clones. ....	88
Table 20. PIUV ORF3 mScarlet fused cloning sequencing results for forward and reverse primer reactions.....	89

Table 21. PIUV ORF3 ZsGreen fused cloning sequencing results for forward and reverse primer reactions.....	92
Table 22. PIUV ORF3 mEmerald fused cloning sequencing results for forward and reverse primer reactions. ....	95
Table 23. Raw data used to calculate titers for all Negevirus stocks.....	100
Table 24. Raw data used to calculate titers for Negevirus using C7/10 cells for the 48hpi sample of growth curves.....	101

## List of Abbreviations

bp	Base pair
BCPV	Big Cypress virus
BIRV	Biratnagar virus
BREJV	Brejeira virus
CFAV	Cell fusing agent virus
CHIKV	Chikungunya virus
CiLV-C	Citrus leprosis virus
CDBV	Cordoba virus
CxFV	Culex flavivirus
CPE	Cytopathic effect
DENV	Dengue virus
DEZV	Dezidougou virus
DMEM	Dulbecco's Modified Eagle's Medium
EGFP	Enhanced green fluorescent protein
FBS	Fetal bovine serum
GANV	Goutanap virus
GFP	Green fluorescent protein
hpe	Hours post electroporation
hpi	Hours post infection
hr	Hour
ISF	Insect specific flaviviruses
ISV	Insect specific virus

JEV	Japanese encephalitis virus
Kb	Kilobases
LORV	Loreto virus
MOI	Multiplicity of infection
MVEV	Murray Valley encephalitis virus
NEGV	Negev virus
NEB	New England Biolabs
NWTV	Ngewotan virus
NHUV	Nhumirim virus
ONNV	O'nyong'nyong virus
ANOVA	Analysis of variance
ORF	Open reading frame
PCV	Palm Creek virus
PCLV	Phasi Charoen-like virus
PIUV	Piura virus
PEG	Polyethylene glycol
+ssRNA	Positive-sense single-stranded RNA
RdRp	RNA dependent RNA polymerase
RT-qPCR	Reverse transcriptase quantitative polymerase chain reaction
RISC	RNA-induced silencing complexes
SBDV	San Bernardo virus
SANV	Santana virus
SFV	Semliki Forest virus

scFv	Single chain variable fragment
STAT	Signal transducer and activator of transcription
siRNA	Small interfering RNA
SD	Standard Deviation
Sq	Starting quantity
TANAV	Tanay virus
TMV	Tobacco mosaic virus
UTMB	University of Texas Medical Branch
VEEV	Venezuelan equine encephalitis virus
VSR	Virus-encoded suppressor RNAi
WALV	Wallerfield virus
WNV	West Nile virus
WT	Wild type from infectious clones
WRCEVA	World Reference Center for Emerging Viruses and Arboviruses
YFV	Yellow fever virus
ZIKV	Zika virus

## Chapter 1 – Literature Review

### *1.1 Introduction to arboviruses and insect-specific viruses*

Hematophagous arthropods, such as mosquitoes, ticks, and phlebotomines, harbour a wide range of infectious agents, including bacteria, parasites, and viruses. **Arthropod-borne** viruses (arboviruses) are dual-host viruses that infect both arthropods and vertebrates. Mosquitoes are among the most medically significant vectors of disease. Mosquito-borne viruses are a threat to public health worldwide, as they are etiologic agents of endemic and (re-)emerging fever syndromes and neurological disorders (1-3). In humans, some of the most relevant arboviruses are West Nile virus (WNV), dengue virus (DENV), Zika virus (ZIKV), chikungunya virus (CHIKV), yellow fever virus (YFV), and Japanese encephalitis virus (JEV). Infections can either be asymptomatic or cause severe symptoms that can progress to secondary conditions or sequelae that affect cognitive performance long-term (4). These arboviruses disproportionately affect tropical areas since environmental conditions benefit the growth and diversity of mosquito populations. However, recent reports demonstrate that climate change has started to shift these patterns, with arboviruses emerging in previously non-native areas (4, 5). The length of the transmission season, and the distribution of vectors or reservoirs, are expected to be influenced by gradual increases in temperature and precipitation (5, 6). Mosquitoes facilitate the transmission of arboviruses through a sequence of steps: 1) they acquire the arbovirus by feeding on an infected host that harbours the virus in its blood, 2) the arbovirus gains entry into the mosquito's digestive system and infects the midgut, 3) the virus disseminates throughout the mosquito's body, ultimately reaching the salivary glands, and 4) the mosquito conveys the virus to another host by introducing it via its saliva (7). Pathogen control strategies for these viruses

rely heavily on vector control with insecticides, which has now become an ineffective remedy for arboviruses (1, 3). Repeated exposure to insecticides has resulted in the development of insecticide resistance genes in mosquito populations, and while alternative approaches that focus on the environmental management of mosquitoes, such as the elimination of oviposition sites, have been beneficial, they often require consistent intervention and can pose challenges in terms of expense and implementation, particularly within urban areas (8, 9). Thus, better strategies to control these pathogens are required.

In addition to arboviruses, an insect's virome also comprises a variety of viruses that are non-pathogenic to vertebrates. Insect-specific viruses (ISVs) are viruses that naturally infect insects and replicate in insect cell lines but cannot replicate in vertebrates (10). ISVs are believed to be prevalent in most wild mosquito populations and can be found within the families of *Bunyaviridae*, *Flaviviridae*, *Mesoniviridae*, *Reoviridae*, *Rhabdoviridae*, *Togaviridae*, and taxon Negeviruses, among many others (1). Mosquitoes infected with ISVs may not show any signs of illness, and many of these viruses do not appear to have a significant negative impact on the mosquito's biological fitness or survival and often establish persistent infections in the insect without causing notable damage (10). Phylogenetic analysis suggests that ISVs likely co-evolved with their insect host. Evidence of this effect is that many ISVs are thought to be transmitted vertically (i.e., transovarian transmission), with some integrating into the host's genome (1, 10). Many ISVs are also found in virus families that have vertebrate pathogenic counterparts such as flaviviruses and reoviruses. Genetic examination indicates high relatedness between ISVs and human arboviruses (10). These virus groups could have diverged from a common ancestor, making their genetic composition, replication strategies, and other aspects of their biology similar (10). Understanding and characterizing the insect virome is crucial for the development

of effective control strategies. While most ISVs are non-pathogenic to their mosquito host, they can interfere with the transmission of arboviruses. A popular theory is that ISVs can inhibit the replication cycle of arboviruses or compete for resources within the insect vector (2, 11). It is believed this occurs during the replication stage in the midgut of the mosquito, where an ISV could compete with an arbovirus for cellular machinery and resources. For this reason, ISVs show potential to be used as a biological control strategy to combat some important human arboviruses (2, 12, 13).

Insect-specific flaviviruses (ISF) are the most studied group of ISV to date. In fact, much of our understanding of the evolution and biology of ISVs derive from experiments focusing on ISFs. Their genomes are composed of single-stranded positive-sense RNA (+ssRNA) of around 11kb in size. Since their genome functions as mRNA and is readily translatable, the replication takes place in cytoplasmic viral factories where double-stranded RNA is created from the original sequence (14, 15). ISF influence on vector competence has been shown repeatedly in both *in vivo* and *in vitro* experiments. Cell fusing agent virus (CFAV) was the first ISF to be isolated and characterized in 1975 after researchers observed its ability to cause fusion of *Aedes albopictus* cells (15). Baidaliuk *et al.* demonstrated that CFAV was capable of reducing DENV and ZIKV replication in *Ae. albopictus* cell culture and live mosquitoes (16). Similarly, Schultz *et al.* found that co-infections with CFAV and Phasi Charoen-like virus (PCLV) repressed replication of the same arboviruses (17). On the other hand, Zhang *et al.* found that CFAV promoted DENV titers *in vitro* which would suggest a mutually beneficial interaction (18). Other ISVs have also shown different effects on vector competence, for example, WNV infection was significantly lowered in cell culture when simultaneously infected with Culex flavivirus (CxFV) (19). Nhumirim virus (NHUV), an ISF isolated in Brazil, showed inhibition of WNV, JEV, and

St. Louis encephalitis virus in mosquito cell culture (20). Likewise, DENV replication was greatly inhibited by the presence of Yichang virus (YCV) an ISV member of the *Mesoniviridae* family (21). Many other ISVs have been documented to have the potential to reduce or inhibit the replication of arboviruses, including the group of interest for the present study: Negevirus (13, 22).

## ***1.2 Negevirus***

Negevirus is a newly discovered taxon of ISV, described by Vasilakis *et al.* in 2013 (22). They have been isolated from various mosquito genera and *Lutzomyia* sand flies, across a wide geographical range. Classified as a Group IV virus, they are comprised of single-stranded, non-segmented, positive sense RNA (1, 22). Their genomes range from 9 to 10 kb in size and are composed of 3 open reading frames (ORFs). The first ORF (ORF1) is the largest and encodes for a non-structural protein(s) that correspond to the replication machinery, the second (ORF2) is responsible for a structural glycoprotein of the virion, and the third (ORF3) codes for a putative membrane protein (13, 22). Negevirus particles are currently known to be spherical or elliptical and between 45-55 nm in diameter. Structural studies using electron microscopy show that the structural proteins are arranged in a round or bullet-like shape with a single protrusion, resembling that of a “hot-air balloon” (22-25). Negevirus, like other ISVs, are believed to be vertically transmitted due to their presence in both larvae and male mosquitoes (24). This suggests that the primary mode of Negevirus transmission is likely through vertical transmission from infected females to their offspring, considering that male mosquitoes, which do not feed on blood as their female counterparts do, rely on alternative means for acquiring viruses (11).

The taxon has been separated into two clades, namely *Nelorpivirus* and *Sandewavirus*. The first clade includes the following species: Big Cypress virus (BCPV), Brejeira virus (BREJV), Cordoba virus (CDBV), Loreto virus (LORV), Negev virus (NEGV), Ngewotan virus (NWTV), Piura virus (PIUV), and San Bernardo virus (SBDV). The second clade *Sandewavirus* contains: Biratnagar virus (BIRV), Dezidougou virus (DEZV), Goutanap virus (GANV), Santana virus (SANV), Tanay virus (TANAV) and Wallerfield virus (WALV) (24, 26). Several other novel isolates have been reported and classified under this taxon. Hitherto, Negevirus have not been classified as a part of any specific order or family of viruses; further phylogenetic analysis is required for such assignment.

Thus far, Negevirus have been distantly linked to citrus leprosis virus C (CiLV-C) of the genus *Cilevirus*, which infects citrus plants via mites (22). Various reports suggest that Negevirus are genetically and evolutionarily related to plant viruses (26). The figure below (Figure 1) depicts both clades and select Negevirus known to be related due to their homology in the RNA-dependent RNA polymerase (RdRp) sequence of the genome, 4316-7309 base pairs (bp) (10).

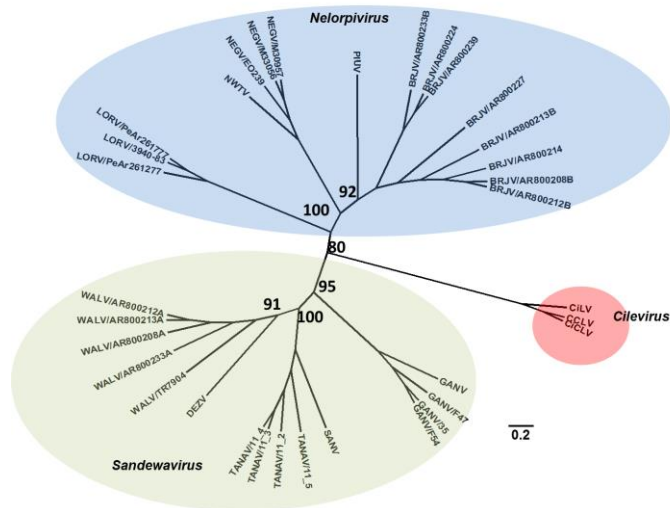


**Figure 1. Maximum likelihood analysis of Negevirus based on the RNA-dependent RNA polymerase region of the genome.**

Figure from Bolling *et al.* (2015) (10), freely available in Open Access.

In insect culture utilizing permissive cell lines, Negevirus cause extensive cytopathic effect (CPE) by disrupting the cell monolayer and causing rounding of the cells from 24 hours post-infection (hpi). Consistent with features of ISVs, these viruses cannot successfully replicate in mammalian cells, as has been shown with Vero (African green monkey), BHK (baby hamster kidney), and HEK 293 (human adrenal ganglion/neuron-derived) cell lines (22). Additionally, no illness was observed in newborn mice after intracerebral injections with Negevirus (22). These characteristics may make them suitable for arboviral control strategies in the arthropod vector as they cannot be transmitted to vertebrates and pose no imminent threat to human or animal health (22). In addition, their genome has shown some stability when modifying it to express fluorescent proteins and other immunogenically relevant sequences (13).

To date there are only a handful of research papers on these novel viruses, and much is still to be investigated about how they interact with their host. By understanding how

Negevirus interact with arthropod vectors, researchers may be able to identify new strategies for controlling the spread of arboviruses.

### *1.3 Co-infections*

The simultaneous infection of a host by two or more infectious agents is defined as a co-infection (27). Even though there is sparse evidence on the effects of co-infections, it is thought that most hosts are continuously exposed to several infectious agents at once. Although some concurrent infections can be harmful for the host, it is not always the case, as some can be beneficial (2, 27).

Studying arboviral co-infections in humans is challenging due to the complexity of the interactions between different arboviruses within a single host. Viral infections can occur simultaneously or sequentially, and their interactions can be intricate, depending on various factors, including the immune response of the host (2). Understanding the dynamics of co-infections requires sophisticated research designs and comprehensive data analysis.

As with any interaction with multiple biological agents, there are four main outcomes that may occur: enhancement, inhibition, competition, or neutral (Figure 2) (2). When it comes to mosquito-borne illnesses, most research focuses on arboviruses in humans and whether infection with multiple vertebrate pathogens can enhance or decrease disease severity in comparison to a single infection. Co-infections can be acquired simultaneously, where both viruses infect the host at the same time, or sequentially, where one viral infection precedes a secondary infection (2).

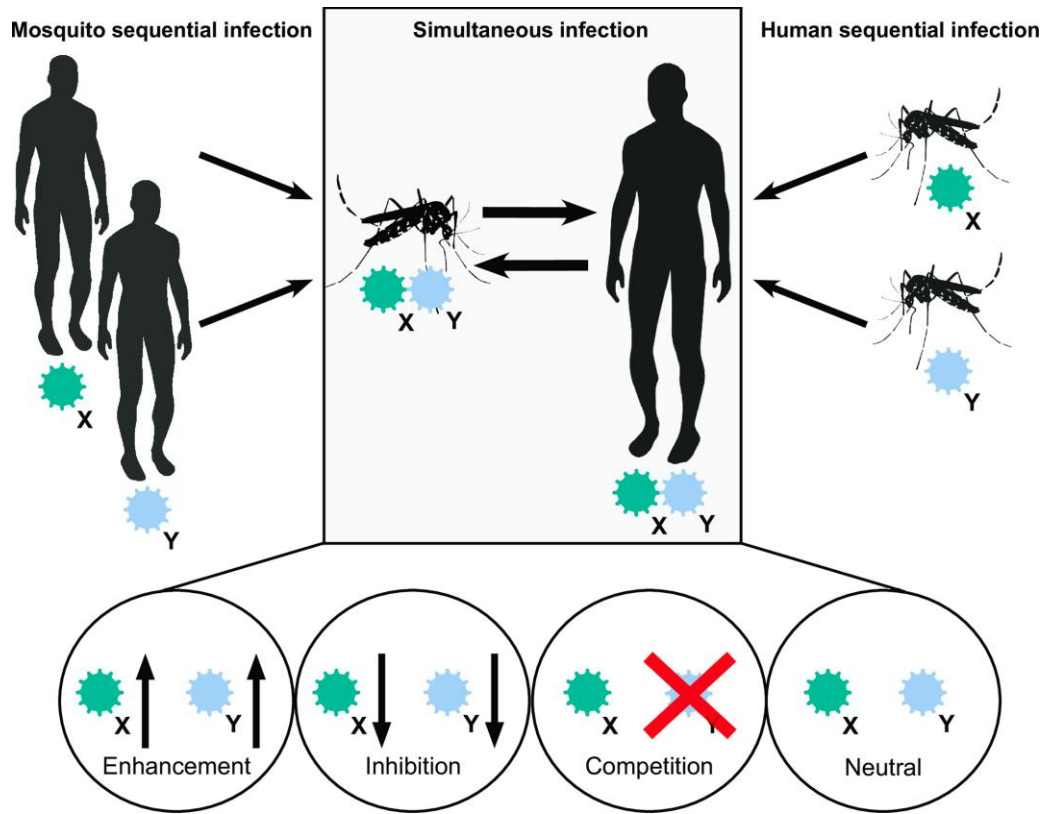


**Figure 2. Co-infection scenarios that may occur from simultaneous or sequential arboviral infections.**

Image from Vogels *et al.* (2), freely available in Open Access.

The enhancement outcome for co-infections is often focused on since it is likely for patients to seek medical treatment due to increased morbidity. For instance, CHIKV is known to interfere with human antiviral response by hindering signal transducer and activator of transcription 1 (STAT1), and DENV is known to disrupt STAT2. Thus, a simultaneous infection with CHIKV and DENV would suggest that these viruses could be able to replicate freely (2). Even if this does not directly increase their replication, the exacerbated immune response would result in an enhanced disease severity. However, the information available for these interactions is narrow since most studies are small-scale or based on individual case reports (2, 28, 29).

The co-infection inhibition outcome, where a simultaneous infection decreases the replication of both pathogens, is much less studied. One reason for this may be that the infected individuals might not look for medical attention if their symptoms are mild. Likewise, it is difficult to determine whether a co-infection results in a neutral outcome. Vogels *et al.* compiled data from numerous reports of human co-infections and determined that disease severity was often comparable to single infections, implying that co-infections have no virological impact or the viruses outcompeted each other and resulted in a single infection (2).

On the other hand, co-infections that result in competition have been investigated, and seem plausible since arboviruses often infect the same human cell type. Therefore, it could be possible for the initial infection to take over and use all cell resources for itself, causing the secondary virus to replicate less (2). For example, Zaidi *et al.* studied a small group of people in Mexico that were co-infected with DENV and CHIKV. They showed that the infections were not associated with increased clinical severity; rather, patients showed an immune response to both viruses while some seroconverted to CHIKV alone (30). These researchers suggest that a sequential infection could have been the cause of such results. The timing of the viral infections could explain why CHIKV outcompeted DENV in some patients (30). This is based on the superinfection exclusion theory, where a preexisting viral infection prevents or reduces a secondary infection. The study is limited by its small sample size, but still results point to some competition between mosquito viruses.

The examples mentioned above all involve multiple arboviruses infecting humans, but none mention co-infections within the insect vector itself. Interestingly, research shows that *Aedes aegypti* and *Ae. albopictus* mosquitoes are capable of transmitting multiple arboviruses during one bite, suggesting co-infections within the vector (2). A clearer example of viral

competition is the *Wolbachia*-mediated pathogen interference in mosquitoes. The proteobacterium *Wolbachia* is an endosymbiont known to infect around 76% of insect species on Earth, including some mosquitoes (8). For many years now, research has shown that the presence of this bacterium interferes with a variety of pathogens in mosquitoes, including other bacteria, nematodes, viruses, and avian plasmodia (8, 9). The mechanism by which *Wolbachia* interferes with arboviruses is not fully understood. It is thought to involve lifespan shortening of the insect host and cytoplasmic incompatibility, which results in the inability to form viable offspring, along with the activation of the mosquito's innate immune system (8, 9).

In addition, co-infection studies demonstrate that these bacteria can inhibit replication of viruses by directly competing for cellular resources. This has been demonstrated with DENV, as *Wolbachia* is speculated to inhibit the replication cycle of the virus through the collective contribution of several *Wolbachia*-mediated host modifications. When the bacterium is present, apparent changes in lipid homeostasis, disruption of intracellular membranes, and changes to the host cytoskeleton occur. These alterations disrupt the efficient formation of DENV virions, thus inhibiting its replication (9). Although there is no definitive answer to how the hindrance of virus infection occurs, it is well-established that *Wolbachia* outcompetes DENV in certain mosquito species (8, 9).

The current increased interest in detection and discovery of ISVs has significantly contributed to the understanding of mosquito virome interactions. As mentioned before, CFAV has shown its capability to reduce arboviral replication in multiple studies (11, 16-18). Another ISF that has shown this capacity is Palm Creek virus (PCV). Previously, Hobson-Peters *et al.*, provided *in-vitro* evidence of the superinfection exclusion theory with PCV. They showed that cells infected with PCV were less permissible to infection from WNV and Murray Valley

encephalitis virus (MVEV) (31). Similarly, Hall-Mendelin *et al.* conducted a study to determine how this ISV impacted the replication and transmission of WNV (32). As they had predicted, mosquitoes infected with PCV were less susceptible to oral infection with WNV and less competent to transmit the virus. Through *in-vitro* experiments, they found that in some mosquito cells PCV replicated quicker than WNV in the early stages of infection, thus giving PCV an advantage that leads it to outcompete WNV. This could explain why WNV replication decreased, along with the upregulation of antiviral responses by the primary infection (32). Both their results demonstrate that ISVs could be used to regulate transmission of pathogenic flaviviruses (31, 32).

Similar to ISFs, a recent study demonstrated the capacity of Negevirus to regulate and inhibit the replication of a different class of pathogens: alphaviruses. Patterson *et al.* demonstrated that some wild-type Negevirus could reduce the replication of Venezuela equine encephalitis virus (VEEV), o'nyong'nyong virus (ONNV) and CHIKV (13). The researchers demonstrated that NEGV and PIUV isolates significantly reduced the replication of VEEV and ONNV at all time points during co-infections. Although CHIKV titers were also reduced when co-infected with Negevirus, the results varied depending on the Negevirus species used. It was clear that CHIKV titers were most inhibited when co-infected with the PIUV isolate from *Lutzomyia evansi* sand flies (13). In general, it was evident that Negevirus also possess the ability to control arboviruses in cell culture, and that they could be good candidates for a novel pathogen or vector control method.

#### ***1.4 Virus Infectious Clones, Reporter Genes, and their Stability in ISVs***

Infectious cDNA clones are powerful tools for virology research. These tools offer valuable information on the functional elements in a virus sequence, including expression and replication of genes, and therefore largely contribute to the understanding of virus-host interactions (33). These artificial plasmids contain a complete copy of the virus genome and can be used to generate virus stock. They also facilitate the manipulation of the virus sequence through mutagenesis, deletions, and insertions, making it easy to explore viral mechanisms (33). The construction of infectious cDNA clones of certain RNA viruses consists of reverse transcribing the viral RNA into single-stranded DNA using virus-specific primers. Despite the challenges faced during the construction process, mainly due to the hampering of the polymerization steps by strong secondary structures on the viral template, many cDNA clones of both positive and negative-strand RNA viruses have been reported (33, 34).

When it comes to mosquito-borne viruses, there are several examples of infectious clones that result in functioning virus progeny. For instance, Kümmerer *et al.* generated a cDNA clone of CHIKV with a T7 promoter (35). They did this by amplifying the CHIKV sequence in four long parts through reverse-transcriptase PCR (RT-PCR), adding a T7 promoter upstream of the 5'-end of the viral cDNA, along with a NotI restriction site near the 3'-end. They cloned each fragment into low copy vectors and then fused them together, resulting in a full-length clone for CHIKV (35). The virus stock was produced through *in vitro* transcription and electroporation of BHK cells and deemed comparable to the original wild-type virus by producing CPE at 36 hours post-electroporation (hpe) and immunofluorescence signal with human anti-CHIKV sera at 24 hpe (35). A similar study was conducted by Shan *et al.*, who constructed a cDNA clone of a ZIKV isolate. Using methods comparable to that of the Kümmerer *et al.*, they retrieved virus

stock that was infectious in both Vero and insect cells, causing CPE in vertebrate cells. They also showed that mice infected with the rescued virus led to neurological disease and weight loss (36). Although in both studies, the parental virus isolate performed slightly “better”— suggesting their recombinant virus was less virulent— they still demonstrated that the cDNA clones created could be used for mutagenesis and pathogenesis analyses (35, 36). In addition to the cDNA clones, both research groups created fluorescent versions of their clones by adding reporters (in this case the mCherry fluorescent protein and the luciferase enzyme, respectively) to demonstrate that their clones could be modified to express foreign protein-coding genes. This way, viral infection can be tracked by monitoring the expression of the reporter gene, facilitating the identification of, as well as the study of viral replication and spread of the virus. Also, the kinetics of these fluorescent viruses can be compared to the wild-type clone to examine whether the replication rates are equal regardless of a reporter gene being present, which indirectly influences insert stability within the genome (35, 36). Likewise, infectious recombinant clones of ISVs have also been created as a platform to study viral transmission and pathogenesis. Unfortunately, the literature available on ISV infectious clones is sparse, but the ultimate goal would be to develop tools to combat pathogenic vertebrate viruses and lessen the burden they cause.

The incorporation of reporter genes into RNA viruses tends to be unstable (37). Inherently, viruses evolve quickly, have a high mutation rate and tend to lean towards a compact genome that does not allow space for non-essential genes and sequences. Therefore, deletions, mutations, or silencing of foreign genes are not unusual, since these would increase the size of their genome (37, 38). Common reporter genes, such as green fluorescent protein (GFP) and mScarlet, tend to range from 600-800 bp in size. Although that might not seem significant, for a

small RNA virus with a genome size around 11-15 kilobases, the extra length can be costly. This is especially true when inserting sequences that add no value to the viral genome. For example, expressing enhanced GFP (eGFP) is known to have a high fitness cost and be toxic for expression systems in certain +ssRNA viruses, like tobacco mosaic virus (TMV). It has been shown that propagating and passaging TMV expressing eGFP caused appearance of spontaneous deletion variants due to the decrease in fitness from carrying the reporter (37). Additionally, RNA viruses often use overlapping reading frames or alternative splicing to maximize the coding capacity of their genome. Insertion of sequences into such regions may disrupt the normal viral gene expression, leading to instability or loss of the reporter gene (37). Also, the size and number of foreign genes that researchers can incorporate into viruses are constrained due to potential disruptions in viral genome packaging. For instance, in the case of TMV, the insertion of foreign genes theoretically holds no limit owing to its rod-shaped nature. However, in practical applications, larger inserts are more susceptible to experiencing insert loss (37, 39). In the case of Negevirus, researchers have yet to fully explore their characteristics, leading to limited knowledge regarding their packaging signals and genome flexibility.

*In vitro*, reporter genes can also be inserted along different sections of a viral genome to determine the area(s) most likely to accept an insertion and retain it longer (37, 38). This approach was taken by Patterson *et al.* who demonstrated that GFP could be inserted into the NEGV genome (13). Using an infectious clone of NEGV, they found that the reporter gene was only tolerated when inserted as cleaved or fusion protein to the C terminus of ORF1 and ORF3, which correspond to the replication machinery and the membrane protein, respectively. These recombinant clones produced viable and stable virus stock that caused both the expression of GFP and CPE comparable to the wild-type. However, inserting GFP into ORF2, the sequence

that corresponds to the glycoprotein, resulted in nonviable virus. Such finding is not surprising since ORF2 is important for cell attachment and entry. Their results indicate that virus yield was directly dependent on placement of the insert.

After finding areas that would accept insertions, Patterson *et al.* replaced the reporter gene for an anti-CHIKV single chain variable fragment (scFv) sequence of similar size. They then demonstrated that the NEGV genome could be altered to express antiviral genes, and that the stock produced from those recombinant clones could inhibit CHIKV replication in cell culture (Figure 3)(13). Overall, these results show that the NEGV genome could be effectively manipulated to express foreign genes and be used as a paratransgenic control strategy.

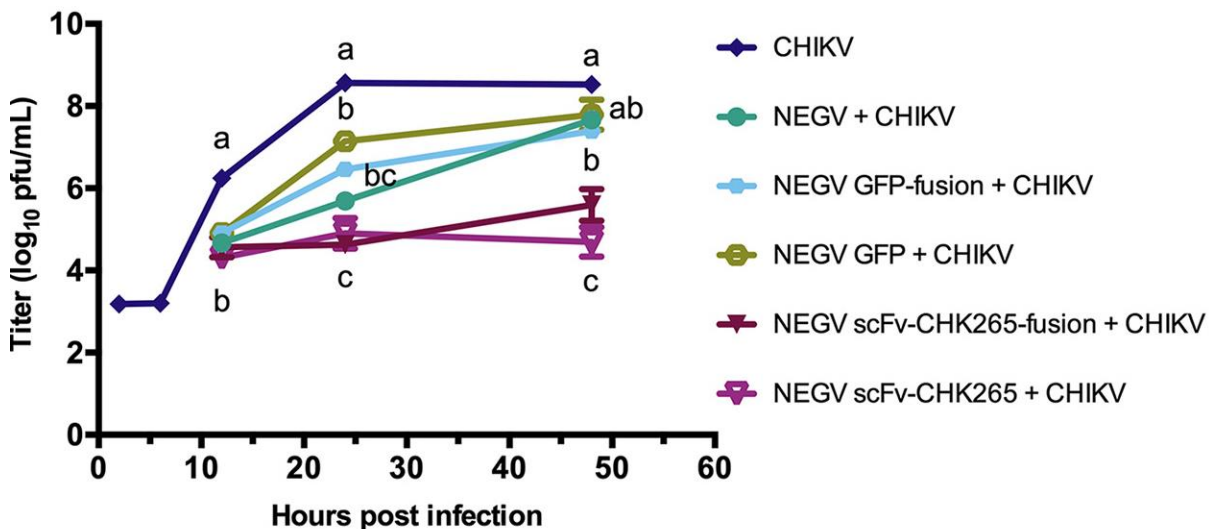


**Figure 3. Co-infection growth curves of CHIKV and paratransgenic NEG on C7/10 cells.** The trends demonstrate that the modified NEG clone expressing the anti-CHIKV single chain variable fragment (scFv) successfully inhibits CHIKV replication in cell culture. Wild-type NEG and clones expressing the reporter gene GFP cause no inhibition of the Alphavirus. Graph taken from Patterson *et al.*, available in Open Access (13).

Paratransgenesis is a strategy that can be used to control arboviruses by manipulating the microbiome of arthropod vectors. ISVs can be used for this since they can be genetically engineered to carry anti-arboviral components, like siRNAs (12, 17). These modified ISVs are introduced into the vector's microbiome, triggering RNAi pathways, potentially reducing vector competence, and limiting arbovirus transmission (12, 17). Challenges to implementing the use of paratransgenic microbes in the field include delivery optimization, stability, and regulatory considerations.

### ***1.5 Mosquito Cell Lines***

The females of hematophagous Diptera require a blood meal during the gonotrophic cycle to nourish egg development. This blood feeding process enables the transmission of pathogens to susceptible hosts, thus making them excellent vectors of disease. Insect cell culture has been a model for viral detection, replication, and interactions of mosquito-borne viruses. Several mosquito cell lines have been developed, many of which are naturally infected with ISVs.

The insect cell lines C6/36 and C7/10 were generated from *Ae. albopictus* larvae, and are derived from the ATC-15 cell line established by Singh in 1967 (40). The C6/36 cell line was selected for high arbovirus yield and increased sensitivity to infection (41). The C7/10 cell line was established from a clonal population selected from the ATC-15 line that showed distinct CPE after infection with Sindbis viruses (42). Both cell lines have been used extensively in the past to identify arboviruses and investigate virus interaction with mosquito vectors (41). These cells are permissive to infection from a variety of arboviruses and ISVs due to the absence of a functional RNA interference response (RNAi) (41, 43).

RNAi is a natural pathway in eukaryotic cells that likely evolved as a self-defence mechanism from viral attacks. It regulates gene expression by destroying viral RNA through the recognition of dsRNA, an intermediate in viral genome replication (43, 44). The pathway starts upon cleavage of viral dsRNA into small interfering RNA (siRNA) by Dicer-2, an endonuclease protein. These newly formed siRNAs are then loaded into RNA-induced silencing complexes (RISCs), which are made up of Argonaute proteins. Once loaded, an RNA helicase unwinds the dsRNA, causing one of the strands to become susceptible to degradation, leaving the guide strand attached to the RISC. The pairing of this guide strand to viral ssRNA causes sequence-specific cleavage that inhibits viral protein expression (43, 44). It is important to note that structured RNA sequences, such as those that form hairpins, are less likely to become accessible to Dicer-2 and therefore can avoid dsRNA cleavage. Some research suggests that the restriction in viral gene expression enables arboviruses to establish persistent infections in insect hosts (44). As a result, less insect fatalities occur due to low pathogenicity, allowing the virus to survive in the insect and infect a vertebrate host (44). Certain flaviviruses, such as DENV, can block RNAi in vertebrates through viral proteins that possess virus-encoded suppressor RNAi (VSR) activity. Due to this blockage, gene regulation is not functional, and pathogenicity increases as the viral genome replicates (44). The lack of Dicer complexes in C6/36 and C7/10 cells lines makes them ideal to grow and isolate mosquito-borne and insect-specific viruses.

Another important cell line used to study arboviruses and ISVs is the Aag2 line, isolated from *Ae. aegypti* mosquitoes in the late 1960s (45). This cell line is used frequently to examine the mosquito immune system since it has a competent RNAi response(41). For example, the antiviral response of insect cells to DENV has been characterized extensively in Aag2 cells due to their immuno-competency (41). Several other cell lines derived from *Ae. aegypti* are known to

be susceptible to DENV among other arboviruses, including CCL-125 and RML-12, but the Aag2 line is most commonly used (41). Additionally, some Aag2 cell lines are known to have pre-existing chronic infections with two ISVs, CFAV and PCLV (46). Those infections can make them a good candidate to study virome interactions since they emulate existing infections that can often be present in a natural insect environment. In this study, C6/36, C7/10 and Aag2 cells lines were used to study Negevirus interactions (Table 1).

**Table 1. Cell cultures used in the present study.**

Modified from Walker et al., 2014 (41)

Cell Line	Mosquito species	Source	Conditions
C6/36	<i>Aedes albopictus</i>	Larvae	RNAi deficient
C7/10	<i>Aedes albopictus</i>	Larvae	RNAi deficient
Aag2	<i>Aedes aegypti</i>	Embryos	Persistent infection with CFAV and PCLV

## Research Purpose and Objectives

The overarching goal of the present study is to further characterize Negevirus and contribute to the understanding of their interactions with the insect virome.

Specific objectives of this work included:

1. *To determine which virus species is most likely to prevail during co-infections in the wild.*

I will produce NEGV and PIUV stocks through both artificially created cDNA clones, and lyophilized virus isolated from wild-caught insects. I will perform a series of co-infection assays in different cell types, both RNAi deficient and competent, to observe how NEGV and PIUV, among other isolates like LORV, interact (Table 2). Competition, inhibition, enhancement, or

neutral interactions will be monitored to determine which virus species is most fit to survive in mosquitoes.

2. *To identify which virus species tolerates genetic modifications better and could act as a backbone for paratransgenesis.*

I aim to successfully create infectious clones of NEGV and PIUV that have fluorescent reporter genes inserted into ORF3 of their genome. The reporter genes GFP, mScarlet, mEmerald, and ZsGreen were used during cloning experiments. Comparing the growth curves of different Negevirus clones and species in these cell lines will allow us to determine the most suitable virus isolate to be used in further experiments with mosquitoes. This will also tell us which virus tolerates genetic modifications better and could act as a backbone for paratransgenesis. In the future, the goal will be to replace these reporter genes with immunologically relevant sequences that can inhibit arboviral replication in mosquitoes, as was demonstrated *in vitro* by Patterson *et al.* (13).

**Table 2. Wild type Negeviruses described in the current study.**

Modified from Nunes *et al.*, 2017 (26).

<b>Genus</b>	<b>Species</b>	<b>Strain</b>	<b>Host source</b>	<b>Location of Isolation</b>	<b>Year of Isolation</b>
	Negev virus	M30957	<i>Culex coronator</i>	Texas, USA	2008
Nelorpivirus	Piura virus	CoR 10	<i>Lutzomyia evansi</i>	Sucre, Colombia	2013
	Loreto virus	3940-83	<i>Anopheles albimanus</i>	Lima, Peru	1983

## Chapter 2 – Materials and Methods

### Materials

#### 2.1 Cell culture and viruses

**Table 3. Reagents used for cell culture maintenance and experiments.**

Reagent	Supplier	Catalog #
Dulbecco's Modified Eagle's Medium - high glucose	Sigma	D6429
Schneider's Insect Medium	Sigma	S0146
Dulbecco's Phosphate Buffered Saline	Sigma	D8662
Tryptose Phosphate Broth solution, 29.5 g/L	Sigma	T8159
Sodium Pyruvate, Liquid 100 mM Solution	Corning	25-000-CI
MEM Nonessential Amino Acids, 100x	Corning	25-025-CI
Gentamicin Sulfate, 50mg/mL	Corning	30-005-CR
Research Grade Fetal Bovine Serum, Canadian Sourced	Thermo Fisher	FB12999102
Fungin™ - Antifungal Reagent	InvivoGen	ant-fn-1
Cell culture plasticware, T-25, T-75, T-175 & plates	Sarstedt	

**Table 4. Reagents used for *in vitro* transcription and electroporation.**

Reagent	Supplier	Catalog #
DTT 100 mM 100 µL, Molecular Grade	Promega	P117A
Ambion™ SP6 RNA Polymerase	Thermo Fisher	AM2071
m7G(5')ppp(5')G RNA Cap Structure Analog	NEB	S1404S
RNaseOUT™ Recombinant Ribonuclease Inhibitor	Thermo Fisher	10777019
Ambion™ 10X Transcription Buffer	Thermo Fisher	AM2071
Promega Riboprobe rNTPs	Thermo Fisher	P1221

## 2.2 Cloning *NEGV* and *PIUV* for exogenous gene expression

**Table 5. Reagents used for bacterial culture during cloning experiments.**

The reagents listed below were used to make LB agar selection plates and LB broth for overnight cultures of bacterial colonies containing the plasmid of interest.

Reagent	Supplier	Catalog #
Agar powder	Thermo Fisher	A360500
Sodium Chloride	Thermo Fisher	S2713
Bio-Tryptone	BioShop	TRP402.500
Yeast Extract	Sigma	70161-500G
Kanamycin Sulfate	Thermo Fisher	BP906-5
Ampicillin	Thermo Fisher	AAJ6097706
SOC Outgrowth Medium	NEB	B9020S

**Table 6. PCR mixes, enzymes, kits, and cells used for cloning experiments.**

Reagent	Supplier	Catalog #
Q5 <sup>®</sup> High-Fidelity 2X Master Mix	NEB	M0492S
NEBuilder <sup>®</sup> HiFi DNA Assembly Master Mix	NEB	E2621L
NotI-HF <sup>®</sup>	NEB	R3189S
NdeI	NEB	R0111S
Monarch <sup>®</sup> Plasmid Miniprep Kit	NEB	T1010L
Monarch <sup>®</sup> PCR & DNA Cleanup Kit	NEB	T1030L
NEB <sup>®</sup> Turbo Competent <i>E. coli</i> (High Efficiency)	NEB	C2984I

**Table 7. Reagents used for gel electrophoresis and gel extraction.**

<b>Reagent</b>	<b>Supplier</b>	<b>Catalog #</b>
Tris-Acetate-EDTA, 50X Solution	Thermo Fisher	BP133220
Quick-Load <sup>®</sup> Purple 1 kb Plus DNA Ladder	NEB	N0550S
Agarose (Low-EEO/Multi-Purpose/Molecular Biology Grade)	Thermo Fisher	BP160-100
SYBR <sup>™</sup> Safe DNA Gel Stain	Thermo Fisher	S33102
Monarch <sup>®</sup> DNA Gel Extraction Kit	NEB	T1020L

**2.3 Plaque assays****Table 8. Reagents using for insect cell plaque assays.**

<b>Reagent</b>	<b>Supplier</b>	<b>Catalog #</b>
Modified Eagle Medium (2X), no phenol red	Gibco	11935046
Alfa Aesar, Tragacanth powder	Thermo Fisher	A18502-22
Crystal Violet (Certified Biological Stain)	Thermo Fisher	C581100
Formaldehyde	Thermo Fisher	BP531

**2.4 Virus growth curves using RT-qPCR****Table 9. RNA extraction and RT-qPCR kit used for growth curve experiments.**

<b>Reagent</b>	<b>Supplier</b>	<b>Catalog #</b>
Quick-RNA Miniprep Kit	Zymo Research	R1055
Quick-RNA 96 Kit	Zymo Research	R1053
Primers (refer to appendix A)	Integrated DNA Technologies	
iTaq <sup>™</sup> Universal SYBR <sup>®</sup> Green One-Step Kit	BioRad	1725150

## Methods

### 2.5 Cell culture and viruses

*Ae. albopictus* C6/36 cells were provided by Dr. Hunter's group at Brock University, *Ae. albopictus* C7/10 cells were obtained from the World Reference Center for Emerging Viruses and Arboviruses (WRCEVA) at the University of Texas Medical Branch (UTMB; Galveston, TX) and *Ae. aegypti* Aag2 cells were obtained from the Liverpool School of Tropical Medicine (LSTM). All insect cell lines were kept in a 27°C incubator with 5% CO<sub>2</sub>, using various media. C6/36 and C7/10 cells were maintained in Dulbecco's Modified Eagle's Medium (DMEM) supplemented with 10% fetal bovine serum (FBS), 1% sodium pyruvate, 1% nonessential amino acids, 1% tryptose phosphate broth, and 0.05 mg/ml gentamicin. Aag2 cells were maintained in Schneiders medium supplemented with 20% FBS and 0.05 mg/mL gentamicin. Anti-mycotic Fungin<sup>TM</sup> was used at a concentration of 0.05 mg/mL to grow virus in cell culture.

NEGV was rescued in C6/36 cells from an infectious clone synthetically produced by Genscript, without further passage. The sequence was derived from NEGV strain M30957, isolated from a pool of *Culex coronator* mosquitoes collected in Harris County, TX, in 2008 (34). The PIUV strain CoR 10 was rescued in C7/10 cells from an infectious clone without further passage. The plasmid was synthetically produced by Genewiz. The sequence was derived from PIUV isolated from a pool of *Lutzomyia evansi* sand flies caught in Ovejas, Sucre, Colombia, in 2013 (26). Lyophilized field-derived wild-type isolates of NEGV, PIUV and LORV were also obtained from the WRCEVA; stocks of these viruses were grown and recovered in C7/10 cells. Henceforth, the wild-type virus stocks produced from infectious clones are referred to as NEGV WT and PIUV WT, and the field-derived virus stock are referred to as NEGV UTMB, PIUV UTMB and LORV UTMB. Modified NEGV and PIUV isolates expressing

reporter sequences are produced from the wild-type infectious clones. Cloning of these modified isolates is described in the following section.

Virus progeny from infectious clones was rescued as previously described by Gorchakov *et al.* (34). 2-3  $\mu\text{g}$  (generally, 5-10  $\mu\text{L}$ ) of each plasmid was linearized using 1  $\mu\text{L}$  of restriction enzyme, 5  $\mu\text{L}$  of 1X NEB CutSmart buffer and nuclease free water to a total volume of 50  $\mu\text{L}$ , according to the manufacturer's instructions. Enzyme NotI-HF was used for both wild-type clones, as well as ZsGreen and mEmerald reporter clones, while NdeI was used for mScarlet variations. The linearized product was purified using the Monarch PCR & DNA Cleanup Kit (NEB) as per manufacturer's instructions. The 50  $\mu\text{L}$  sample was diluted in 100  $\mu\text{L}$  of binding buffer and mixed by pipetting up and down. Sample was loaded onto the spin column with a collection tube and spun at 10,000 X *g* for 1 minute. After discarding the flowthrough, two wash steps with 200  $\mu\text{L}$  with DNA wash buffer were performed, and the column was transferred to a clean 1.5 mL tube. 50  $\mu\text{L}$  of elution buffer heated to 50°C was added to the matrix and spun down for a minute. The product was stored at -20°C until needed.

*In vitro* transcription of the linearized plasmids was carried out using the following reagents in this exact order: 2.5  $\mu\text{L}$  DTT, 5  $\mu\text{L}$  of 10X transcription buffer, 2.5  $\mu\text{L}$  of 10 mM rNTPs, 2.5  $\mu\text{L}$  of 10 mM RNA cap, 5  $\mu\text{L}$  of linearized template, 7  $\mu\text{L}$  of RNase/DNase free H<sub>2</sub>O, 0.5  $\mu\text{L}$  of RNA guard RNase inhibitor and 1 $\mu\text{L}$  of SP6 RNA Polymerase. This transcription mixture was incubated at 37°C for 1 hr and placed on ice for subsequent electroporation or stored at -80°C.

A confluent T175 flask of C7/10 or C6/36 cells was scraped with 10 mL of fresh media, centrifuged at 200  $\times$  *g* in a 15 ml tube for 5 min and resuspended in 7 ml of cold PBS, cells were washed with PBS twice and spun down a last time for 3 min, then cells were resuspended in 450

$\mu\text{L}$  of PBS in a 1.5 mL tube. 10  $\mu\text{L}$  of the corresponding transcribed RNA sample was placed into the tube and mixed thoroughly. The mixture was transferred to an electroporation cuvette on ice and pulsed using the BTX ECM 830 Electro Square Porator by Harvard Apparatus using the following settings: 680 V, pulse length 99  $\mu\text{s}$ , 200 ms intervals and 5 pulses. The cuvette was left at room temperature for 10 min, after which the solution was transferred into a 15 mL tube with 10 mL of media in the biosafety cabinet. A new T75 was then seeded with this mixture and incubated as usual. Virus stock was collected at 24- and 48-hours post-electroporation (hpe).

## ***2.6 Cloning NEGV and PIUV for exogenous gene expression***

The NEGV and PIUV infectious clones were used as backbones to express foreign genes. mScarlet (696bp), mEmerald (720bp) or ZsGreen (693bp) were inserted on the C-terminus of ORF3 to create fusion proteins. Cloning was performed using an NEBuilder HiFi DNA Assembly kit (NEB) and the correct insertion of the reporter was confirmed by Sanger sequencing (Appendix A). Infectious clones of NEGV and PIUV containing exogenous genes were rescued in C6/36 and C7/10 cells as previously described without further passage, extensive details for the cloning process are below.

To amplify the vector and insert fragments, NEB's Q5 high-fidelity 2X master mix was used. The reaction consisted of 2.5  $\mu\text{L}$  of 10  $\mu\text{M}$  forward primer, 2.5  $\mu\text{L}$  of 10  $\mu\text{M}$  reverse primer, 1  $\mu\text{L}$  of the template DNA, 25  $\mu\text{L}$  of the master mix and 19  $\mu\text{L}$  of nuclease-free water, for a total volume of 50  $\mu\text{L}$ . This was transferred to a thermocycler under the following conditions: initial denaturation at 98°C for 30 seconds, 35 cycles of 98°C for 10 seconds, 68°C for 20 seconds and 72°C for 20 seconds, then a final extension at 72°C for 2 minutes after which the reaction was kept at 4°C. For reactions meant to amplify the vector backbone, in this case the

virus sequence, the extension period for each cycle was increased to 10 min to ensure enough time was given for construction of a sequence larger than 10 kb.

The entire reaction volume was mixed with 10  $\mu\text{L}$  of purple loading dye and added to a 1% agarose gel with 1:40,000 x SYBR Safe dye (i.e., used 2.5  $\mu\text{L}$  of SYBR Safe Dye when casting 100 ml of gel). Electrophoresis was ran at 90 V for 45 min in TBE buffer. The gel was then imaged to visualize DNA fragments and estimate their size based on the NEB Quick-Load Purple 1kb Plus DNA ladder. Bands corresponding to fragments of interest were excised from the gel and individually placed in 1.5 mL tubes. The samples were purified using the Monarch DNA Gel Extraction Kit by NEB as per manufacturer's instructions. The agarose slice was dissolved using 400  $\mu\text{L}$  of dissolving buffer and incubating this reaction at 50°C on a water bath for 15-30 min. The sample was then loaded onto the columns with collection tubes and spun for a minute at 10,000 X *g*. Two wash steps followed, using 200  $\mu\text{L}$  of DNA wash buffer and spinning at the same speed for 1 min, discarding the flowthrough at each step. The column was transferred to a clean 1.5 mL microfuge tube and 20  $\mu\text{L}$  of DNA elution buffer that had been warmed to 50°C was added onto the center of the matrix. After incubating at room temperature for 1 min, the column was spun, and the concentration of each DNA sample was taken.

As mentioned previously, the NEBuilder HiFi DNA Assembly kit was used to clone the recombinant infectious clone plasmids. DNA fragments from the gel extraction protocol were added to a 0.2 mL tube in a 1:2 ratio of vector to insert (generally, 50-100 ng/ $\mu\text{L}$  of vector) along with 10  $\mu\text{L}$  of NEBuilder Hi-Fi DNA assembly master mix and deionized water to a total volume of 20  $\mu\text{L}$ . The reaction was incubated in a thermocycler at 50°C for 15 min and then used for transformation, or stored at -20°C. For transformations, 5  $\mu\text{L}$  of the assembled product was added to NEB® Turbo Competent *E. coli* (High Efficiency) cells that had been thawed on ice.

The reaction was mixed by flicking 5 times and then incubated on ice for 30 min, after which it was heat shocked at 42°C on a water bath for 40 seconds. After resting on ice for 2 min, 950 µL of SOC media was added to each tube and incubated in an orbital shaker at 37°C for 1 hr at 250 rpm. 100-200 µL of cells were spread on selection plates with 50 µg/mL ampicillin or kanamycin and incubated overnight at 37°C. Isolated colonies were picked from the plates and used to make overnight cultures for the miniprep plasmid kit.

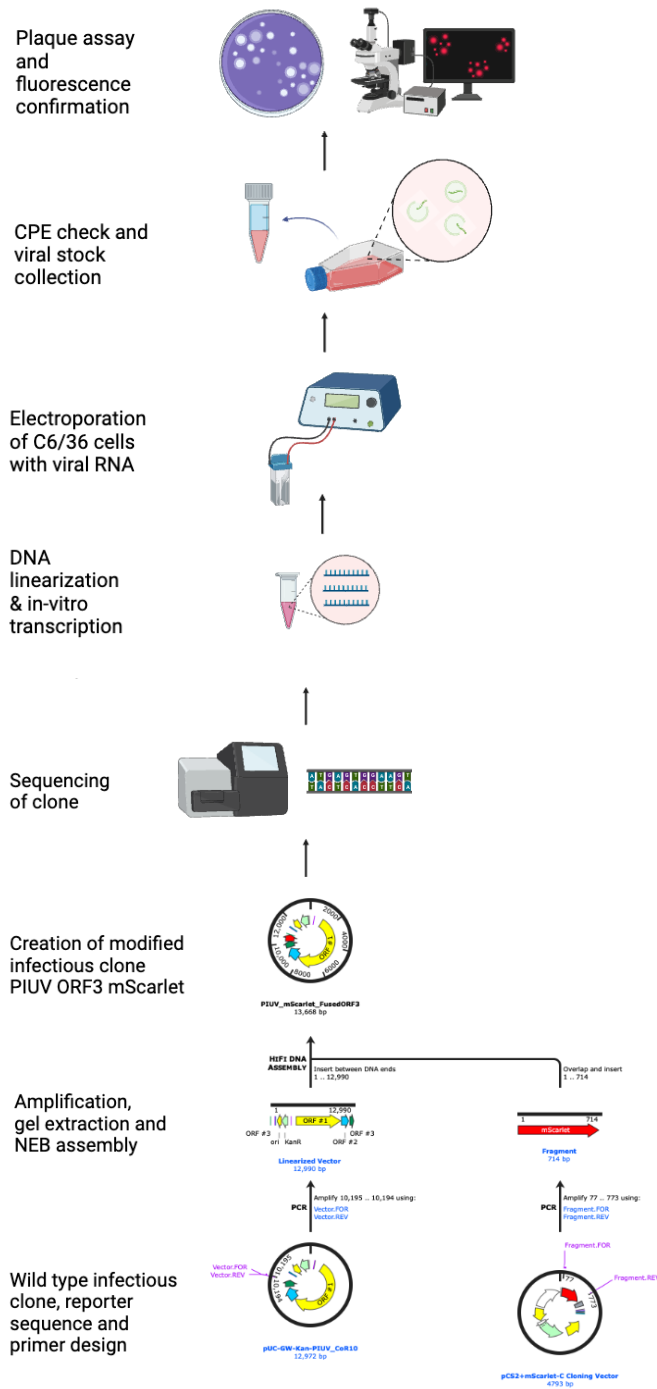


**Figure 4. Flow chart demonstrating all steps taken to clone mScarlet into ORF3 of PIUV.**

The figure, bottom-up, depicts the cloning process of PIUV ORF3 mScarlet, as described in section 2.6 of the methods. Each step is described by the text to the left.

## **2.7 Virus Purification**

The virus purification protocol was modified from Colmant *et al.*, 2020 (23). The supernatant of infected C6/36 cells was collected and centrifuged at 3,000 x g at 4°C for 10 min. One part of 40% polyethylene glycol (PEG) 8000 was mixed with four parts of clarified supernatant containing virus and left to precipitate overnight. The next day, this mixture was centrifuged for 30 minutes at 4°C at 3000 x g, after which the supernatant was discarded and the pellet was left to air dry for 30 min. The PEG-precipitated virions were resuspended in 4 ml cold NTE (12 mM Tris at pH 8, 120 mM NaCl, 1 mM EDTA pH 8) prior to ultracentrifugation through a 20% sucrose cushion at 100,000 x g (28,000 rpm; SW41Ti Rotor Beckman Coulter) for 2 hr at 4 °C. This pellet was resuspended in 1 mL of NTE buffer and added onto a 10–40% potassium tartrate gradient and centrifuged at 180,000 x g (38,000 rpm; SW41Ti Rotor, Beckman Coulter) for 1.5 hr at 4 °C. The virus band was extracted, and the buffer was exchanged into NTE pH 8 using a centrifugal concentrator with a molecular weight cut-off of 100 kDa. The final volume collected from the concentrators was between 150-300 µL.

## **2.8 Plaque assays**

Plaque assays were performed in 6-well plates using C6/36 cells seeded at  $0.5 \times 10^6$  cells/mL. Plates were seeded 2 days prior to ensure a ~90% confluent monolayer the day of infection. Tenfold serial dilutions of the infectious samples were prepared using a 96-well plate. Each well was provided 225 µL of fresh media, then 25 µL of each virus stock was added to the first column, corresponding to the  $10^{-1}$  dilution. Using a multichannel pipette, the first column was mixed by pipetting up and down 20 times. 25 µL of the first column was deposited into the second column and the tips were discarded in a waste container with a 10% bleach solution.

Using new pipette tips, the mixing and dilution steps were repeated in each column until reaching the desired dilution.

Media was removed from the plates seeded with C6/36 cells and 150  $\mu$ L of each virus dilution was added to its corresponding well. Plates were rocked gently to ensure even coverage and placed in the incubator for 30 min; they were rocked again at the 15-min mark. After the incubation period, 2-3 mL of the overlay was slowly added to each well to avoid disturbing the cells. The overlay consisted of a 1:1 mixture of 2% tragacanth and 2X DMEM media with 5% FBS and additives (1% sodium pyruvate, 1% nonessential amino acids, 1% tryptose phosphate broth, and 0.05 mg/ml gentamicin) which had been warmed to room temperature before adding it to the cells. Plates were placed in the incubator for 48 hr without any disruption. After this time, the overlay was removed slowly to avoid interfering with plaques, and 2 mL of 10% formaldehyde fixing solution was added to each well. After incubating for 30 min, formaldehyde was discarded in a waste container and approximately 1 mL of 0.25% crystal violet stain was added to each well. After 1 min, stain was removed and lightly washed with tap water. Plates were placed on a light box for visualizing countable plaques. Titers were calculated and used for growth curve experiments.

## ***2.9 Virus growth curves using RT-qPCR***

A preliminary real-time quantitative PCR (RT-qPCR) to determine the approximate genome copy number per microliter of virus stock was carried out using the iTaq Universal SYBR Green One-Step Kit for real time PCR. The concentration of the wild-type plasmids was determined using a nanodrop prior to PCR preparation to obtain a concentration value from which a standard curve could be generated. The NEGV 6812/6971 (appendix A, primers 25 &

26) and PIUV 7881/8101 (appendix a, primers 27 & 28) primers were used at a concentration of 10 mM, as designed by Dr. Patterson using the Primer3 interface (<https://primer3.ut.ee/>) (47). Each well on a 96-well qPCR plate was loaded with 5  $\mu$ L of iTaq Universal SYBR Green master mix, 0.125  $\mu$ L iScript reverse transcriptase, 0.3  $\mu$ L forward primer, 0.3  $\mu$ L reverse primer, 2.28  $\mu$ L nuclease free H<sub>2</sub>O and 2  $\mu$ L of RNA template. The plate was then sealed with optically transparent film, gently vortexed and centrifuged for 30 seconds before running. The thermocycler protocol was programmed on the CFX Real-Time PCR instrument by Bio-Rad according to the manufacturer's recommendations. Conditions included an initial reverse transcription reaction for 10 min at 50°C, polymerase activation and DNA denaturation for 1 min at 95°C, and 40 cycles of denaturation at 95°C for 10 seconds, and annealing/extension at 60°C for 20 seconds. The melt curve was generated in 0.5°C increments from 65 to 95°C. Genome copy numbers were calculated from the starting quantity (Sq) values from the qPCR results using an online calculator (<http://sciprim.com/html/copyNumb.v2.0.html>).

Growth curves were carried out using 24-well plates with C7/10 and Aag2 cells in triplicates. Plates were seeded with 500  $\mu$ L of a suspension of cells at a concentration of  $0.5 \times 10^6$  cells/ml and left to incubate for 24 hr. Media was removed from the plates and cells were infected with the appropriate amount of virus stock for a multiplicity of infection (MOI) of 1, based on the plaque assay results. Plates were placed back into the incubator to await collection, which occurred at 2, 6, 24 and 48-hours post-infection (hpi). For each 24-well plate, 500  $\mu$ L of the corresponding wells for a single time point were collected and individually placed in 1.5 mL tubes. These were centrifuged at  $2,300 \times g$  for 5 minutes, after which 150  $\mu$ L of supernatant was transferred to a new 1.5 mL tube for RNA extraction and 350  $\mu$ L left over was stored at -80°C for further experiments.

RNA from liquid media was extracted using the Zymo Quick-RNA 96-well plate kit with modifications of the manufacturer's protocol. 300  $\mu\text{L}$  of RNA lysis buffer was added to each 100  $\mu\text{L}$  sample and briefly vortexed. 400  $\mu\text{L}$  of 100% ethanol (1:1) was added to each sample and mixed well before transferring the solution to the Zymo Silicon A plate mounted on a collection plate. This was centrifuged at  $2,500 \times g$  for 5 minutes, and flowthrough was discarded. 400  $\mu\text{L}$  of RNA wash buffer was added to each well and flowthrough was discarded after spinning. A DNase step followed: 40  $\mu\text{L}$  of treatment solution was added to the matrix of each column on the plate, which consisted of 5  $\mu\text{L}$  of DNase and 35  $\mu\text{L}$  of digest buffer, then the plate was incubated for 15 minutes at room temperature. After incubation, 400  $\mu\text{L}$  of RNA prep buffer was added to each well and spun again, discarding flowthrough, after which 2 wash steps with 500  $\mu\text{L}$  RNA wash buffer followed. RNA was eluted in 25  $\mu\text{L}$  of DNase/RNase-free water and stored at  $-80^\circ\text{C}$ .

RT-qPCR was performed using the RNA samples from the growth curve time points in duplicates for each biological replicate. The same primers, reagents and protocol for the thermocycler mentioned prior were used to generate standard curves and estimate Sq values for the samples at different time points. The copy number calculator was used to convert Sq values into genome copy number per microliter of sample, data available in supplementary files. The data from this protocol was exported to GraphPad Prism software for analysis.

### ***2.10 Negevirus co-infections***

Co-infection experiments were carried out using 24-well plates with C7/10 and Aag2 cells in triplicates. Plates were seeded with 500  $\mu\text{L}$  of a suspension of cells at a concentration of  $0.5 \times 10^6$  cells/ml and left to incubate for 24 hr. Media was removed from the plates and cells were infected with the appropriate amount of virus stock for infection with an MOI of 1 for each

virus pair of co-infections (Table 10). Plates were placed back into the incubator until further collection, which occurred at 2, 6, 24 and 48 hpi. For time collections, 500  $\mu$ L was recovered for each well and individually placed in 1.5 mL tubes. They were centrifuged at  $2,300 \times g$  for 5 min, after which aliquots of the supernatant were made. 100  $\mu$ L was transferred to a 2 mL screw cap tube for plaque assays and 400  $\mu$ L was transferred to a new 1.5 mL tube for RNA extraction using the same protocol mentioned prior using the Zymo Quick-RNA 96-well plate kit. Both aliquots were stored at  $-80^{\circ}\text{C}$  until further use.

RT-qPCR was performed using the same protocol used for the growth curves with the RNA samples from the co-infection time points in technical duplicates for each biological replicate. The same reagents and protocol mentioned prior were used to generate standard curves and estimate  $S_q$  values for the time points of each co-infection. The copy number calculator was used to convert  $S_q$  values into genome copy number per microliter of sample. This data was exported to GraphPad Prism software for analysis.

**Table 10. Negevirus co-infection pairs used in the present study.**

<i>Co-infection #</i>	<i>Virus pair in co-infection</i>		
1	PIUV WT	X	NEGV WT
2	PIUV WT	X	NEGV UTMB
3	PIUV UTMB	X	NEGV WT
4	PIUV UTMB	X	LORV UTMB
5	NEGV UTMB	X	LORV UTMB
6	PIUV ORF3 mScarlet	X	NEGV ORF3 GFP

### ***2.11 Statistical analysis***

Analysis for virus growth curves (single infections) was performed using one-way analysis of variance (ANOVA), followed by a Tukey's multiple comparisons test for each time point. To evaluate differences in reporter gene and virus sequence quantity for genome copies, unpaired t-tests were carried out at each time point as well. A one-way ANOVA followed by a Dunnett's multiple comparisons test was used to analyze the differences between growth trends in the co-infection experiments, using the virus' single infection data as a control against the co-infection trend. Variances between reporter gene signal and virus sequence signal was evaluated using unpaired t-tests at each time point. To assess statistical differences between virus titers at 48 hpi, a one-way ANOVA was carried out. To determine the significance between regular and fluorescent plaques for modified viruses in single/dual infections, unpaired t-tests were performed. Differences for all analyses were reported if they were highly significant ( $P < 0.0001$ ). All statistical tests were performed using GraphPad Prism 8.0.

## Chapter 3 – Cloning Results

### *3.1 Construction of modified NEGV and PIUV infectious clones*

Molecular cloning is a useful technique that involves the insertion of a specific DNA fragment into a suitable vector which can be easily amplified by the appropriate host. Cloning allows researchers to manipulate DNA through insertions, deletions or mutations, all while being able to yield their desired sequence in an expression vector that can be produced by quickly replicating organisms, like bacteria. One of the objectives of this study was to clone reporter genes onto Negevirus. The following sections describe the process by which modified NEGV and PIUV clones expressing reporters were constructed.

#### *3.1.1 Cloning of fluorescent reporters onto virus infectious clones: PIUV*

Sequences for NEGV and PIUV wild-type clones were made available by Dr. Patterson and uploaded to SnapGene. Using this software and its built-in NEBuilder HiFi assembly tool, I designed the primers necessary for amplification of fragments and was able to simulate the cloning steps with the kit available. Reporter genes mScarlet and mEmerald were kindly provided by Anel Turgambayeva and Marvel Megaly, members of Dr. Necakov's lab, while ZsGreen was provided by Dr. Patterson. For purposes of visualization, the Addgene (<https://www.addgene.org/fluorescent-proteins/plasmid-backbones/>) sequences were used in the construction scheme below (Figure 5). The PCR products recovered from the Q5 Hi-Fi reaction used to clone PIUV ORF3 mScarlet are shown in Figure 5.

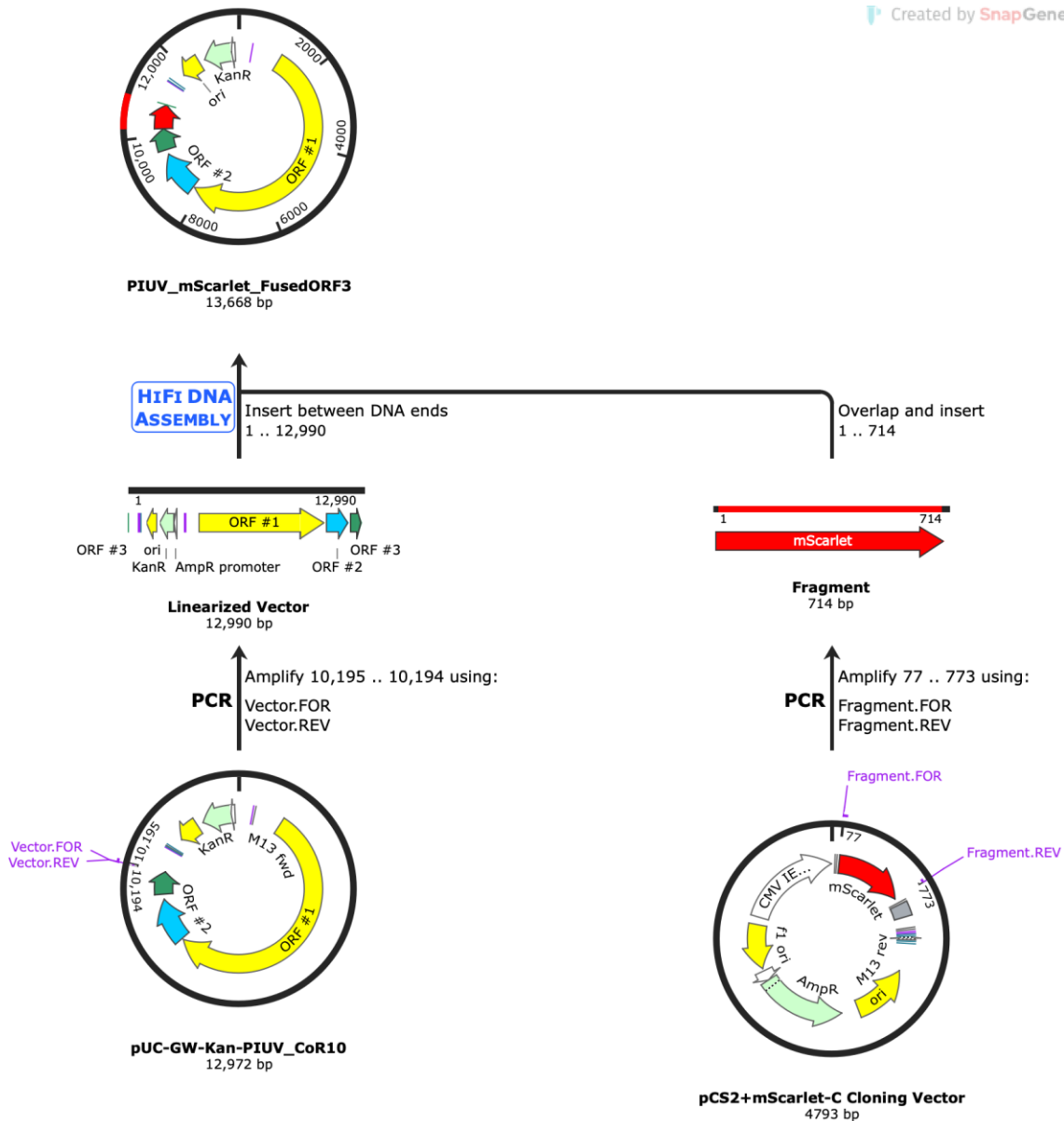


**Figure 5. Simulation of the cloning process for PIUV ORF3 mScarlet.**

The figure, bottom-up, depicts the starting products for the cloning process; the infectious clone for PIUV on the left and the vector expressing mScarlet on the right. The primers shown in purple were designed via SnapGene, using their NEBuilder HiFi assembly tool, these were used for a Q5 Hi-Fi PCR step to amplify the fragments for assembly. In this case, the entire PIUV plasmid sequence (12,990 bp) and the reporter fragment mScarlet (714 pb). The primers were designed to create overhangs on either end of the amplified fragment to facilitate the ligation of

the insert and vector. The linearized products from the PCR that were used for the NEB assembly kit are also shown, these products were extracted and purified from the gel electrophoresis step (Figure 6). The final product is observed at the top. Cloning scheme created with the SnapGene software.

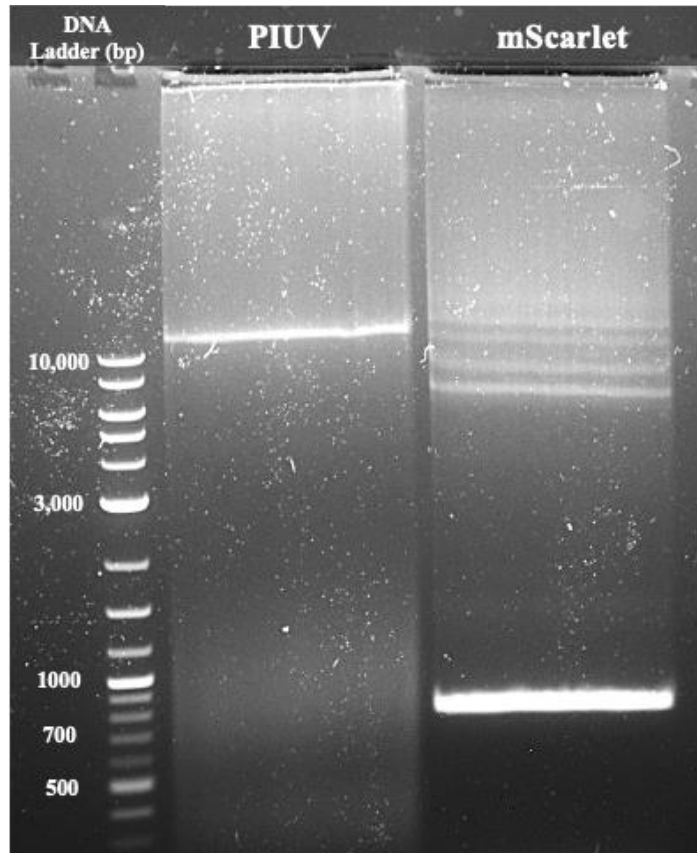


**Figure 6. Gel image for Q5 Hi-Fi PCR products used to clone PIUV ORF3 mScarlet.**

The products were run on a 1% agarose gel with SYBR Safe and electrophoresed at 90 V for 45 min in TBE buffer. The estimated size of the PIUV plasmid amplicon was around 13kb and mScarlet around 700bp. The DNA bands were individually excised using a razor and used for a gel extraction kit.

Using a 1:2 ratio of vector to insert and the master mix provided in the NEBuilder Hi-Fi DNA assembly kit, the product was created as shown in Panel C of the scheme. The assembled product was transformed into high efficiency competent *E. coli* cells and plated onto kanamycin selection plates. Isolated single colonies were picked from the plate to make overnight cultures for subsequent plasmid DNA isolation. Once the DNA for the infectious clone was isolated, it was sent for sequencing to confirm the insertion as shown in Figure 7 below. Out of the 6 colonies screened all 6 contained the fluorescent reporter, but only 4 had acceptable sequence alignment to both ORF3 of PIUV and mScarlet. Colony #6, shown in Figure 7, was chosen to use for rescuing virus stock since sequencing results showed excellent quality scores throughout the forward and reverse reads and especially within the junction sites ORF3-mScarlet and mScarlet-plasmid backbone.

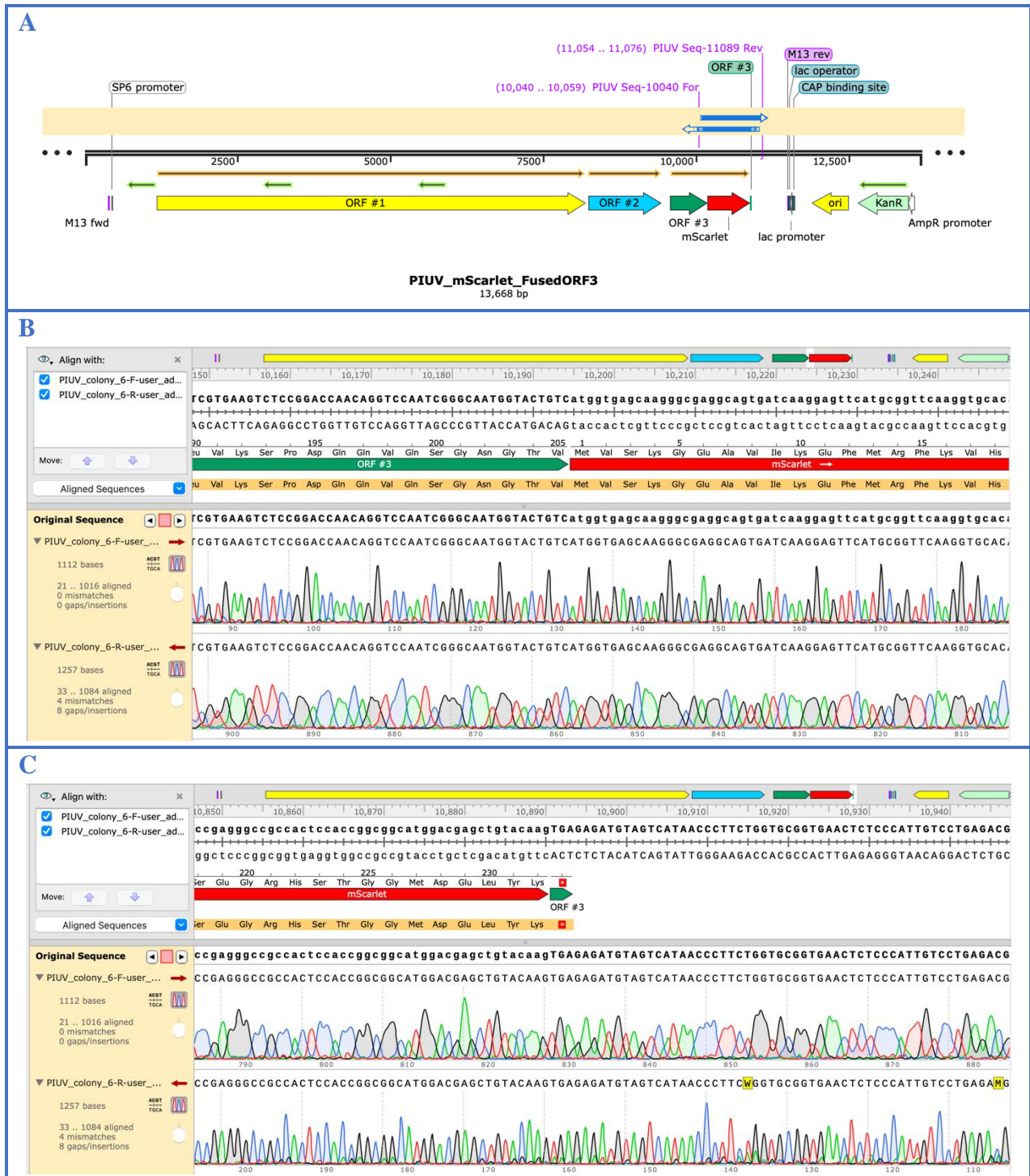


**Figure 7. Sequencing data chromatograms for PIUV ORF3 mScarlet-fused infectious clone.**

Plasmids purified from a bacterial colony as a result of cloning were sent for sequencing at the Centre for Applied Genomics (TCAG). Panel A shows the sequence map of the infectious clone with its labelled ORFs and features. The sequencing primers for PIUV (21, 22) can be seen on

the map, and the blue arrows demonstrate the forward and reverse sequence results. Panel B demonstrates the chromatograms for the sequences at the junction site ORF3-mScarlet, where the forward sequence demonstrates a perfect match to the reference sequence. Panel C shows that of the mScarlet-PIUV backbone site, with the reverse sequence having good homology to the reference. Quality scores for the sequencing were on average between 30-45, indicating excellent accuracy.

Once positive sequencing results were obtained, the next step was to produce virus stock from the infectious clone. First, the plasmid was linearized using a restriction enzyme, NdeI for PIUV ORF3 mScarlet, and the product purified using a PCR cleanup kit. The linearized plasmid was then used for *in vitro* transcription, which yielded the RNA necessary for subsequent electroporation with C7/10 cells. The electroporated cells were seeded onto a T75 flask and monitored for CPE and fluorescence. The virus stock created from the infectious clone was collected at 24, 48, 72 and 96 hpe, until all cells had died. CPE and fluorescence were first observed at 48 hpe and continued until 96 hpe. The 48 and 72 hpe stocks were used for plaque assays to observe fluorescent plaques and determine titer, as seen below.

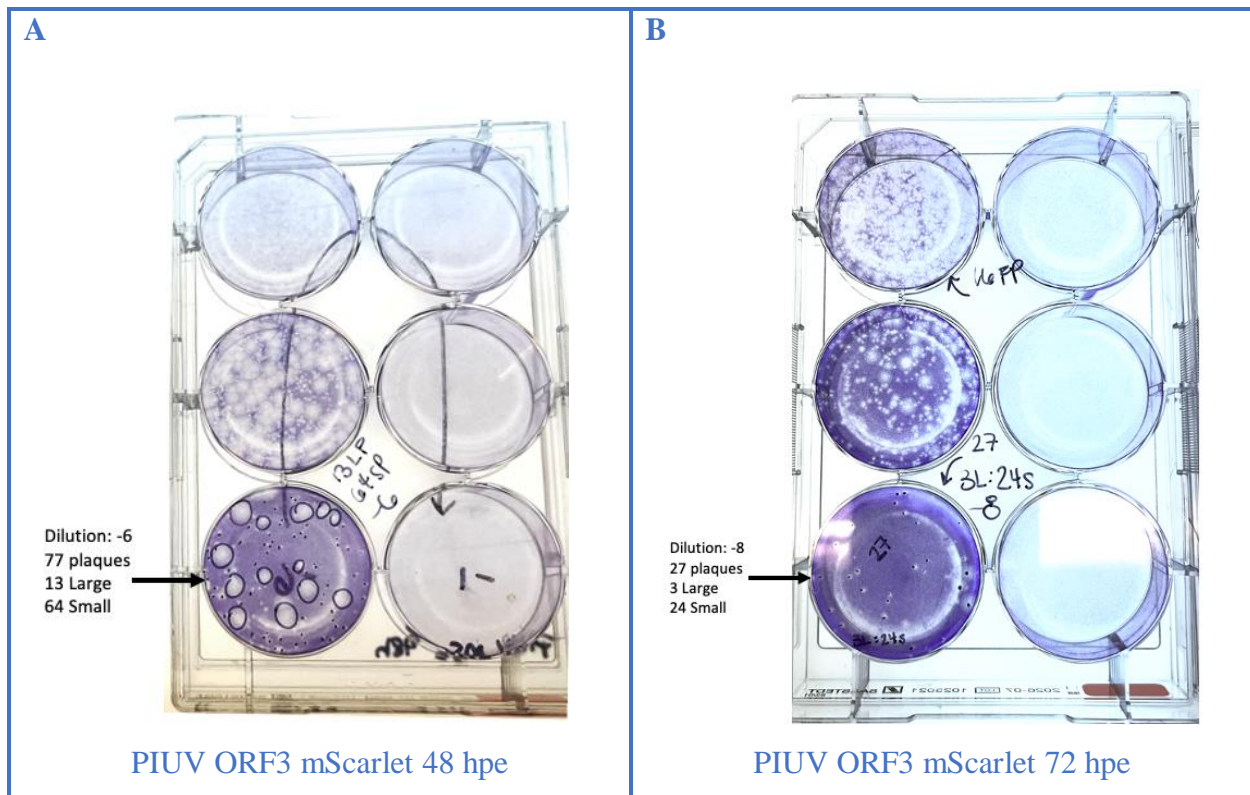


**Figure 8. Plaque assay using C6/36 cells to determine titers of PIUV ORF3 mScarlet stocks.**

Panel A shows plaques formed at the  $10^{-6}$  dilution by PIUV mScarlet 48 hpe, with a total of 77 plaques counted in that well with different morphologies, 13 large and 64 small. At this same dilution, 12 fluorescent plaques were seen. Panel B shows plaques at the  $10^{-8}$  dilution with PIUV ORF3 mScarlet 72 hpe, with a total of 27 plaques, composed of 3 large and 24 small. At the  $10^{-6}$  dilution, 16 fluorescent plaques were seen.

Plaque assays showed two plaque morphologies for PIUV ORF3 mScarlet. For the 48hr stock at the  $10^{-6}$  dilution 77 plaques were counted, of which 13 were large and 64 were small, for the stock collected at 72hr at the  $10^{-8}$  dilution, there was a total of 27 plaques, of which 3 were large and 24 were small. In addition to this, the number of fluorescent plaques observed was not comparable to the total amount of plaques seen, for 48hr only 12 out of 77 plaques were

fluorescent at the  $10^{-6}$  dilution, while for the 72 hr stock 16 fluorescent plaques were counted at the  $10^{-6}$  dilution. Moreover, when a purified and concentrated fraction of this virus was assessed by SDS-PAGE, it resulted in a notable band below the expected product from ORF3 in comparison to the wild-type viruses (Figure 9).

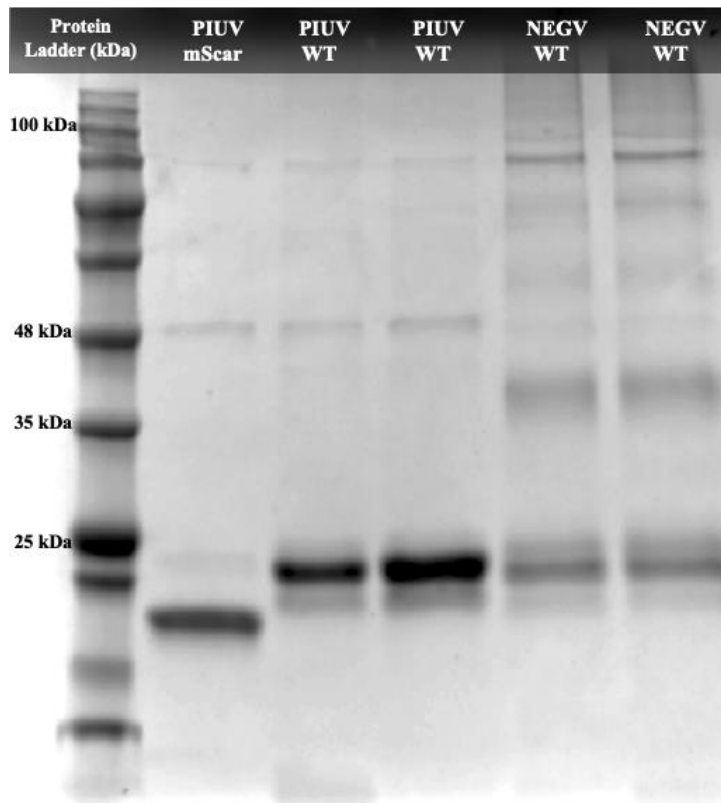


**Figure 9. SDS-PAGE image for purified and concentrated Negevirus.**

Negevirus were isolated using the purification protocol, after which 10  $\mu$ L of concentrated virus sample was ran on a 10% SDS-polyacrylamide gel. All virus samples demonstrate light bands at around 46 kDa, corresponding to the putative glycoprotein encoded from ORF2. It is notable that the sample from PIUV ORF3 mScarlet shows a unique band, different than the wild type viruses, under the expected 22 kDa protein product from ORF3.

The same strategy was used to create PIUV ORF3 ZsGreen and PIUV ORF3 mEmerald (Appendix A). Fewer colonies were seen when transformed with the cloned PIUV ORF3 ZsGreen product. Out of 7 colonies screened, only 1 showed the correct insertion of the reporter through sequencing (Appendix A), this colony was thus used for the production of virus stock. The cells electroporated with the RNA from the *in vitro* transcription of this clone demonstrated CPE similar to that of PIUV wild-type, and stock was collected at 24 and 48 hpe, since no cells remained after 48 hr. Green fluorescence was observed during collection those time points, yet none was observed when infecting cells for plaque assays (appendix B). However, plaques formed with both the 24- and 48-hpe stocks, showing comparable titers to those of the wild-type clones. Titters for PIUV ORF3 ZsGreen 24 and 48 hr was  $1.47 \times 10^{10}$  pfu/mL and  $1.27 \times 10^9$  pfu/mL respectively.

The cloning of mEmerald to ORF3 of PIUV was ineffective. While colonies were present on the selection plates for this modified plasmid, from 5 screened none had 100% sequence homology to the reference junction they were designed to assess, and there were several gaps and mismatches on both the PIUV sequence and the reporter gene. In addition to this, when attempting to collect virus stock from this clone, no CPE or fluorescence was observed, suggesting there was no viable virus infecting the cells.

### ***3.1.2 Cloning of fluorescent reporters into infectious viral clones: NEGV***

The same strategy used for the PIUV modified clones was used to design and construct the following infectious clones: NEGV ORF3 mScarlet and NEGV ORF3 mEmerald (appendix A). NEGV infectious clones carried an ampicillin resistance gene rather than a kanamycin resistance gene, thus ampicillin was used for selection plates and overnight cultures.

As seen in Figure 10, the amount of fragment recovered from the Q5 PCR for the NEG V clones was much lower than that for PIUV. After extracting the bands from the gel and running the extraction and purification kit, the concentration of DNA was often below 2 ng/ $\mu$ L. In comparison, when recovering PIUV fragments the concentration varied from 260-380 ng/ $\mu$ L per reaction.

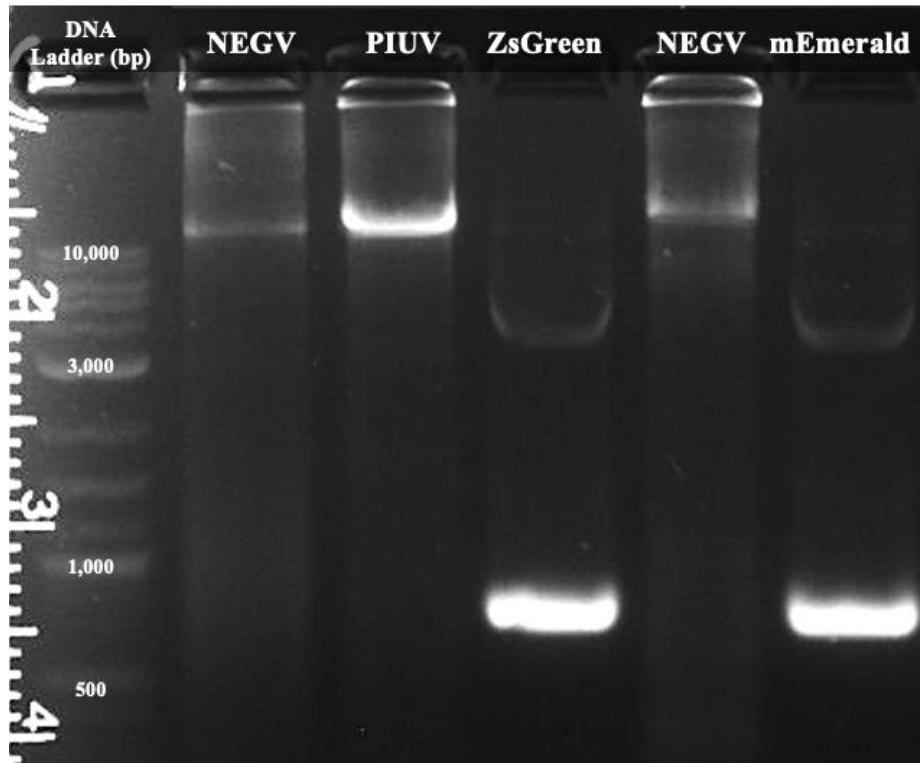


**Figure 10. Gel image for PCR products for cloning reporter genes into infectious clones.**

The products were run on a 1% agarose gel with SYBR Safe at 90 V for 45 min in TBE buffer. The DNA bands were individually excised using a razor and used for a gel extraction kit. There is a clear difference in intensity between the NEG V and PIUV fragments, indicating more DNA yield in the PIUV sample. There are 2 NEG V lanes that correspond to separate PCR amplification reactions. ZsGreen and mEmerald lanes are shown at approximately 750 bp, these were excised and used for subsequent NEB assembly reactions.

Whilst the concentration of NEGV product recovered was low, a sample with a concentration of 65 ng/μL was achieved by combining 2-3 fragment products from replicates. Using this new “stock” of NEGV backbone, cloning of mScarlet and mEmerald was attempted. The transformation of the assembled product appeared to be successful, since some colonies were present on the ampicillin selection plates, suggesting they had taken up the plasmid. However, from 5 colonies tested for NEGV ORF3 mScarlet and 3 screened for NEGV ORF3 mEmerald, none had positive sequencing results, as seen in Figure 11.

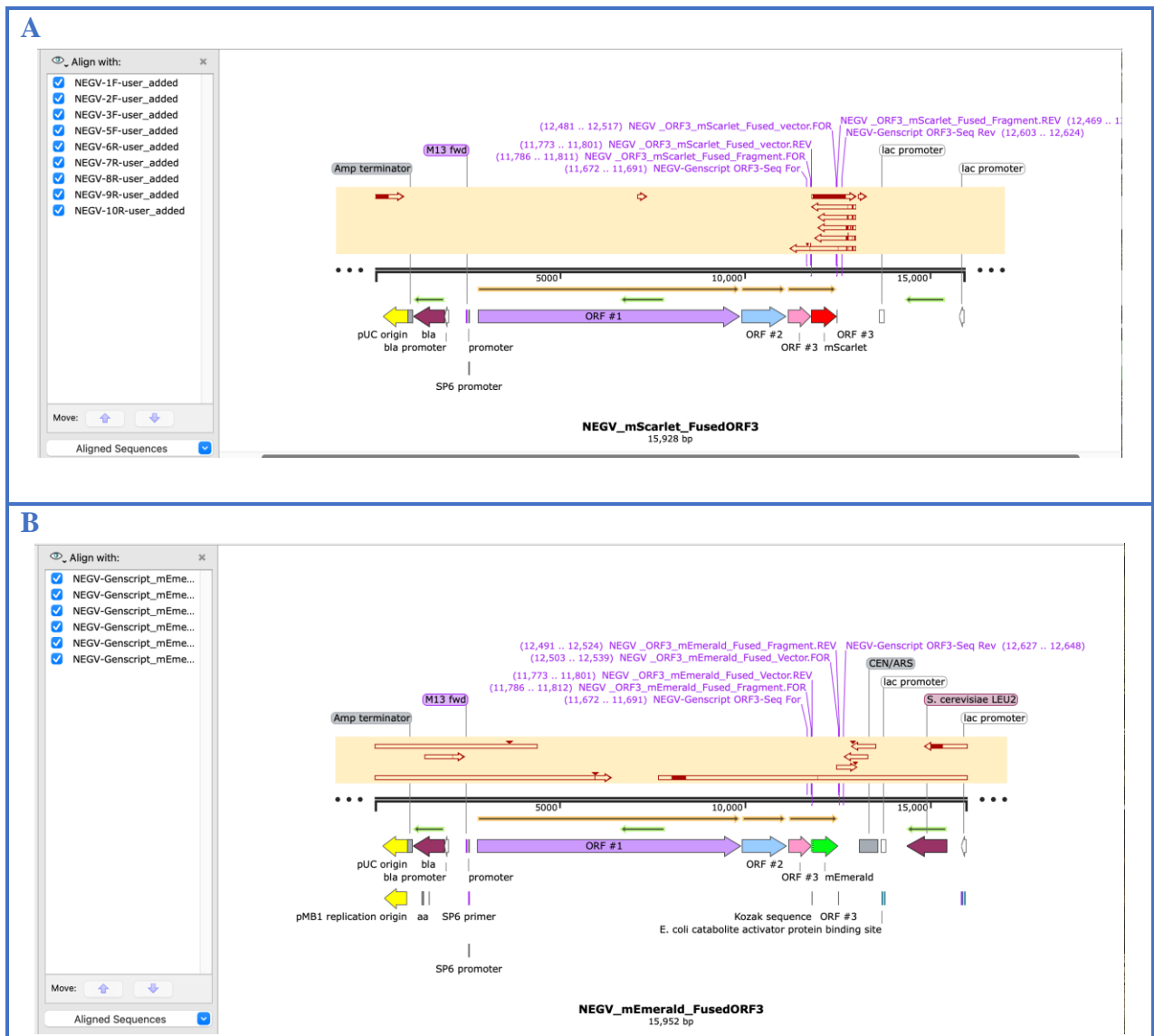
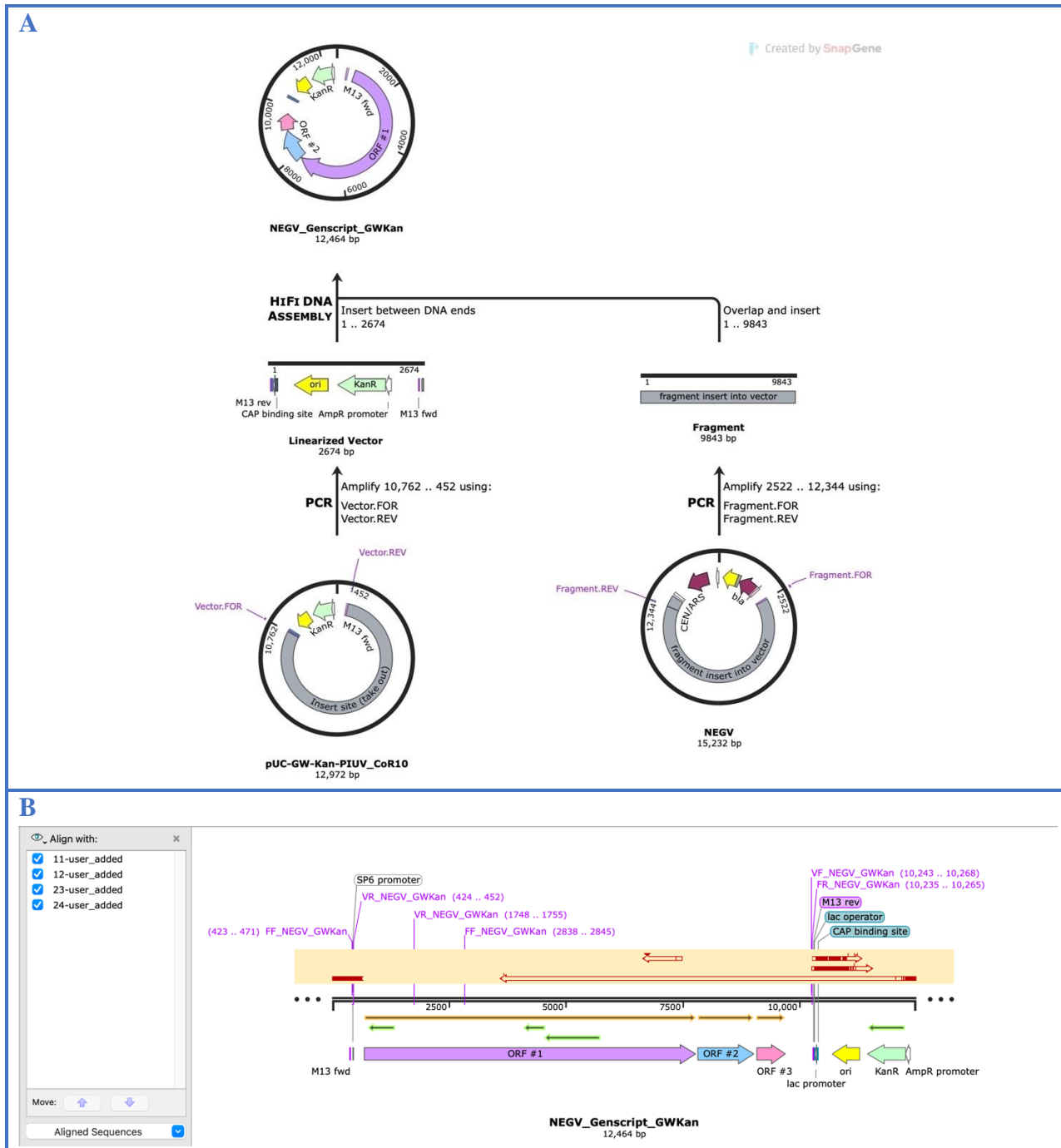


Figure 11. Sequencing results for NEGV modified infectious clones.

Panel A demonstrates the sequencing results for NEG V ORF3 mScarlet, while panel B shows the sequencing results for NEG V ORF3 mEmerald. The red segments of the arrows show portions of the experimental sequence that align with the reference plasmid sequence. In both panels there is a lack of alignment to neither the reference nor reporter gene.

A backbone switch experiment was carried out in an effort to reduce the plasmid size for NEG V (Figure 12). This was done through a separate NEB assembly reaction, similar to the protocol used for the fluorescent reporter. As demonstrated below, the NEG V virus sequence and the pUC vector with a kanamycin resistance gene within the PIUV infectious clone were amplified. Using the overhanging sequence created by the primers used, both fragments were annealed to produce a new NEG V clone with kanamycin resistance and having a total size of 12,464 bp. The plasmid product was transformed into bacterial cells and plated on LB plates containing kanamycin. From 4 plates, only 2 small colonies grew, and both were sent for confirmation via sequencing. Unfortunately, the sequencing results were not satisfactory, demonstrating several mismatches and gaps on both the forward and reverse reads. It was apparent that the lac promoter/operator and the origin of replication were cloned in correctly, but the kanamycin resistance gene sequence had several insertions and deletions. Thus, no infectious clone was recovered from this process.

To continue with the stated project goals, a NEG V ORF3 GFP clone that was synthesized previously by Dr. Patterson was used for the comparison of performance to the newly generated PIUV ORF3 mScarlet clone.



**Figure 12. NEGV clone backbone switch experiment scheme and sequencing results.**

The SnapGene software was used to simulate and design the construction of a kanamycin resistant version of the NEGV infectious clone. Panel A shows the simulation cloning scheme used to assemble the product. Panel B shows the sequencing results from the colonies tested.

### 3.2 Plaque assay results for all virus stocks

Following the recovery of virus stock from infectious clones (WT) and lyophilized viruses (UTMB), plaque assays were conducted to determine titer. C6/36 cells were used for plaque assays of all viruses, with an incubation period of 48 hr. Table 11 summarizes the titers determined for each virus species. Raw data for these results can be found in appendix section B.

**Table 11. Negevirus titers (PFU/mL) determined by plaque assay.**

Virus Stock Name	PFU/mL	Fluorescent PFU/mL
PIUV WT 24 hpe	$6.67 \times 10^9$	N/A
PIUV UTMB 24 hpe	$1.3 \times 10^{10}$	N/A
PIUV ORF3 mScarlet 72 hpe	$1.8 \times 10^{10}$	$1.1 \times 10^8$
PIUV ORF3 mScarlet 48 hpe	$5.13 \times 10^8$	$8.0 \times 10^7$
PIUV ORF3 ZsGreen 24 hpe	$1.5 \times 10^{10}$	0
NEGV WT 24 hpe	$6.0 \times 10^9$	N/A
NEGV UTMB 24 hpe	$1.3 \times 10^9$	N/A
LORETO WT 24 hpe	$5.3 \times 10^8$	N/A
NEGV ORF3 GFP 24 hpe	$8.0 \times 10^7$	$2.7 \times 10^6$
NEGV ORF3 GFP 48 hpe	$1.8 \times 10^8$	$1.2 \times 10^8$

## Chapter 4 – Growth Curve Results

### *4.1 Virus growth curves in C7/10 cells using RT-qPCR*

Growth curves for virus stocks produced from infectious clones and lyophilized viruses were quantified using RT-qPCR. The standard curves were generated using the wild-type infectious clone for NEGV and PIUV, since there was a known starting quantity (Sq). Using these standard curves, the Sq values from the experimental samples were converted into genome copy numbers.

Analysis of the genome copy values was carried out using one-way ANOVA. Results showed that there was no significant difference between the genome copy numbers from the wild-type NEGV and PIUV infectious clones at all time points, which can be seen in panel A of Figure 13. Three NEGV isolates were also compared: the infectious clone wild-type (NEGV WT), the field-derived wild-type (NEGV UTMB), and the modified clone with GFP attached to ORF3 (NEGV ORF3 GFP). As observed in panel B, there was no significant difference between the three viruses at 2, 6, 24, and 48 hr. A similar growth trend was observed for the PIUV isolates tested: the infectious clone wild-type (PIUV WT), the UTMB wild-type (PIUV UTMB), and the modified clone with mScarlet attached to ORF3 (PIUV ORF3 mScarlet). No significant differences were observed amongst these 3 viruses at 2, 6, and 24 hpi. PIUV WT and PIUV UTMB showed a significant difference at 48 hpi, but PIUV ORF3 mScarlet was not statistically different than either wild-type virus at 48 hpi. The trend can be observed in panel C of Figure 13. Additionally, a comparison between the reporter and the virus sequence in both modified clones showed no significant differences, suggesting the virus and reporter were present in similar quantities.

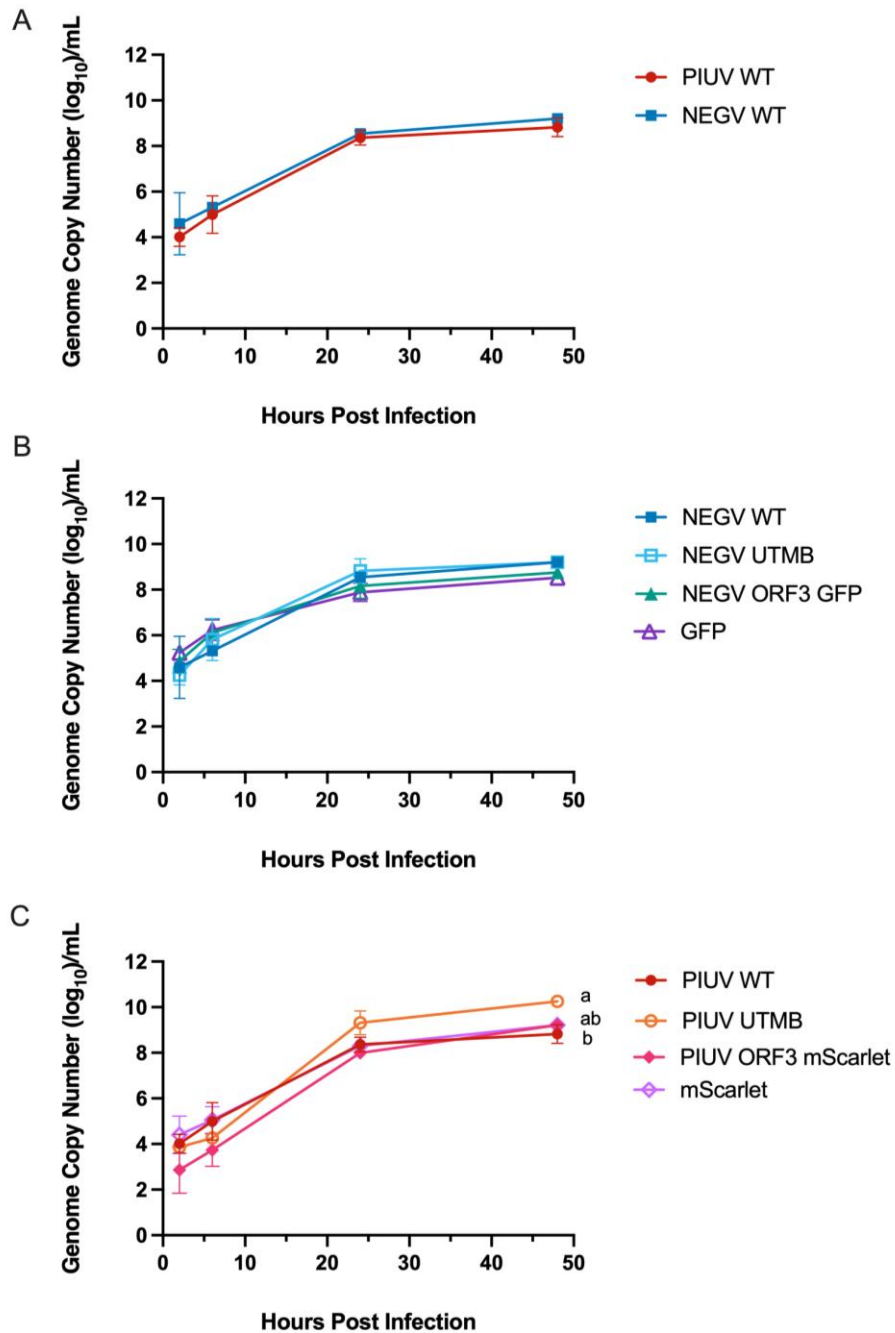


**Figure 13. Growth curves of Negevirus by genome copy number in C7/10 cells.**

Panel A shows the growth curves of the wild-type NEG V and PIUV generated from infectious clones. Panel B shows the growth curves of NEG V WT, NEG V UTMB and NEG V ORF3 GFP. Panel C displays the growth trend of PIUV WT, PIUV UTMB and PIUV ORF3 mScarlet. All

isolates were inoculated at an MOI of 1. Points represent the means from  $n=3$ ,  $\pm$  SD. Letters indicate significant differences at  $P<0.0001$ .

#### 4.1.1 Plaque assays for growth curves samples using C7/10 cells

As a way to further confirm the growth curve results, end-point plaque assays were performed using the 48 hpi sample collected from the growth curve experiments. Figure 14 shows the titers calculated from the experiment in C7/10 cells. A one-way ANOVA was used to evaluate variances between viruses, and unpaired t-tests were used to analyze the differences between fluorescent and regular plaques for PIUV ORF3 mScarlet and NEGV ORF3 GFP. Table 12 summarizes the results from this analysis.

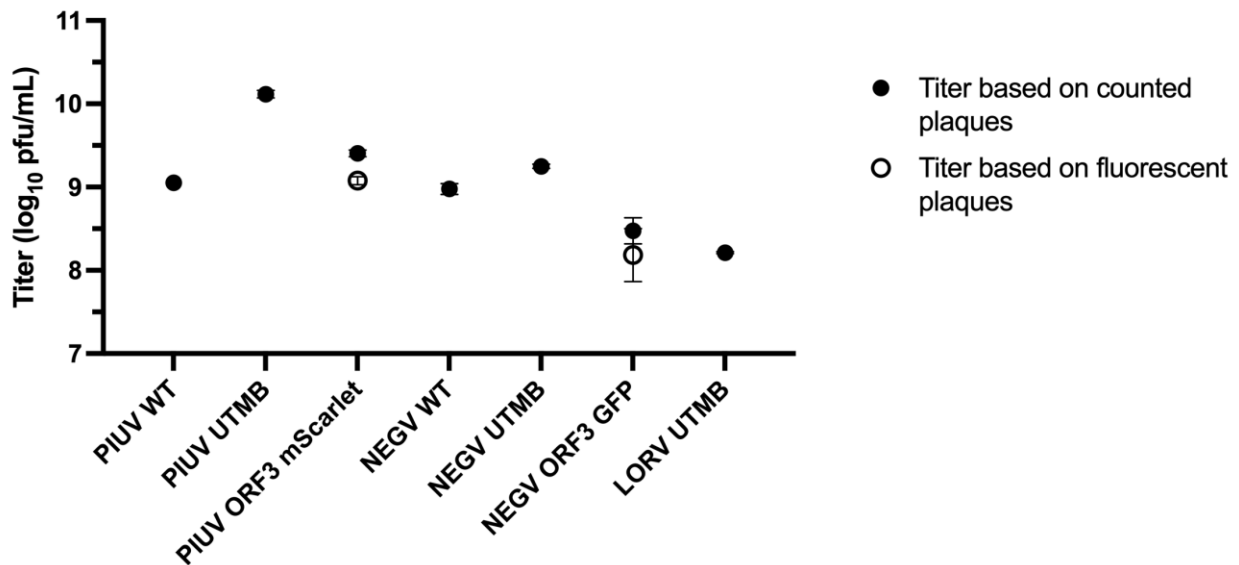


**Figure 14. Titers for Negevirus using C7/10 cells for the 48hpi sample of growth curves.**

The graph shows the titer calculated for each virus stock, as well as the fluorescent titer calculated for PIUV ORF3 mScarlet and NEGV ORF3 GFP. Error bars represent the standard deviation (SD) from the mean of biological replicates ( $n=3$ ).

**Table 12. Statistical results for Negevirus plaque assays at 48hpi in C7/10 cells.**

The pairs mentioned below are those that had statistically significant differences at  $P < 0.0001$ .

Virus #1		Virus #2
PIUV UTMB	vs	PIUV WT PIUV ORF3 mScarlet NEGV WT NEGV UTMB NEGV ORF3 GFP
PIUV ORF3 mScarlet	vs	NEGV WT NEGV ORF3 GFP PIUV UTMB mScarlet Fluorescent Plaques
NEGV ORF3 GFP	vs	NEGV UTMB NEGV WT PIUV WT PIUV UTMB
LORV UTMB	vs	NEGV UTMB NEGV WT PIUV WT PIUV UTMB PIUV ORF3 mScarlet

The statistical analysis revealed significant differences among the studied viruses, with notable variations observed for PIUV UTMB, LORV UTMB, and both modified viruses. Specifically, PIUV UTMB exhibited a higher average number of plaque-forming units at 48 hpi than its infectious clone counterpart (PIUV WT), both NEGV isolates and modified clones. Similarly, LORV UTMB displayed significantly higher titers compared to all other wild-type isolates and PIUV ORF3 mScarlet. Furthermore, PIUV ORF3 mScarlet demonstrated similar titers to PIUV WT but significantly lower titers compared to PIUV UTMB, NEGV WT, LORV UTMB, and NEGV ORF3 GFP. Interestingly, the titer calculated for fluorescent plaques

containing mScarlet was substantially lower than the overall titer for that virus group. Notably, no significant differences were observed between the wild-type infectious clones.

#### ***4.2 Virus growth curves in Aag2 cells using RT-qPCR***

Growth curves for the same virus stocks tested prior were also carried out in the Aag2 cell line. The same process carried out for the C7/10 experiments were repeated to calculate genome copy numbers using this cell line, including one-way ANOVA to evaluate differences.

Analysis of the Aag2 genome copies yielded contrasting outcomes to the C7/10 growth curve results. Panel A of Figure 15 demonstrates a significant difference in genome copy numbers between wild-type NEG V and PIUV infectious clones at the 24 and 48-hour time points. Moving on to panel B, a significant difference was observed amongst all three NEG V isolates at 2 hpi and between NEG V WT and NEG V ORF3 GFP at 48 hpi. In panel C, which focused on PIUV isolates, no significant differences were found at 2, 6, and 24 hpi among the three viruses. However, at 48 hpi, a significant difference emerged between PIUV WT and PIUV UTMB, while PIUV ORF3 mScarlet displayed no discernible differences in comparison to either wild-type group. As panels B and C indicate, the reporter genes GFP and mScarlet exhibited similar trends to the viruses they were fused to, with no significant differences observed in their quantifications.

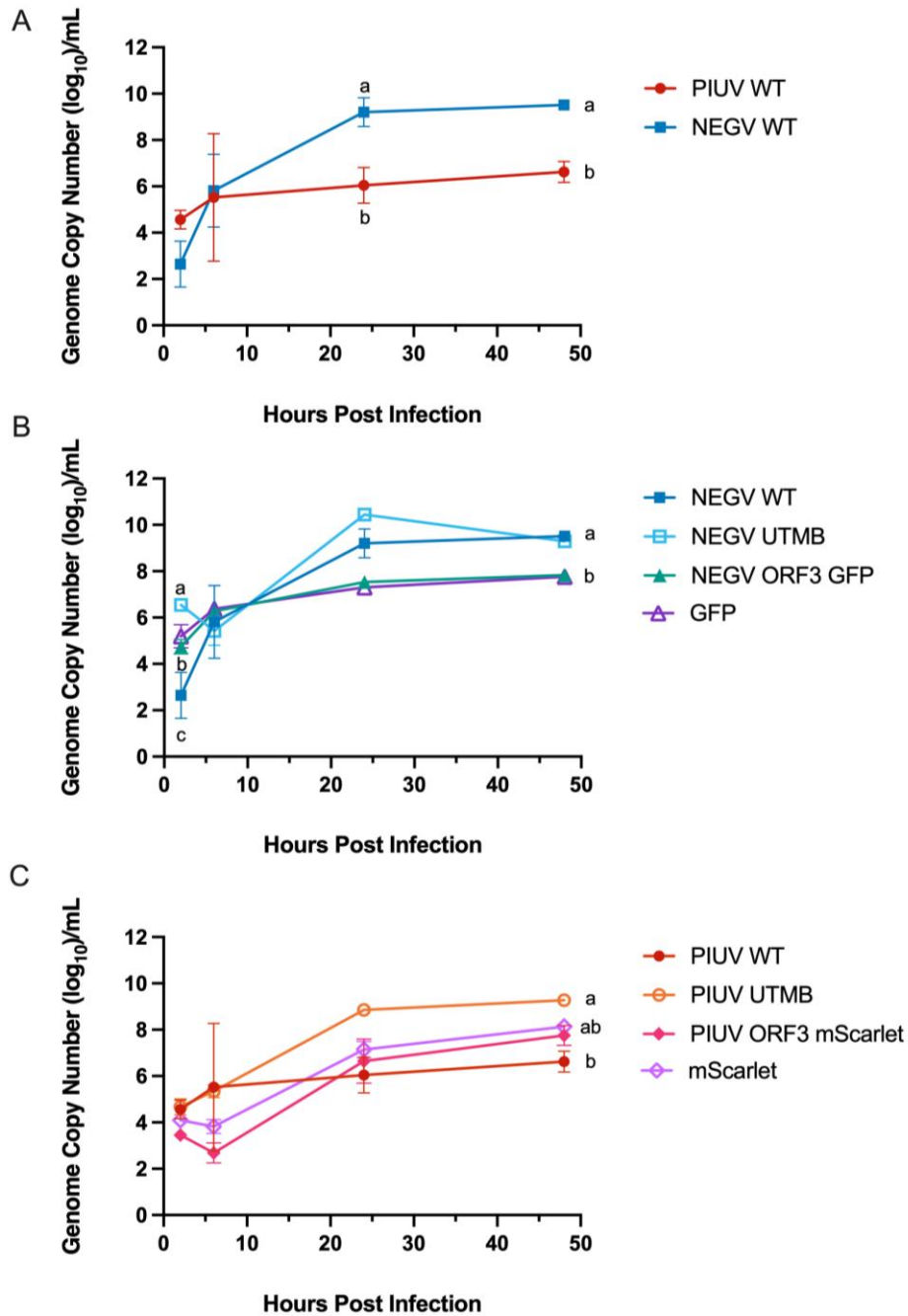


**Figure 15. Growth curves of Negeviruses by genome copy number in Aag2 cells.**

Panel A shows the growth curves of the wild-type NEG V and PIUV generated from infectious clones. Panel B shows the growth curves of NEG V WT, NEG V UTMB, NEG V ORF3 GFP and the curve from GFP as a target. Panel C displays the growth trend of PIUV WT, PIUV UTMB, PIUV ORF3 mScarlet and the curve from the reporter, mScarlet. All isolates were inoculated at

an MOI of 1. Points represent the means from  $n=3$ ,  $\pm$  SD. Letters indicate significant differences at  $P<0.0001$ .

#### 4.2.1 Plaque assays for growth curves samples using Aag2 cells

Plaque assays were performed on Aag2 growth curve samples collected at 48 hpi, these results are shown in Figure 16. Parallel to the analysis carried out prior, a one-way ANOVA was used to evaluate differences between viruses, and t-tests were used to evaluate differences between fluorescent and regular plaques for the modified viruses. Results from those analyses are summarized in Table 13.

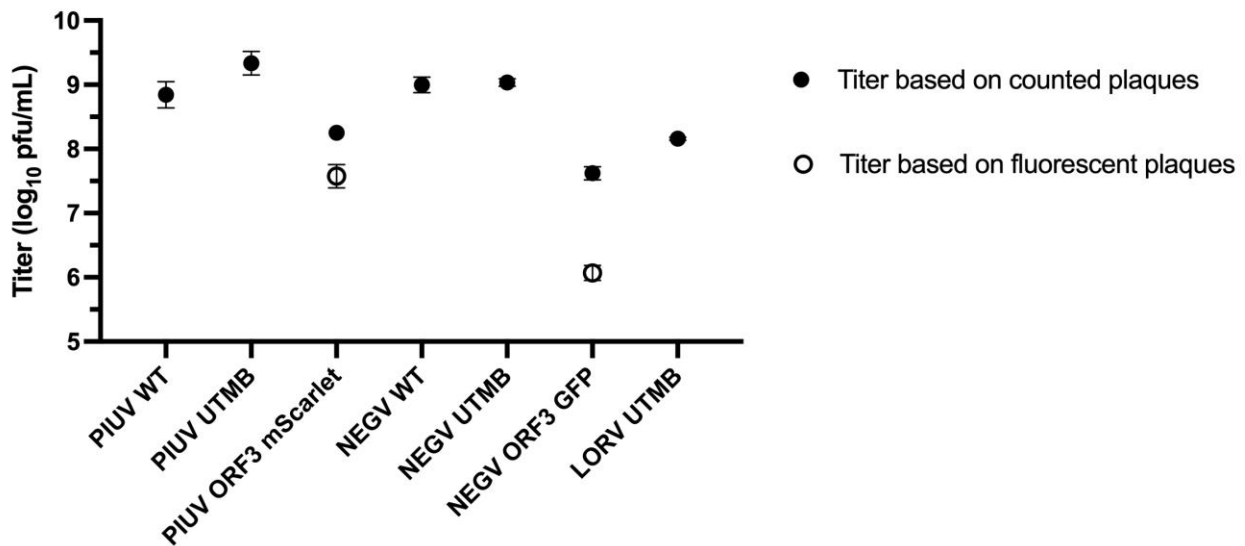


**Figure 16. Titers for Negevirus using Aag2 cells for the 48 hpi sample of growth curves.**

The graph shows the titer calculated for each virus stock, as well as the fluorescent titer calculated for PIUV ORF3 mScarlet and NEG V ORF3 GFP. Error bars represent the SD from the mean of biological replicates ( $n=3$ ).

**Table 13. Statistical results for Negevirus plaque assays at 48 hpi in Aag2 cells.**

The pairs mentioned below are those that had statistically significant differences at  $P < 0.0001$ .

Virus #1		Virus #2
PIUV ORF3 mScarlet	vs	PIUV UTMB NEGV UTMB NEGV WT
NEGV ORF3 GFP	vs	NEGV WT PIUV WT NEGV UTMB PIUV UTMB GFP Fluorescent Plaques
LORV UTMB	vs	PIUV UTMB NEGV WT NEGV UTMB

Similar to the statistical findings obtained from the C7/10 plaque assays, the experiments conducted using the Aag2 cell line revealed intriguing outcomes. Among the viruses studied, those exhibiting the most pronounced variations were PIUV ORF3 mScarlet, NEGV ORF3 GFP, and LORV UTMB. Remarkably, the modified clone containing mScarlet displayed a significantly lower titer than PIUV UTMB, NEGV UTMB, and NEGV WT but exhibited titers comparable to those of PIUV WT. In contrast, NEGV ORF3 GFP demonstrated substantially lower titers than its wild-type counterpart, in addition to NEGV UTMB, PIUV WT, and PIUV UTMB. Notably, the quantification of green fluorescent plaques for this virus was considerably lower than the total number of plaques counted, clearly indicating a statistically significant variance between the virus and the reporter tag. Lastly, LORV UTMB exhibited a significantly higher titer than both field-derived PIUV and NEGV, as well as the infectious clone NEGV.

### 4.3 Genome copy vs titer comparison for single infections

Comparing and relating genome copy numbers calculated through RT-qPCR to the titers determined from plaque assays can provide valuable insights into viral replication and infectivity. Genome copy number reflects the amount of viral genetic material present in a sample, while plaque assay titer represents the number of infectious viral particles capable of forming visible plaques. Both measurements provide different perspectives on viral replication dynamics. Thus, to determine the relationship between viral genome replication and production of infectious viral particles, ratios of genome copy number over titer were calculated. Individual ratios were plotted for the biological replicates of the 7 virus isolates tested, as seen in Figure 17. The average genome copy number to titer ratios for each virus are visually presented on Figure 18, and stated on Table 14.

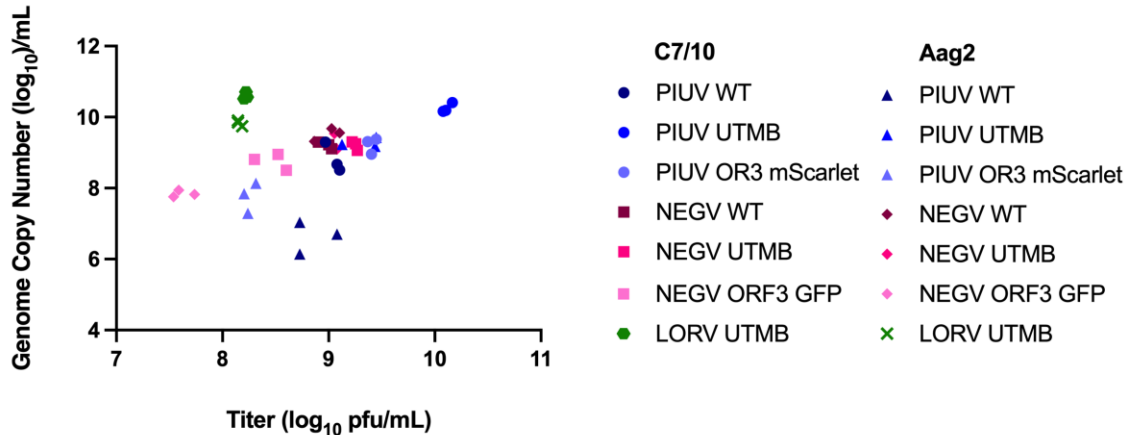


**Figure 17. Plot comparing genome copy numbers/mL vs. pfu/mL of Negeviruses in C7/10 & Aag2 cells.**

Biological replicates (n=3) are plotted for both cell types using their genome copy number (Y-axis) vs plaque titer (X-axis). PIUV sample are in shades of blue, NEGV samples are in shades of red and LORV is depicted in green.

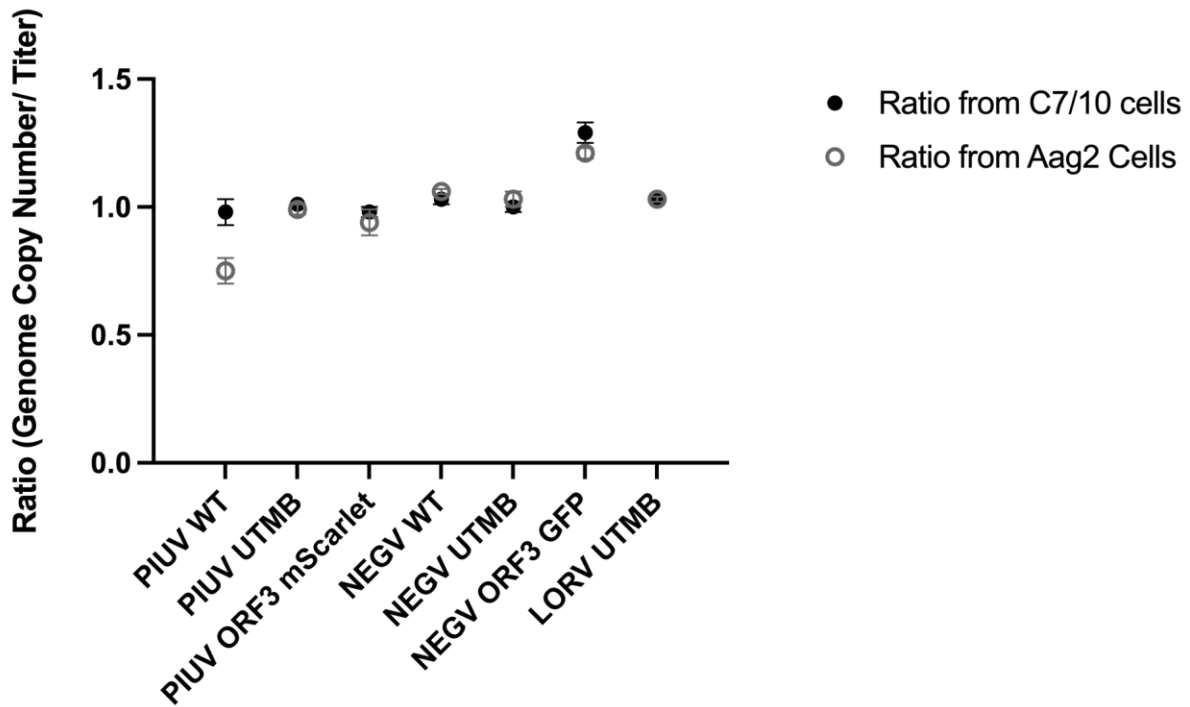


**Figure 18. Plot depicting the ratio of genome copy numbers/mL vs pfu/mL for Negevirus in different cell types.**

The average ratio of biological replicates (n=3) for each virus species is shown above for experiments carried out in C7/10 cells (solid circle) and Aag2 cells (open circle). Error bars represent the  $\pm$  SD. A t-test revealed no statistically significant difference between cell types.

Evaluation of the ratios shows that NEGV WT, NEGV UTMB, PIUV UTMB and LORV UTMB have ratios close to 1 in both cell types, indicating an equal proportion of genome copy number-to-plaque forming units. PIUV WT results from C7/10 cells have a ratio close to 1, yet a lower ratio for the Aag2 cell type, indicating greater amount of plaque forming units to genome copies present in the latter culture. PIUV ORF3 mScarlet demonstrated a similar ratio for both cell types, under 1, suggesting a slightly lower number of genome copies to plaque forming

units. On the other hand, NEG V ORF3 GFP, showed a much higher ratio, implying a higher number of genome copies than infectious particles present.

**Table 14. Average genome copy number vs plaque titer ratio for Negevirus at 48 hpi.**

Biological replicate ratios were averaged ( $n=3$ )  $\pm$  SD for each cell type tested. A t-test revealed no statistically significant difference between cell types.

Virus Name	Cell Type			
	C7/10	SD	Aag2	SD
PIUV WT	0.98	0.05	0.75	0.05
PIUV UTMB	1.01	0.01	0.99	0.02
PIUV ORF3 mScarlet	0.98	0.02	0.94	0.05
NEGV WT	1.03	0.02	1.06	0.01
NEGV UTMB	1.00	0.02	1.03	0.03
NEGV ORF3 GFP	1.29	0.04	1.21	0.02
LORV UTMB	1.03	0.01	1.03	0.01

## Chapter 5 – Co-infection Results

### 5.1 C7/10 cell co-infection results using RT-qPCR

C7/10 cells were infected with previously characterized Negeviruses to investigate co-infections. The results of co-infections were compared to data from single infections as controls, as depicted in Figure 19. To assess significant differences between viral genome copy numbers in single and dual infections, I conducted one-way ANOVAs. A t-tests was employed to evaluate the similarity of genome copy numbers between single infections and co-infections for PIUV ORF3 mScarlet and NEG V ORF3 GFP. The summarized results of these analyses are presented in Table 15.

Statistical analysis revealed that NEG V WT, NEG V UTMB, and NEG V ORF3 GFP exhibited consistent growth curves, regardless of whether they were involved in co-infections with other Negeviruses. PIUV UTMB displayed a consistent growth curve in co-infections at 2, 6, and 24 hpi, compared to its control. However, at 48 hpi, statistically significant differences were observed between PIUV UTMB in a single infection and its co-infections with NEG V WT and LORV UTMB. Similarly, LORV UTMB exhibited no differences at 2, 6, and 24 hpi, but displayed significant variations from its control when co-infected with NEG V UTMB at 48 hpi. PIUV WT exhibited differences in its replication curve compared to single infection at 24 and 48 hpi in co-infections with NEG V WT, as well as with NEG V UTMB at 48 hpi. Furthermore, PIUV ORF3 mScarlet demonstrated significant differences from its control at 24 hpi when co-infected with the NEG V mutant clone.

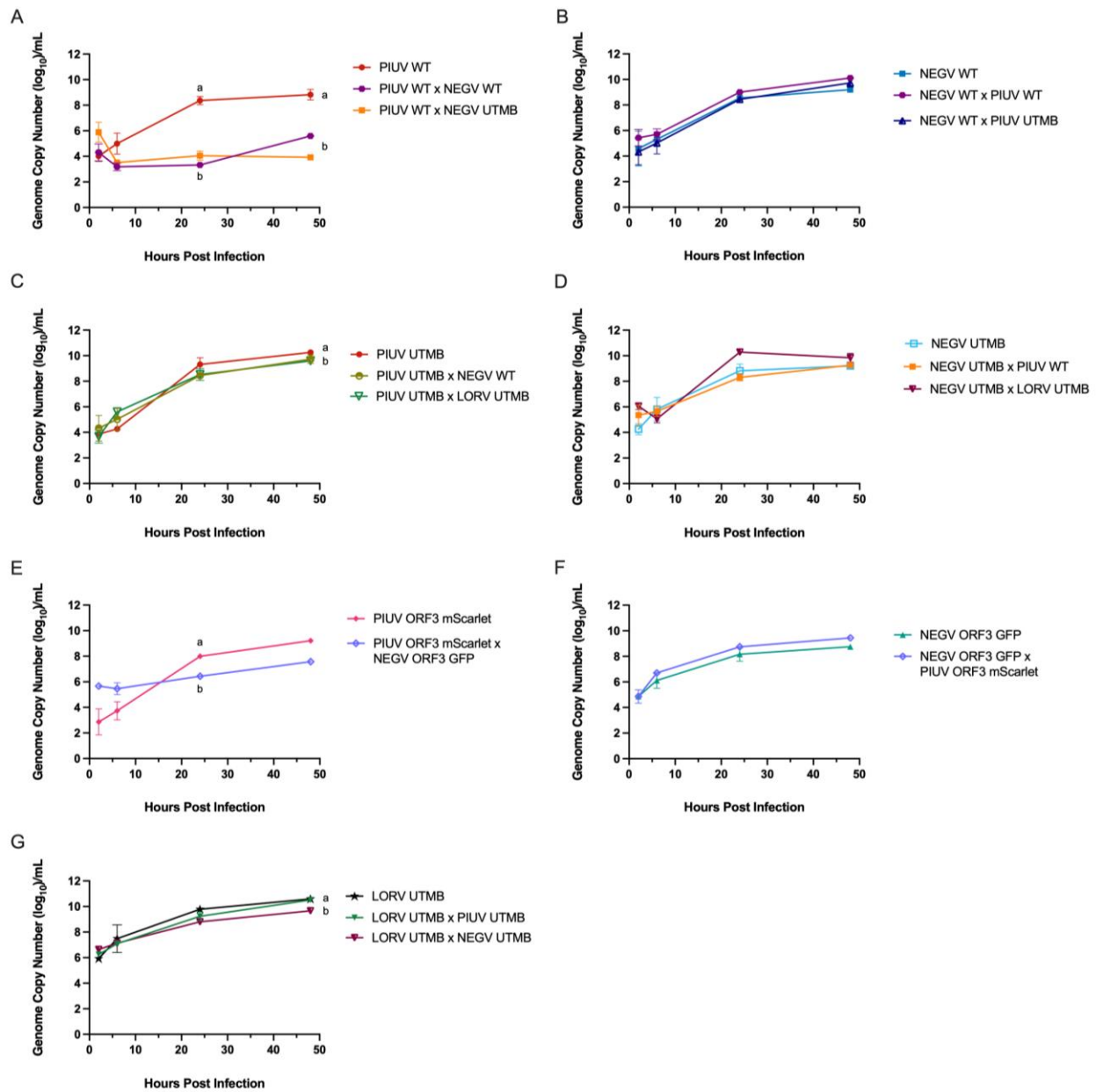


**Figure 19. Co-infection growth curves of Negevirus by genome copy number in C7/10 cells.**

Panels A to G show the growth curves of Negevirus at 2, 6, 24 and 48 hpi during co-infections in C7/10 cells. Each panel shows a single target control curve and the co-infection pairs evaluated: PIUV WT (A), NEGV WT (B), PIUV UTMB (C), NEGV UTMB (D), PIUV ORF3 mScarlet (E), NEGV ORF3 GFP (F), and LORV UTMB (G). Negevirus were inoculated at an

MOI of 1 for all conditions. All points represent means from n=3, and error bars represent SD. Letters indicate significant differences (P<0.0001).

**Table 15. Statistical results for Negevirus during co-infections in C7/10 cells.**

The control virus used, and its co-infection pair are mentioned below if statistically significant differences are notable at P < 0.0001 for each time point.

Virus Control		Co-infection pair and time point
PIUV WT	vs	PIUV WT x NEGV WT 24 hpi PIUV WT x NEGV UTMB 24 hpi PIUV WT x NEGV WT 48 hpi PIUV WT x NEGV UTMB 48 hpi
PIUV UTMB	vs	PIUV UTMB x NEGV WT 48 hpi
LORV UTMB	vs	LORV UTMB x NEGV UTMB 48 hpi
PIUV ORF3 mScarlet	vs	PIUV ORF3 mScarlet x NEGV ORF3 GFP 24 hpi

### **5.2 Aag2 cell co-infection results using RT-qPCR**

In order to delve deeper into co-infections involving Negevirus, I employed an immune-competent cell line, Aag2, for our experimental investigations. I performed co-infections using the same pairs of viruses mentioned earlier with this culture, and the outcomes of these experiments are visually presented in Figure 20. Additionally, a concise summary of the statistical differences between them is observed in Table 16 below.

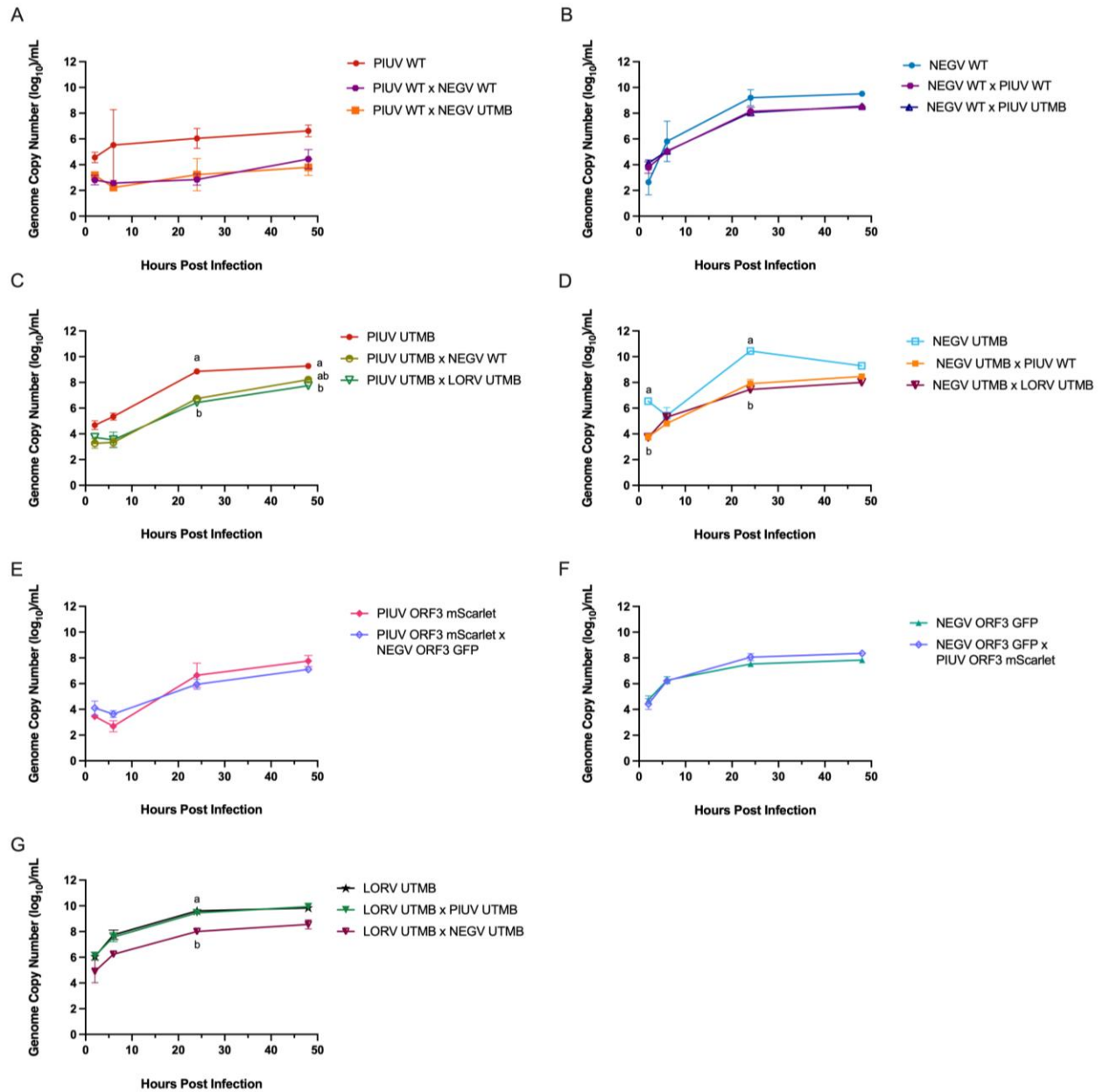


**Figure 20. Co-infection growth curves of Negevirus by genome copy number in Aag2 cells.**

Panels A to G show the growth curves of Negevirus when inoculated on cells at 2, 6, 24 and 48 hpi during co-infections. Each panel shows a single target control curve and the co-infection pairs evaluated: PIUV WT (A), NEG V WT (B), PIUV UTMB (C), NEG V UTMB (D), PIUV ORF3 mScarlet (E), NEG V ORF3 GFP (F), and LORV UTMB (G). Negevirus were

inoculated at an MOI of 1 for all conditions. All points represent means from n=3, and error bars represent SD. Letters indicate significant differences (P<0.0001).

**Table 16. Statistical results for Negevirus during co-infections in Aag2 cells.**

The control virus used, and its co-infection pair are mentioned below if statistically significant differences arise at P < 0.0001 for each time point.

Virus Control		Co-infection pair and time point
NEG V UTMB	vs	NEG V UTMB x PIUV WT 2 hpi NEG V UTMB x LOR V UTMB 2 hpi NEG V UTMB x PIUV WT 24 hpi NEG V UTMB x LOR V UTMB 24 hpi
PIUV UTMB	vs	PIUV UTMB x NEG V WT 24 hpi PIUV UTMB x LOR V UTMB 24 hpi PIUV UTMB vs LOR V UTMB 48 hpi
LOR V UTMB	vs	LOR V UTMB x NEG V UTMB 24 hpi

Statistical analysis revealed that PIUV WT, NEG V WT, PIUV ORF3 mScarlet, and NEG V ORF3 GFP had insignificant variations from its growth curve during single infections when in co-infections with other Negevirus. On the contrary, PIUV UTMB showed significant differences between its single infection in Aag2 cells and its dual infection with NEG V WT at 24 hpi and LOR V UTMB at 24 and 48 hpi (Figure 20, Panel C). NEG V UTMB had a growth trend consistent with its control at 6 and 48 hpi but showed variances at 2 and 24 hpi during co-infections with LOR V UTMB and PIUV WT. LOR V UTMB only showed deviation from its single infection trend at 24 hpi when co-infected with NEG V UTMB (Figure 20, Panel G).

### ***5.3 Co-infection plaque assay: NEGV ORF3 GFP X PIUV ORF3 mScarlet***

Plaque assays were performed to assess the interactions between the two modified viruses, NEGV ORF3 GFP and PIUV ORF3 mScarlet. The total and fluorescent titers calculated from the co-infection of NEGV ORF3 GFP and PIUV ORF3 mScarlet in both cell types are displayed in Table 17. To examine these results, the ratio of fluorescent plaques to the total counted plaques was calculated since this can give insights into the stability of the reporter in an infectious clone.

The co-infection between PIUV ORF3 mScarlet and NEGV ORF3 GFP in C7/10 cells demonstrated a lower number of red fluorescent plaques than green plaques, corresponding to mScarlet and GFP, respectively. This phenomenon can be clearly seen in Figure 21, as there is a great number of plaques fluorescing green than red at the same dilution.

In Aag2 cells, the trend is similar, since green fluorescence far outweighs red fluorescence, having a much lower fluorescent to total plaque ratio for red plaques. This can be observed in Figure 22, which shows the large discrepancy between plaques fluorescing red and green during this co-infection at 48 hpi. A t-test was carried out to assess the differences in ratios between the cell types used. Results from this analysis showed a significant difference in the ratio of green fluorescent plaques to total titer between C7/10 and Aag2 cells.

**Table 17. Titers resulting from the co-infection of NEGV ORF3 GFP and PIUV ORF3 mScarlet at 48 hpi.**

Titers represent means from biological replicates (n=3) with  $\pm$  SD.

<b>Condition</b>	<b>Cell Type</b>	<b>Total Titer</b>	<b>Fluorescent Titer</b>	<b>Ratio Total Titer/Fluorescent Titer</b>
Total Stained Plaques		$1.84 \times 10^8 \pm 3.67 \times 10^7$	-	-
Red Plaques	C7/10	-	$6.22 \times 10^5 \pm 1.68 \times 10^5$	296:1
Green Plaques		-	$1.58 \times 10^8 \pm 2.04 \times 10^7$	1:1
Combined		$1.84 \times 10^8$	$1.58 \times 10^8$	14% non-fluorescent
Total Stained Plaques		$2.0 \times 10^7 \pm 9.08 \times 10^6$	-	-
Red Plaques	Aag2	-	$5.1 \times 10^5 \pm 1.39 \times 10^5$	40:1
Green Plaques		-	$2.3 \times 10^6 \pm 3.01 \times 10^5$	9:1
Combined		$2.0 \times 10^7$	$2.8 \times 10^6$	86% non-fluorescent

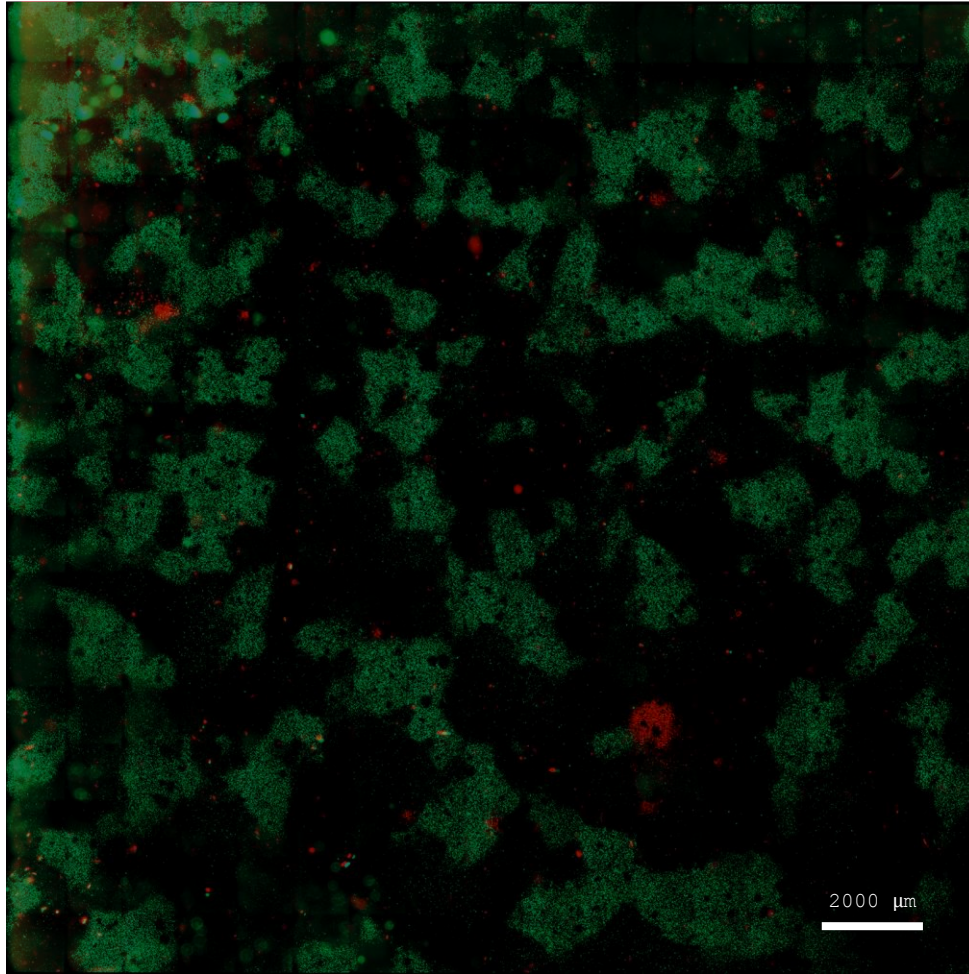


**Figure 21. Fluorescent plaques formed from co-infection with NEGV ORF3 GFP and PIUV ORF3 mScarlet in C7/10 cells at 48hpi.**

The figure shows the entire well (2 cm x 2 cm, 17 x 17 tiles) from the  $10^{-4}$  dilution of a plaque assay from a co-infection with modified Negevirus. The merged image shows fluorescent plaques formed by PIUV ORF3 mScarlet and NEGV ORF3 GFP at 48hpi. A greater number of green plaques produced than red plaques are depicted at this dilution.

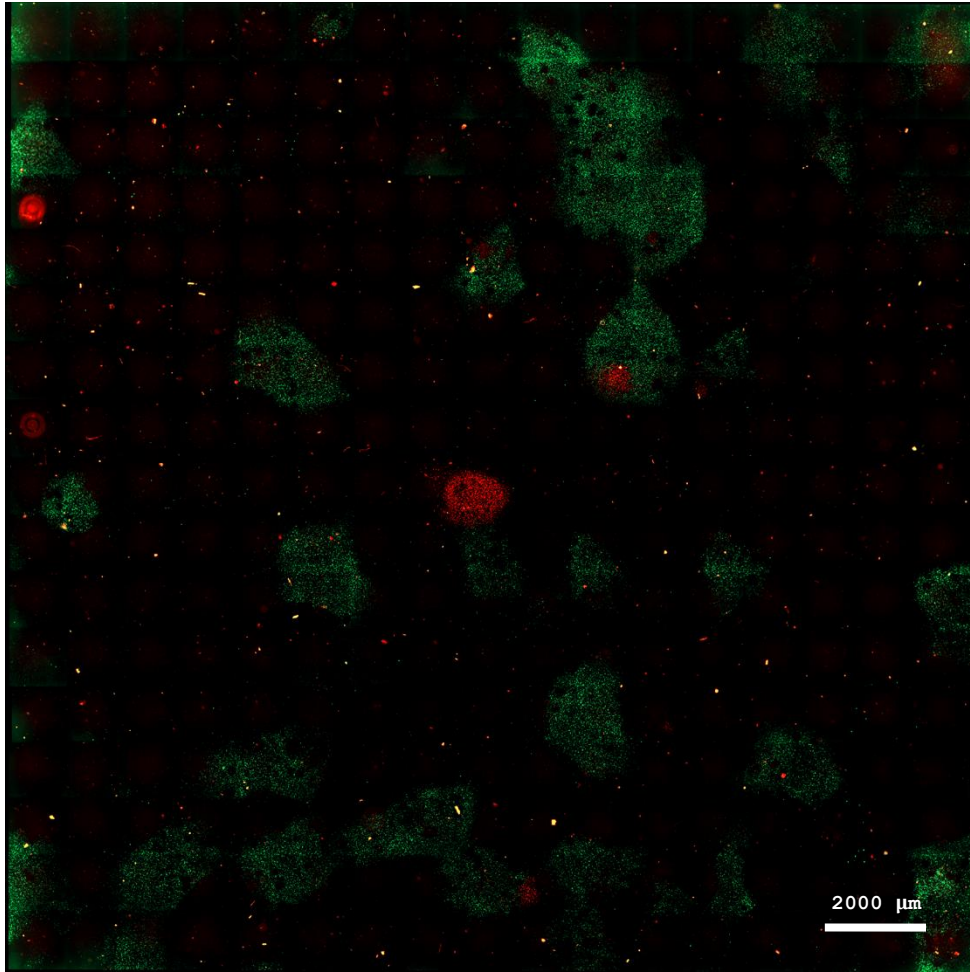


**Figure 22. Fluorescent plaques formed from co-infection with NEG V ORF3 GFP and PIUV ORF3 mScarlet in Aag2 cells at 48hpi.**

Figure shows the entire well (2 cm x 2 cm, 17 x 17 tiles) from the  $10^{-4}$  dilution of a plaque assay from a co-infection with modified Negevirus at 48hpi. A greater number of green plaques from NEG V ORF3 GFP are observed in comparison to red plaques produced by PIUV ORF3 mScarlet.

## Chapter 6 – Discussion

### *Part I – Cloning Experiments*

The results of the cloning experiments differed depending on the Negevirus species. I achieved successful cloning of mScarlet into the third open reading frame of PIUV; however, concerns arose regarding the stability of the insert within the genome. Remarkably, two distinct plaque morphologies were observed when quantifying PIUV ORF3 mScarlet plaques. Furthermore, the number of fluorescent plaques observed did not correspond to the total plaque count after staining. These findings collectively suggest the presence of different PIUV isolates within the same stock, resulting in different plaque morphologies and variations in fluorescence. Substantiating this observation, the purified virus fraction subjected to protein gel electrophoresis (Figure 9) yielded a smaller product than anticipated for the virus membrane protein. This discrepancy implies that the fusion of mScarlet to ORF3 may have caused alterations in the final protein product. I postulate that the reporter construct may not exhibit stability within the genome, potentially leading to the introduction of mutations or stop codons to prevent its expression. This phenomenon could elucidate the discrepancy between the lower number of observed fluorescent plaques and the total plaque count.

These results are similar to previous studies that compared the stability of marker genes in viral genomes. For example, Tamberg et al. (2007) successfully achieved stable propagation of EGFP-expressing Semliki Forest virus (SFV) by strategically inserting EGFP between nsP3 and nsP4 (48). Prior attempts to insert EGFP after amino acid position 452 of SFV nsP3 had resulted in the production of an unstable virus, since a truncated form of the fusion protein was found, even when cells were directly transfected with RNA (48). Likewise, Pierson et al (2005) constructed a WNV reporter virus with GFP and found that the reporter was unstable in the viral

genome since there was a loss of GFP expression over time (49). This decline was attributed to deletions or point mutations before the reporter sequence, a conclusion supported by the observation of truncated variants of the reporter virus (49). It could be possible that the positioning of mScarlet on the PIUV or the occurrence of mutations/deletions could lead the virus to shed the reporter and create truncated variations in order to be more efficient. There could also be a limit to how flexible the viral genome is to insertions, which could explain the reporter loss. Although there was some instability, only 1 passage with a 2-step growth curve (MOI=1, does not guarantee all cells will become infected) was studied in this paper. Thus, to ascertain the stability of the reporter, additional investigations involving viral passaging are imperative for drawing definitive conclusions.

During attempts to clone ZsGreen and mEmerald into the PIUV genome, additional challenges were encountered. Despite obtaining sequencing results with satisfactory overall quality scores and confirming the accurate insertion of the reporter in PIUV ORF3 ZsGreen, no detectable fluorescence was observed upon infecting cells for plaque assays. Although plaques did form, the underlying reasons for the lack of fluorescence remain poorly understood.

Hurdles encountered during the cloning process for PIUV species were different than those encountered for NEGV. Diligent efforts were made to accurately insert fluorescent reporters into the NEGV genome, yet several challenges impeded successful cloning. Amplification of the NEGV virus backbone posed significant difficulties, resulting in PCR products with a DNA concentration of less than 2 ng/ $\mu$ L per reaction. To circumvent this issue, multiple replicates of the reactions were combined, resulting in a sample concentration of 65 ng/ $\mu$ L, which remained considerably lower than the recovered PIUV concentrations. The recommended minimal vector concentration for the NEB reaction was 0.03 pmol, equivalent to

297 ng of DNA for a vector length of 15,000 bp. Regrettably, this concentration could not be achieved, potentially explaining the lack of successful cloning.

I hypothesized that the discrepancy in size between the PIUV and NEG V clones contributed to the lower DNA yield during the amplification step. The PIUV infectious clone, excluding the PIUV sequence, possessed a backbone of approximately 2,700 bp, whereas the NEG V clone had a backbone of approximately 5,000 bp. This difference of over 2,000 bp was deemed responsible for the reduced yield observed in the NEG V clone. Moreover, the reactions employed Q5 polymerase, and although the supplier states this polymerase is designed for template lengths up to 20 kb for "simple" templates or 10 kb for "complex" templates, a substantial discrepancy was noticed when amplifying a 12 kb fragment compared to a 15 kb fragment. To address this challenge, one potential solution would involve replacing the conventional PCR with a circular polymerase extension reaction (CPE R) cloning method.

The CPE R cloning method is based on the extension of overlapping regions between vector and insert fragments to construct a circular plasmid (50, 51). In contrast, traditional PCR utilizes primers targeting specific flanking regions of the target sequence, resulting in linear amplification products. To minimize errors during amplification, a high-fidelity polymerase suitable for long sequence generation is required, as the amplification process can accumulate or propagate errors (50). Multi-cycle CPE R cloning technology offers broad utility and advantages over regular PCR by enabling the seamless joining of multiple DNA fragments with overlapping ends. This method demonstrates high efficiency and fidelity since it does not involve amplification. The fragments utilized in this method are typically shorter in length, and their annealing through overlapping overhangs minimizes the generation of unwanted errors or mutations (50, 51). Conveniently, this method has been successfully employed for constructing

large viruses. In 2021, Amarilla *et al.* utilized CPER technology for the construction of SARS-CoV-2 and Casuarina virus, demonstrating its potential as a reverse genetics platform for viruses with large, complex genomes containing polyA tails (51).

Overall, the results indicate challenges in amplifying the complete NEGV infectious clone due to various reasons. However, alternate methods employing advanced amplification technology can be considered replacements for the cloning protocols employed in this research.

## ***Part II – Single & Co-infection Experiments***

Clear differences can be observed between experiments depending on the cell type used. As mentioned in the introduction, C7/10 cells are RNAi deficient, rendering them permissive to viral infection. This permissiveness provides a clear pathway for viral replication, where the influence of host factors on viral growth is minimal. In contrast, Aag2 cells are RNAi competent and already harbour two pre-existing infections. These pre-existing viruses may impact the outcome of co-infections with Negevirus. For instance, the presence of CFAV and PCLV in Aag2 cells could trigger the host's immune response, activating antiviral factors and defense mechanisms (17, 46). Thus, the infection with a third virus may encounter interference at an early stage. The variability in growth curves observed in Aag2 cells has been previously documented by Schultz *et al.* in 2018 (17). They tried to characterize the growth trends of ZIKV in Aag2 cells but encountered unpredictable results. They proposed that the unreliable growth trends could be attributed to the presence of pre-existing infections in the Aag2 cell culture. In addition to this, there are also indications that levels of CFAV and PCLV in Aag2 cell lines vary greatly, thus the levels of ISVs present in the culture in our lab should be characterized (46).

When examining differences in growth trends between the same virus species derived from different sources, variations can arise due to variable fitness and adaptations. For these experiments, only PIUV WT showed significant differences from PIUV UTMB in both cell types. It could be that field-derived isolates (UTMB) may exhibit better fitness or adaptations to infect a specific mosquito species more effectively. These genetic differences can lead to variations in replication efficiency, replication kinetics, and the ability to exploit host cellular machinery. Furthermore, genetic variations, including point mutations, insertions, deletions, or rearrangements in the viral genome, can impact viral replication (52, 53). Each virus isolate may possess different fitness levels, reflecting their ability to efficiently replicate and propagate within a specific cellular environment. Fitness differences can arise due to mutations that enhance or impair viral replication, transcription, translation, or assembly processes, ultimately affecting the efficiency and speed of viral replication (52, 54). In this particular case, our infectious clone virus stock (WT) is “new” and has not yet adapted to infecting insect cells. In contrast, the field-derived viruses have inherent advantages as they already exist in the wild as an optimized quasispecies that has been infecting insects for some generations. Unlike a traditional species with a single genome, a quasispecies consists of a diverse set of viral variants. This genetic variation allows them to adapt rapidly to changing environments and helps viruses evade the host immune response (54). This could be attributed to high mutation rates during replication and purifying selection pressures in RNA viruses (54). It is also worth noting that the mRNA produced from infectious clones during *in-vitro* transcription are produced from an SP6 RNA polymerase, which introduces some mutations into the population with no penalty for reduced fitness. This could also be why the viruses from infectious clones performed differently than their field-derived counterparts. It could very well be the case that our viruses recovered from

infectious clones just require some passaging in cell culture to select for positive mutations and “catch up” to the field-derived viruses through purifying selection. As mentioned in the introduction, Shan et al. constructed an infectious clone of ZIKV that performed slightly “worse” than the parental virus (36). They mention that the observed differences in replication and virulence between the parental and synthetic viruses could be attributed to the limited genetic heterogeneity of the recombinant virus population and the greater genetic diversity inherent in the quasispecies nature of the parental virus (36). To bypass this issue, an alternative approach to infectious cloning using CPER could be employed to generate a quasispecies of the virus that more accurately represents the genetic diversity observed in the parental virus population (55). Nonetheless, the ZIKV clone can be used for several applications: for vaccine development, antiviral drug screening with reporter virus and transmission/pathogenicity studies (36).

When comparing viral isolates from different species, it becomes crucial to investigate if one species may replicate more or less efficiently than another. The results from the single infections indicate that both NEGV isolates and LORV reach higher genome copies than PIUV WT. Additionally, growth curves characterized in Aag2 cells showed that the mutant clones reached fewer genome copy numbers than their wild-type equivalent. This points towards a disadvantage when carrying a fluorescent reporter, which was somewhat expected since the fluorescent proteins are a bulky addition to their genome (13, 48).

The evaluation of genome copy to plaque titer ratios provides valuable insights into various aspects of viral biology, such as replication efficiency, fitness, infectivity, and the potential impact of host factors on viral replication (56). In this project, the genome copy to plaque titer ratios for these viruses were found to be very close to 1, indicating their efficiency in generating infectious viral particles that can form plaques. This is highly advantageous for

potential pathogen control in the vector, as it suggests that a single genome copy can lead to the production of an infectious virus particle. For example, ratios for genome copies to pfu for SARS-CoV-2 have been reported to be in the range of  $10^3$ - $10^6$ :1 (57). This high ratio implies that a larger number of genome copies are produced compared to infectious viral particles. The presence of non-infectious or defective genome copies in SARS-CoV-2 can confer benefits, as it can diminish the efficacy of the host's immune response. By diverting or overwhelming the immune response with defective genomes, viable infectious particles are able to replicate and propagate more efficiently within the host prior to their recognition and elimination by the immune system (57). Similarly, NEGV ORF3 GFP demonstrated a higher ratio of genome copies to pfu in both cell types. This would suggest that the reporter affected the ability of NEGV to form viable viral particles, thus making more genome copies to compensate.

In the co-infection experiments, it was observed that outcomes varied significantly depending on the cell type involved. This variation may be attributed to the presence of a functional RNAi pathway in Aag2 cells or the chronic infections with other ISVs discussed earlier. It is important to acknowledge the limitations associated with cell line experiments in this research, as they lack the biological complexity present in live mosquitoes and may not comprehensively represent *in vivo* processes. In contrast, mosquito experiments closely emulate natural transmission dynamics, allowing us to explore vector competence and intricate host-pathogen interactions. However, it is crucial to note that these mosquito experiments come with technical challenges, substantial costs, and considerations related to ethics and regulations. The selection of the experimental approach was guided by the imperative to strike a balance between biological relevance and practical constraints.

Aside from cell type variations however, most differences were seen with PIUV WT. There was a significant difference in replication rate from PIUV WT's single infection and during co-infections with NEG V WT and NEG V UTMB. Moreover, co-infection results suggest that NEG V isolates and LORV exhibited the highest fitness, as their replication rates consistently matched those of their respective single infection controls. The absence of literature reporting investigations of LORV makes it challenging to draw specific comparisons. However, these novel outcomes suggest that LORV has a better fitness than PIUV, indicating that this virus should be used as a backbone for paratransgenesis. In addition to this, LORV has shown the same profile as PIUV to be able to infect both sand flies and mosquito species, thus this virus could be the key to using Negevirus for pathogen/vertebrate control strategies (22, 26).

When examining the ratio from the co-infection involving the mutant clones, the ratio of total plaques counted to fluorescent plaques varied largely. The PIUV clone with mScarlet had a ratio of 296:1 and 40:1 in C7/10 and Aag2 cells respectively, while the NEG V mutant had a ratio of 1:1 in C7/10 cells and 9:1 in Aag2 cells. Once again, the greatest variation was due to the cell type, which was not surprising. One possible explanation for the observed variation in these ratios could be mutations in the binding sites for the primers, which can lead to a preserved amino acid sequence but impaired protein expression. Another factor that can contribute to the variation is frame shift, which is relatively easy to occur, whereas the complete deletion of the sequence is less likely (11, 50). The ratios for green fluorescence seen were comparable to results from Patterson *et al.*, who found ratios of total plaques to fluorescent plaques at around 2:1 and 3:1 for NEG V ORF3 GFP (13).

## *Conclusions*

In conclusion, the cloning experiments revealed variability in the stability and expression of fluorescent reporter constructs within the Negevirus genomes. Concerns were raised regarding the stability of the insert within the PIUV genome, as evidenced by the presence of two distinct plaque morphologies, unexpected membrane protein size on SDS-PAGE, and variations in fluorescence.

Cell type played a significant role in the outcomes of single and co-infection experiments. RNAi competence and pre-existing infections in Aag2 cells influenced viral replication rates and outcomes, while C7/10 cells, being RNAi deficient, provided a permissive environment for viral replication. Field-derived Negevirus isolates exhibited better fitness and adaptations, likely due to their long history of infecting insects in the wild. The genome copy to plaque titer ratios suggested high efficiency in generating infectious viral particles.

Co-infection experiments revealed that NEGV and LORV exhibited the highest fitness, with their replication rates closely matching those of their respective single infection controls. The novel outcomes observed with LORV highlight its potential as a backbone for paratransgenesis and its ability to infect both sand flies and mosquito species, suggesting its suitability for pathogen control strategies.

Further investigations are necessary to elucidate the stability and expression issues observed in the cloning experiments and to better understand the variations in viral replication and infectivity. The utilization of advanced amplification technologies, such as CPER cloning, could overcome the challenges encountered during the cloning process. Also, CPER technology allows for the generation of more heterogeneous virus populations through the switching of fragments. This could facilitate studies investigating the potential role of viral heterogeneity of

ISVs. Overall, these findings shed light on the important role of cell types, pre-existing infections, fitness variations, and genome copy to plaque titer ratios in influencing viral replication and infectivity. The findings contribute to our understanding of Negevirus biology and pave the way for future research in the field of vector-borne disease control. The next steps for this project involve the host adaptation of virus stocks derived from the infectious clones through serial passaging, followed by the repetition of growth curve experiments. This should be carried out in Aag2 cell culture since the presence of PCLV and CFAV can create selection pressures that favor variants better adapted to a more “natural” host. As a further step from this, passaging should also occur in mosquitoes, as this would increase selection pressures for variants that can evade the host’s immune response and replicate quicker. Passaging is also needed for the reporter viruses to observe loss or maintenance of fluorescence over time. The growth curves of passaged viruses should be compared to the “original” or previous passage number viral growth curves to ascertain the occurrence of positive selection pressures. Sequencing of the virus obtained from PIUV ORF3 mScarlet is necessary to elucidate the specific mutations responsible for the generation of truncated viral forms. Furthermore, the application of CPER technology could be employed to generate a novel infectious clone for reporter PIUV and NEGV, enabling a comparative analysis of reporter stability using different cloning methods. Additionally, it is crucial to investigate the impact of superinfection exclusion on these insect-specific viruses (ISVs) as it can provide insights into the predominant Negevirus species in the natural environment and determine the most suitable species for paratransgenesis strategies.

## References

1. Vasilakis N, Tesh RB. 2015. Insect-specific viruses and their potential impact on arbovirus transmission. *Curr Opin Virol* 15:69-74.
2. Vogels CB, Rückert C, Cavany SM, Perkins TA, Ebel GD, Grubaugh ND. 2019. Arbovirus coinfection and co-transmission: A neglected public health concern? *PLoS Biol* 17:e3000130.
3. Jones KE, Patel NG, Levy MA, Storeygard A, Balk D, Gittleman JL, Daszak P. 2008. Global trends in emerging infectious diseases. *Nature* 451:990-993.
4. LaBeaud A, Bashir F, King CH. 2011. Measuring the burden of arboviral diseases: the spectrum of morbidity and mortality from four prevalent infections. *Population health metrics* 9:1-11.
5. Colón-González FJ, Sewe MO, Tompkins AM, Sjödin H, Casallas A, Rocklöv J, Caminade C, Lowe R. 2021. Projecting the risk of mosquito-borne diseases in a warmer and more populated world: a multi-model, multi-scenario intercomparison modelling study. *Lancet Planet Health* 5:e404-e414.
6. Ng V, Fazil A, Gachon P, Deuymes G, Radojević M, Mascarenhas M, Garasia S, Johansson MA, Ogden NH. 2017. Assessment of the probability of autochthonous transmission of chikungunya virus in Canada under recent and projected climate change. *Environ Health Perspect* 125:067001.
7. Wu P, Yu X, Wang P, Cheng G. 2019. Arbovirus lifecycle in mosquito: acquisition, propagation and transmission. *Expert Rev Mol Med* 21:e1.
8. Iturbe-Ormaetxe I, Walker T, O'Neill SL. 2011. Wolbachia and the biological control of mosquito-borne disease. *EMBO reports* 12:508-518.

9. Edenborough KM, Flores HA, Simmons CP, Fraser JE. 2021. Using Wolbachia to eliminate dengue: Will the virus fight back? *J Virol* 95:e02203-20.
10. Bolling BG, Weaver SC, Tesh RB, Vasilakis N. 2015. Insect-specific virus discovery: significance for the arbovirus community. *Viruses* 7:4911-4928.
11. Blitvich BJ, Firth AE. 2015. Insect-specific flaviviruses: a systematic review of their discovery, host range, mode of transmission, superinfection exclusion potential and genomic organization. *Viruses* 7:1927-1959.
12. Patterson EI, Villinger J, Muthoni JN, Dobel-Ober L, Hughes GL. 2020. Exploiting insect-specific viruses as a novel strategy to control vector-borne disease. *Curr Opin Insect Sci* 39:50-56.
13. Patterson EI, Kautz TF, Contreras-Gutierrez MA, Guzman H, Tesh RB, Hughes GL, Forrester NL. 2021. Negeviruses reduce replication of alphaviruses during co-infection. *J Virol* 95:e0043321.
14. Stollar V, Thomas VL. 1975. An agent in the *Aedes aegypti* cell line (Peleg) which causes fusion of *Aedes albopictus* cells. *Virology* 64:367-377.
15. Roundy CM, Azar SR, Rossi SL, Weaver SC, Vasilakis N. 2017. Insect-specific viruses: a historical overview and recent developments. *Adv Virus Res* 98:119-146.
16. Baidaliuk A, Miot EF, Lequime S, Moltini-Conclois I, Delaigue F, Dabo S, Dickson LB, Aubry F, Merklings SH, Cao-Lormeau V-M. 2019. Cell-fusing agent virus reduces arbovirus dissemination in *Aedes aegypti* mosquitoes in vivo. *J Virol* 93:e00705-19.
17. Schultz MJ, Frydman HM, Connor JH. 2018. Dual Insect specific virus infection limits Arbovirus replication in *Aedes* mosquito cells. *Virology* 518:406-413.

18. Zhang G, Asad S, Khromykh AA, Asgari S. 2017. Cell fusing agent virus and dengue virus mutually interact in *Aedes aegypti* cell lines. *Sci Rep* 7:1-8.
19. Bolling BG, Olea-Popelka FJ, Eisen L, Moore CG, Blair CD. 2012. Transmission dynamics of an insect-specific flavivirus in a naturally infected *Culex pipiens* laboratory colony and effects of co-infection on vector competence for West Nile virus. *Virology* 427:90-97.
20. Kenney JL, Solberg OD, Langevin SA, Brault AC. 2014. Characterization of a novel insect-specific flavivirus from Brazil: potential for inhibition of infection of arthropod cells with medically important flaviviruses. *J Gen Virol* 95:2796.
21. Ye G, Wang Y, Liu X, Dong Q, Cai Q, Yuan Z, Xia H. 2020. Transmission competence of a new mesonivirus, Yichang virus, in mosquitoes and its interference with representative flaviviruses. *PLoS Negl Trop Dis* 14:e0008920.
22. Vasilakis N, Forrester NL, Palacios G, Nasar F, Savji N, Rossi SL, Guzman H, Wood TG, Popov V, Gorchakov R. 2013. Negevirus: a proposed new taxon of insect-specific viruses with wide geographic distribution. *J Virol* 87:2475-2488.
23. Colmant AM, O'Brien CA, Newton ND, Watterson D, Hardy J, Coulibaly F, Bielefeldt-Ohmann H, Warrilow D, Huang B, Paramitha D. 2020. Novel monoclonal antibodies against Australian strains of negeviruses and insights into virus structure, replication and host-restriction. *J Gen Virol* 101:440-452.
24. O'Brien CA, McLean BJ, Colmant AM, Harrison JJ, Hall-Mendelin S, van den Hurk AF, Johansen CA, Watterson D, Bielefeldt-Ohmann H, Newton ND. 2017. Discovery and characterisation of Castlerea virus, a new species of Negevirus isolated in Australia. *Evolutionary Bioinformatics* 13:1176934317691269.

25. Okamoto K, Song C, Sakaguchi M, Chalkiadaki C, Miyazaki N, Nabeshima T, Morita K, Inoue S, Murata K. 2023. Structure and its transformation of elliptical nege-like virus Tanay virus. bioRxiv doi:10.1101/2023.01.20.523382:2023.01.20.523382.
26. Nunes MR, Contreras-Gutierrez MA, Guzman H, Martins LC, Barbirato MF, Savit C, Balta V, Uribe S, Vivero R, Suaza JD. 2017. Genetic characterization, molecular epidemiology, and phylogenetic relationships of insect-specific viruses in the taxon Negevirus. *Virology* 504:152-167.
27. McArdle AJ, Turkova A, Cunnington AJ. 2018. When do co-infections matter? *Curr Opin Infect Dis* 31:209.
28. Chahar HS, Bharaj P, Dar L, Guleria R, Kabra SK, Broor S. 2009. Co-infections with chikungunya virus and dengue virus in Delhi, India. *Emerging infectious diseases* 15:1077.
29. Schilling S, Emmerich P, Günther S, Schmidt-Chanasit J. 2009. Dengue and Chikungunya virus co-infection in a German traveller. *J Clin Virol* 45:163-164.
30. Zaidi MB, Garcia-Cordero J, Rivero-Gomez R, Corzo-Gomez J, González y Almeida ME, Bonilla-Moreno R, Bustos-Arriaga J, Villegas-Sepulveda N, Flores-Romo L, Cedillo-Barron L. 2018. Competitive suppression of dengue virus replication occurs in chikungunya and dengue co-infected Mexican infants. *Parasites & vectors* 11:1-11.
31. Hobson-Peters J, Yam AWY, Lu JWF, Setoh YX, May FJ, Kurucz N, Walsh S, Prow NA, Davis SS, Weir R, Melville L, Hunt N, Webb RI, Blitvich BJ, Whelan P, Hall RA. 2013. A New Insect-Specific Flavivirus from Northern Australia Suppresses Replication of West Nile Virus and Murray Valley Encephalitis Virus in Co-infected Mosquito Cells. *PLoS One* 8:e56534.

32. Hall-Mendelin S, McLean BJ, Bielefeldt-Ohmann H, Hobson-Peters J, Hall RA, van den Hurk AF. 2016. The insect-specific Palm Creek virus modulates West Nile virus infection in and transmission by Australian mosquitoes. *Parasites & Vectors* 9:1-10.
33. Boyer J-C, Haenni A-L. 1994. Infectious transcripts and cDNA clones of RNA viruses. *Virology* 198:415-426.
34. Gorchakov RV, Tesh RB, Weaver SC, Nasar F. 2014. Generation of an infectious Negev virus cDNA clone. *J Gen Virol* 95:2071-2074.
35. Kümmerer BM, Grywna K, Gläsker S, Wieseler J, Drosten C. 2012. Construction of an infectious Chikungunya virus cDNA clone and stable insertion of mCherry reporter genes at two different sites. *J Gen Virol* 93:1991-1995.
36. Shan C, Xie X, Muruato AE, Rossi SL, Roundy CM, Azar SR, Yang Y, Tesh RB, Bourne N, Barrett AD. 2016. An infectious cDNA clone of Zika virus to study viral virulence, mosquito transmission, and antiviral inhibitors. *Cell Host Microbe* 19:891-900.
37. Willemsen A, Zwart MP. 2019. On the stability of sequences inserted into viral genomes. *Virus Evolution* 5:vez045.
38. Kautz TF, Jaworski E, Routh A, Forrester NL. 2020. A Low Fidelity Virus Shows Increased Recombination during the Removal of an Alphavirus Reporter Gene. *Viruses* 12:660.
39. Lindbo JA. 2007. High-efficiency protein expression in plants from agroinfection-compatible *Tobacco mosaic virus* expression vectors. *BMC Biotechnol* 7:1-11.
40. Singh K. 1967. Cell cultures derived from larvae of *Aedes albopictus* (Skuse) and *Aedes aegypti* (L.). *Curr Sci* 36:506-508.

41. Walker T, Jeffries CL, Mansfield KL, Johnson N. 2014. Mosquito cell lines: history, isolation, availability and application to assess the threat of arboviral transmission in the United Kingdom. *Parasites Vectors* 7:1-9.
42. Sarver N, Stollar V. 1977. Sindbis virus-induced cytopathic effect in clones of *Aedes albopictus* (Singh) cells. *Virology* 80:390-400.
43. Sanchez-Vargas I, Travanty EA, Keene KM, Franz AW, Beaty BJ, Blair CD, Olson KE. 2004. RNA interference, arthropod-borne viruses, and mosquitoes. *Virus Res* 102:65-74.
44. Gammon DB, Mello CC. 2015. RNA interference-mediated antiviral defense in insects. *Curr Opin Insect Sci* 8:111-120.
45. Peleg J. 1968. Growth of arboviruses in primary tissue culture of *Aedes aegypti* embryos. *The American journal of tropical medicine and hygiene* 17:219-223.
46. Fredericks AC, Russell TA, Wallace LE, Davidson AD, Fernandez-Sesma A, Maringer K. 2019. *Aedes aegypti* (Aag2)-derived clonal mosquito cell lines reveal the effects of pre-existing persistent infection with the insect-specific bunyavirus Phasi Charoen-like virus on arbovirus replication. *PLoS Negl Trop Dis* 13:e0007346.
47. Untergasser A, Nijveen H, Rao X, Bisseling T, Geurts R, Leunissen JA. 2007. Primer3Plus, an enhanced web interface to Primer3. *Nucleic Acids Res* 35:W71-W74.
48. Tamberg N, Lulla V, Fragkoudis R, Lulla A, Fazakerley JK, Merits A. 2007. Insertion of EGFP into the replicase gene of Semliki Forest virus results in a novel, genetically stable marker virus. *J Gen Virol* 88:1225.
49. Pierson TC, Diamond MS, Ahmed AA, Valentine LE, Davis CW, Samuel MA, Hanna SL, Puffer BA, Doms RW. 2005. An infectious West Nile virus that expresses a GFP reporter gene. *Virology* 334:28-40.

50. Quan J, Tian J. 2009. Circular polymerase extension cloning of complex gene libraries and pathways. *PLoS One* 4:e6441.
51. Amarilla AA, Sng JD, Parry R, Deerain JM, Potter JR, Setoh YX, Rawle DJ, Le TT, Modhiran N, Wang X. 2021. A versatile reverse genetics platform for SARS-CoV-2 and other positive-strand RNA viruses. *Nature Communications* 12:3431.
52. Domingo E. 2020. Molecular basis of genetic variation of viruses: Error-prone replication. *Virus as Populations* doi:10.1016/B978-0-12-816331-3.00002-7:35.
53. Patterson EI, Khanipov K, Swetnam DM, Walsdorf S, Kautz TF, Thangamani S, Fofanov Y, Forrester NL. 2020. Measuring alphavirus fidelity using non-infectious virus particles. *Viruses* 12:546.
54. Andino R, Domingo E. 2015. Viral quasispecies. *Virology* 479:46-51.
55. Edmonds J, van Grinsven E, Prow N, Bosco-Lauth A, Brault AC, Bowen RA, Hall RA, Khromykh AA. 2013. A novel bacterium-free method for generation of flavivirus infectious DNA by circular polymerase extension reaction allows accurate recapitulation of viral heterogeneity. *J Virol* 87:2367-2372.
56. Fernandes-Monteiro AG, Trindade GF, Yamamura AM, Moreira OC, de Paula VS, Duarte ACM, Britto C, Lima SMB. 2015. New approaches for the standardization and validation of a real-time qPCR assay using TaqMan probes for quantification of yellow fever virus on clinical samples with high quality parameters. *Hum Vaccin Immunother* 11:1865-1871.
57. Despres HW, Mills MG, Shirley DJ, Schmidt MM, Huang M-L, Jerome KR, Greninger AL, Bruce EA. 2021. Quantitative measurement of infectious virus in SARS-CoV-2 Alpha, Delta and Epsilon variants reveals higher infectivity (viral titer: RNA ratio) in

clinical samples containing the Delta and Epsilon variants. MedRxiv

doi:<https://doi.org/10.1101/2021.09.07.21263229>.

## Appendix

### *Part A – Cloning and sequencing*

**Table 18. Primer sets used for cloning of exogenous genes into NEG V and PIUV infectious clones.**

Primers were used for amplification of vector and insert fragments through NEB Q5 Hi-fi PCR for subsequent gel electrophoresis.

#	Primer name	Primer 5'-3'
1	NEG V ORF3 mEmerald/Scarlet fused – Vector Rev	ctcaccattgcggaagttgaattcgggtgc
2	NEG V ORF3 mEmerald fused – Vector For	tgtacaagtaatagacgaactccacaggagatgtagt
3	NEG V ORF3 mScarlet fused – Vector For	ctgtacaagtagacgaactccacaggagatgtagtct
4	NEG V ORF3 mEmerald/Scarlet fused – Fragment For	cttccgcaatggtgagcaagggcgagg
5	NEG V ORF3 mEmerald fused – Fragment Rev	gagttcgtctattactgtacagctcgtccatgc
6	NEG V ORF3 mScarlet fused – Fragment Rev	agttcgtctactgtacagctcgtccatgcc
7	PIUV ORF3 mEmerald/Scarlet fused – Vector Rev	gctcacatgacagtaccattgcccgattgg
8	PIUV ORF3 mEmerald fused – Vector For	tgtacaagtaatgagagatgtagtcataacccttctgg
9	PIUV ORF3 mScarlet fused – Vector For	ctgtacaagtgagagatgtagtcataacccttctggt
10	PIUV ORF3 mEmerald/Scarlet fused – Fragment For	gtactgtcatggtgagcaagggcgag
11	PIUV ORF3 mEmerald fused – Fragment Rev	ctacatctctcattactgtacagctcgtccatgc
12	PIUV ORF3 mScarlet fused – Fragment Rev	acatctctcactgtacagctcgtccatgcc
13	NEG V Backbone Switch KAN– Vector Rev	tagtgcacctaataatctctagaggatccc
14	NEG V Backbone Switch KAN– Vector For	gatccgcatagatcccaatggcgcg

15	NEGV Backbone Switch KAN– Frag Rev	cgccattgggatctatgcggatccgatgcgg
16	NEGV Backbone Switch KAN– Frag For	ggggatcctctagagatttaggtgacactatagataaaa ccatacaca
17	PIUV ORF3 ZsGreen fused – Vector Rev	gactgggcatgacagtagcattgcccattgg
18	PIUV ORF3 ZsGreen fused – Vector For	cgccttgcctgagagatgtagtcataacccttctgg
19	PIUV ORF3 ZsGreen fused – Frag Rev	acatctctcagggaaggcggagcc
20	PIUV ORF3 ZsGreen fused – Frag For	atggtactgtcatggcccagccaagcac

**Table 19. Primer sets used for sequencing and growth curves of negevirus infectious clones.**

#	Primer name	Primer 5'- 3'
21	PIUV Seq-10040 For	ttctgcaggcactcgtctg
22	PIUV Seq-11089 Rev	ggcaaatcaaacgttcgtccag
23	NEGV-Genscript ORF3-Seq For	tgacctgcagaactcccgc
24	NEGV-Genscript ORF3-Seq Rev	acgttccaagaggagttcacc
25	NEGV-6812 For	tcaggagacgcttcacttt
26	NEGV-6971 Rev	cgaaatgctgtgcgttctta
27	PIUV-7881 For	atcaaacctttcccaccc
28	PIUV-8101 Rev	agtcttgtcgggatggtacg

**Table 20. PIUV ORF3 mScarlet fused cloning sequencing results for forward and reverse primer reactions.**

Where R is a purine, Y a pyrimidine, M an amino (A or C) and K a keto (G or T). S shows a strong interaction (G or C) and W a weak interaction (A, C or T).

**>PIUV mScarlet Forward Seq (1112 bp)**

AAGTCATYYTYCGSWGRGCTCAGCAGTCACGACTTTTCATCATGGTTGTGGTTGTT  
TTCCTGTACTTCATGGGGTATCTCACCCCTCGTGAAGTCTCCGGACCAACAGGTCCA  
ATCGGGCAATGGTACTGTCATGGTGAGCAAGGGCGAGGCAGTGATCAAGGAGTTC  
ATGCGGTTCAAGGTGCACATGGAGGGCTCCATGAACGGCCACGAGTTCGAGATCG  
AGGGCGAGGGCGAGGGCCGCCCTACGAGGGCACCCAGACCCGCAAGCTGAAGG  
TGACCAAGGGTGGCCCCCTGCCCTTCTCCTGGGACATCCTGTCCCCTCAGTTCATG  
TACGGCTCCAGGGCCTTCACCAAGCACCCCGCCGACATCCCCGACTACTATAAGC  
AGTCCTTCCCCGAGGGCTTCAAGTGGGAGCGCGTGATGAACTTCGAGGACGGCGG  
CGCCGTGACCGTGACCCAGGACACCTCCCTGGAGGACGGCACCCCTGATCTACAAG  
GTGAAGCTCCGCGGCACCAACTTCCCTCCTGACGGCCCCGTAATGCAGAAGAAGA  
CAATGGGCTGGGAAGCGTCCACCGAGCGGTTGTACCCCGAGGACGGCGTGCTGAA  
GGGCGACATTAAGATGGCCCTGCGCCTGAAGGACGGCGGCCGCTACCTGGCGGAC  
TTCAAGACCACCTACAAGGCCAAGAAGCCCGTGCAGATGCCCGGCGCCTACAACG  
TCGACCGCAAGTTGGACATCACCTCCCACAACGAGGACTACACCGTGGTGGAAACA  
GTACGAACGCTCCGAGGGCCGCCACTCCACCGGCGGCATGGACGAGCTGTACAAG  
TGAGAGATGTAGTCATAACCCTTCTGGTGCGGTGAACTCTCCCATTGTCCTGAGAC  
GTAGTCGTCGGTCCTTCTGACCGCGGTGAACTCAAATATTACTGCCCTTCTGGGC  
GGAGACGTAGAGATCGTTCCTTCTGAACCCTCGAACTCCACCGAGTCCCTTCTGGA  
CGAACGTTTTGATTTGCCCAAGACGTGAAGTTATTAATCTTCGAATATTCTAAATT  
CTATCAGCGCCGATTTYCTGYCGGCAATTATCATTTTCTTAATYCTTTTACCTWA  
ATTGG

**>PIUV mScarlet Reverse Seq (1257 bp)**

TTTTYAACMYGGYGGAGTCKATGGTTCAGACSGACGATCTCTACGTCTCCGCCAS  
AAGGGGCAGTAATATTTGAGTTCACCGCGGTCAGAAGGACCGACRACTACKTCTC  
AGGACAATGGGAGAGTTCACCGCACCWGAAGGGTTATGACTACATCTCTCACTTG

TACAGCTCGTCCATGCCGCCGGTGGAGTGGCGGCCCTCGGAGCGTTCGTA CTGTTC  
CACCACGGTGTAGTCCTCGTTGTGGGAGGTGATGTCCA ACTTGCGGTTCGACGTTGT  
AGGCGCCGGGCATCTGCACGGGCTTCTTGGCCTTGTAGGTGGTCTTGAAGTCCGCC  
AGGTAGCGGCCGCCGTCCTTCAGGCGCAGGGCCATCTTAATGTCGCCCTTCAGCA  
CGCCGTCCTCGGGGTACAACCGCTCGGTGGACGCTTCCCAGCCCATTGTCTTCTTC  
TGCATTACGGGGCCGTCAGGAGGGAAGTTGGTGCCGCGGAGCTTCACCTTG TAGA  
TCAGGGTGCCGTCCTCCAGGGAGGTGTCCTGGGTACGGTACGGCGCCGCCGTC  
CTCGAAGTTCATCACGCGCTCCCACTTGAAGCCCTCGGGGAAGGACTGCTTATAGT  
AGTCGGGGATGTCGGCGGGGTGCTTGGTGAAGGCCCTGGAGCCGTACATGAACTG  
AGGGGACAGGATGTCCCAGGAGAAGGGCAGGGGGCCACCCTTGGTCACTTCAG  
CTTGGCGGTCTGGGTGCCCTCGTAGGGGCGGCCCTCGCCCTCGCCCTCGATCTCGA  
ACTCGTGGCCGTTTCATGGAGCCCTCCATGTGCACCTTGAACCGCATGAACTCCTTG  
ATCACTGCCTCGCCCTTGCTCACCATGACAGTACCATTGCCCGATTGGACCTGTTG  
GTCCGGAGACTTCACGAGGGTGAGATACCCCATGAAGTACAGGAAAACAACCAC  
AACCATGATGAAAGTCGTGACTGCTGGAGCCTCACGCGAAGTACGAATGCAGAGC  
GAGTGCCTGCAGAACGTA CTCAAGGACGGAGGCTTGAGGACAACATCACCCAGA  
GAAGGTCGCGAGTGCAAGACACGCGTAGCTTCTCGGCGATGAGCACGGCGGGGG  
CAAAGATAGCCATCAGAACTGAATGATTTCTGCACCACTAGCTAGAARTTGYYG  
CCGTCGCAACTATTGCGACGCACGAAGAAAAATCCA YTGATR TGATCGAGCTCAA  
CATACCTGAAAGAAGACGAGCGTCCTGTTTARAGCCGCTGTA



**Figure 23. Sequencing data chromatograms for PIUV ORF3 ZsGreen-fused infectious clone.**

Plasmids purified from a bacterial colony as a result of cloning was sent for sequencing at the Centre for Applied Genomics (TCAG). Image A shows the sequence map of the infectious clone with its labelled ORFs and features. The sequencing primers for PIUV (21, 22) can be seen on the map, and the blue arrows demonstrate the forward and reverse sequence results. Image B demonstrates the chromatograms for the sequences at the junction site ORF3-ZsGreen, where the forward sequence demonstrates a perfect match to the reference sequence. Image C shows that of the ZsGreen-PIUV backbone site, with the reverse sequence having a near perfect match to the original sequence. Quality scores for the sequencing were an average of 30-35, indicating good sequence read.

**Table 21. PIUV ORF3 ZsGreen fused cloning sequencing results for forward and reverse primer reactions.**

Where R is a purine, Y a pyrimidine, M an amino (A or C) and K a keto (G or T). S shows a strong interaction (G or C) and W a weak interaction (A, C or T).

<p><b>&gt;PIUV ZsGreen Forward Seq (1254 bp)</b></p> <p>GGACCAGCTTCGCGTGAGCTCAGCAGTCACGACTTTTCATCATGGTTGTGGTTGTT  TTCCTGTACTTCATGGGGTATCTCACCCCTCGTGAAGTCTCCGGACCAACAGGTCCA  ATCGGGCAATGGTACTGTCATGGCCCAGTCCAAGCACGGCCTGACCAAGGAGATG  ACCATGAAGTACCGCATGGAGGGCTGCGTGGACGGCCACAAGTTCGTGATCACCG  GCGAGGGCATCGGCTACCCCTTCAAGGGCAAGCAGGCCATCAACCTGTGCGTGGT  GGAGGGCGGCCCTTGCCCTTCGCCGAGGACATCTTGTCGCCCGCCTTCATGTACG  GCAACCGCGTGTTACCGAGTACCCCCAGGACATCGTCGACTACTTCAAGAATC  CTGCCCCGCCGGCTACACCTGGGACCGCTCCTTCCTGTTCGAGGACGGCGCCGTGT  GCATCTGCAACGCCGACATCACCGTGAGCGTGGAGGAGAAGTGCATGTACCACGA  GTCCAAGTTCTACGGCGTGAACCTCCCCGCCGACGGCCCCGTGATGAAGAAGATG  ACCGACAAGTGGGAGCCCTCCTGCGAGAAGATCATCCCCGTGCCAAGCAGGGCA  TCTTGAAGGGCGACGTGAGCATGTACCTGCTGCTGAAGGACGGTGGCCGCTTGCG  CTGCCAGTTCGACACCGTGTACAAGGCCAAGTCCGTGCCCCGCAAGATGCCCGAC  TGGCACTTCATCCAGCACAAAGCTGACCCGCGAGGACCGCAGCGACGCCAAGAACC  AGAAGTGGCACCTGACCGAGCACGCCATCGCCTCCGGCTCCGCCTTGCCCTGAGA  GATGTAGTCATAACCCTTCTGGTGCGGTGAACCTCTCCATTGTCCTGAGACGTAGT</p>
---

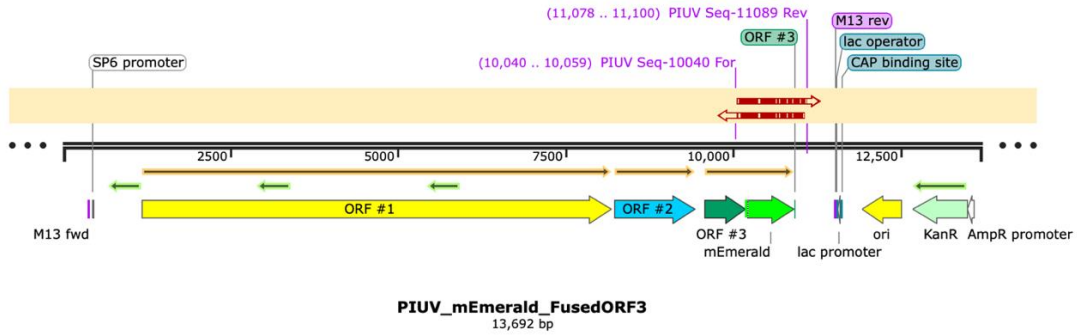
CGTCGGTCCTTCTGACCGCGGTGAACTCAAATATTACTGCCCTTCTGGGCGGAGA  
CGTAGAGATCGTTCCTTCTGAACCCTCGAACTCCACCGAGTCCCTTCTGGACGAAC  
GTTTGATTTGCCCAAGACGTGAAGTTATTATTCTTCGATATCTAATTCCTATCAGC  
GCGATTTCTGTTCGCATATCATTCTATCTTACTAATGGCCAGAAAAAAGAAAA  
GSGACCSATCCATGRCSAGCGTRMTAGAWCGAGCGTCTCARTACGAKCGMACYSY  
ATCGCTTTTMTTCTTCAACGACTWGKAGYTGAAGACAGCTGTGGAACGTTARTT  
TAATCCTTTCSTTCAGTTCCATTGGCGRAAACGTAG

**> PIUV ZsGreen Reverse Seq (1270 bp)**

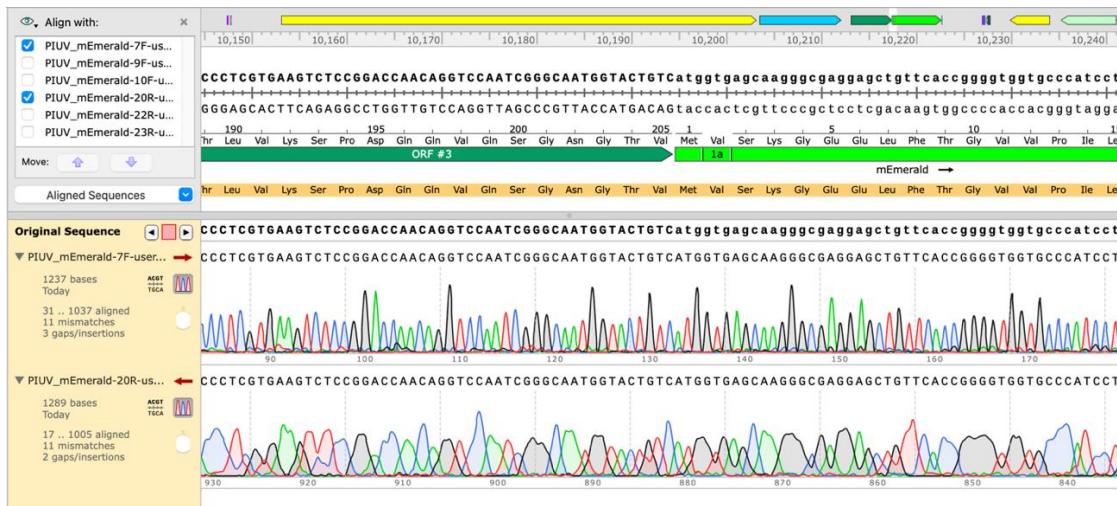
GGGRACMAYGGGTGGTGTTCGAGWRITCAGAGGAACGATCTCTACGTCTCCGCC  
AGAAGGGGCAGTAATATTTGAGTTCACCGCGGTCAGAAGGACCGACGACTACGTC  
TCAGGACAATGGGAGAGTTCACCGCACCAGAAGGGTTATGACTACATCTCTCAGG  
GCAAGGCGGAGCCGGAGGCGATGGCGTGTCTCGGTCAGGTGCCACTTCTGGTTCTT  
GGCGTCGCTGCGGTCTCGCGGGTCAGCTTGTGCTGGATGAAGTGCCAGTCGGGC  
ATCTTGCGGGGCACGGACTTGGCCTTGTACACGGTGTTCGAACTGGCAGCGCAAGC  
GGCCACCGTCCTTCAGCAGCAGGTACATGCTCACGTCGCCCTTCAAGATGCCCTGC  
TTGGGCACGGGGATGATCTTCTCGCAGGAGGGCTCCAGTTGTCGGTCATCTTCTT  
CATCACGGGGCCGTCGGCGGGGAAGTTCACGCCGTAGAACTTGGACTCGTGGTAC  
ATGCAGTTCTCCTCCACGCTCACGGTGTGTCGGCGTTGCAGATGCACACGGCGCC  
GTCCTCGAACAGGAAGGAGCGGTCCCAGGTGTAGCCGGCGGGGCAGGAGTTCTTG  
AAGTAGTCGACGATGTCCTGGGGGTACTCGGTGAACACGCGGTTGCCGTACATGA  
AGGCGGCGGACAAGATGTCCTCGGCGAAGGGCAAGGGGCCGCCCTCCACCACGC  
ACAGGTTGATGGCCTGCTTGCCCTTGAAGGGGTAGCCGATGCCCTCGCCGGTGAT  
CACGAACTTGTGGCCGTCCACGCAGCCCTCCATGCGGTACTTCATGGTCATCTCCT  
TGGTCAGCCGTGCTTGGACTGGGCCATGACAGTACCATTGCCCGATTGGACCTGTT  
GGTCCGGAGACTTCACGAGGGTGAGATACCCCATGAAGTACAGGAAACAACCAC  
AACCATGATGAAAAGTCGTGACTGCTGGAGCCTCACGCGGAAGTACGAATGCAGA  
GCGAGTGCCTGCAGAACGTACTCAAGACGGAGCTTGGAGACCAACATCACCCAGA  
RAAGGGTCGCGAGTGCAGACACGCGTAGCTTCTCGGGCGATGAGCACGGCGGGG  
CAAGATAGCATCAGAACTTGAATGCTTCTGCACCACTAGCTAGAGAGTGTCTCGG  
CCGTCGCACTATGCGAACGCACGAGAAATCCYTGATGATGAATCCAGCACACCTA

CTGAAGAGCACGCTGTTAAGCKAAAGGTGAGAAMCGCTCGAATCGACYTTATTG  
 ATYG

A



B



C



**Figure 24. Sequencing data chromatograms for PIUV ORF3 mEmerald-fused infectious clone.**

Plasmids purified from a bacterial colony as a result of cloning was sent for sequencing at the Centre for Applied Genomics (TCAG). Image A shows the sequence map of the infectious clone with its labelled ORFs and features. The sequencing primers for PIUV (21, 22) can be seen on the map, and the red arrows demonstrate the forward and reverse sequence results. Image B demonstrates the chromatograms for the sequences at the junction site ORF3-mEmerald, where the forward sequence shows 11 mismatches and 3 gaps in comparison to the reference sequence. Image C shows that of the mEmerald-PIUV backbone site, with the reverse sequence having some mismatches and gaps as well. Quality scores for the sequencing were an average of 25-35, less than was observed for PIUV ORF3 mScarlet.

**Table 22. PIUV ORF3 mEmerald fused cloning sequencing results for forward and reverse primer reactions.**

Where R is a purine, Y a pyrimidine, M an amino (A or C) and K a keto (G or T). S shows a strong interaction (G or C) and W a weak interaction (A, C or T).

<p>&gt;PIUV mEmerald Forward Seq (1237 bp)</p> <p>TTAGTTTGCTTCGCGCGAGCTCAGCAGTCACGACTTTTCATCATGGTTGTGGTTGTT TTCCTGTACTTCATGGGGTATCTCACCCCTCGTGAAGTCTCCGGACCAACAGGTCCA ATCGGGCAATGGTACTGTCATGGTGAGCAAGGGCGAGGAGCTGTTACCGGGGTG GTGCCCATCCTGGTCGAGCTGGACGGCGACGTAACGGCCACAAGTTCAGCGTGT CCGGCGAGGGCGAGGGCGATGCCACCTACGGCAAGCTGACCCTGAAGTTCATCTG CACCACCGGCAAGCTGCCCCTGCCCTGGCCCACCCTCGTGACCACCCTGACCTAC GGCGTGCAGTGCTTCAGCCGCTACCCCGACCACATGAAGCAGCACGACTTCTTCA AGTCCGCCATGCCCGAAGGCTACGTCCAGGAGCGCACCATCTTCTTCAAGGACGA CGGCAACTACAAGACCCGCGCCGAGGTGAAGTTCGAGGGCGACACCCTGGTGAA CCGCATCGAGCTGAAGGGCATCGACTTCAAGGAGGACGGCAACATCCTGGGGCAC AAGCTGGAGTACAACACTACAACAGCCACAACGTCTATATCATGGCCGACAAGCAGA AGAACGGCATCAAGGTGAACCTCAAGATCCGCCACAACATCGAGGACGGCAGCG TGCAGCTCGCCGACCACTACCAGCAGAACACCCCCATCGGCGACGGCCCCGTGCT</p>
---

GCTGCCCGACAACCACTACCTGAGCACCCAGTCCGCCCTGAGCAAAGACCCCAAC  
GAGAAGCGCGATCACATGGTCCTGCTGGAGTTCGTGACCGCCGCCGGGATCACTC  
TCGGTATGGACGAGCTGTACAAGTAATGAGAGATGTAGTCATAACCCTTCTGGTG  
CGGTGAACTCTCCCATTGTCCTGAGACGTAGTCGTGGTCCTTCTGACCGCGGTGA  
ACTCAATATTACTGCCCTTCTGGGCGGAGACGTAGAGATCGTTCCTTCTGAACCC  
TCGAACTCCACCGAGTCCCTTCTGGACGACGTTTGATTTGCCAGACGTGAAGTAT  
ATTCTCGATATCTAATCCTATCAGCGCGATTTTCTGTGCATATCATTCTATCTTT  
ACTAATGGCCAAAAAAAAAAAAAAAAACAAGCGGCGCATCCAATGCCGCCAGCTGCT  
CGACATGTCWAGCGTCTGGTGATGTWCGTCAATCACACATCGACCGAACTAAGTT  
ACCTGGGGTGCCTATGAGTGA

**>PIUV mEmerald Reverse Seq (1289 bp)**

GGAACMYGGGTGGARTCGAGGGTTCAGAAGGAACGATCTCTACGTCTCCGCCCA  
GAAGGGGCAGTAATATTTGAGTTCACCGCGGTCAGAAGGACCGACTACGTCT  
CAGGACAATGGGAGAGTTCACCGCACCAGAAGGGTTATGACTACATCTCTCATTA  
CTTGTACAGCTCGTCCATACCGAGAGTGATCCCGGCGGCGGTCACGAACTCCAGC  
AGGACCATGTGATCGCGCTTCTCGTTGGGGTCTTTGCTCAGGGCGGACTGGGTGCT  
CAGGTAGTGGTTGTCGGGCAGCAGCACGGGGCCGTCGCCGATGGGGGTGTTCTGC  
TGGTAGTGGTCGGCGAGCTGCACGCTGCCGTCCTCGATGTTGTGGCGGATCTTGAA  
GTTACCTTGATGCCGTTCTTCTGCTTGTCGGCCATGATATAGACGTTGTGGCTGTT  
GTAGTTGTA CTCCAGCTTGTGCCCCAGGATGTTGCCGTCCTCCTTGAAGTCGATGC  
CCTTCAGCTCGATGCGGTTACCAGGGTGTCGCCCTCGAACTTCACCTCGGCGCGG  
GTCTTGTAGTTGCCGTCGTCCTTGAAGAAGATGGTGCGCTCCTGGACGTAGCCTTC  
GGGCATGGCGGACTTGAAGAAGTCGTGCTGCTTCATGTGGTTCGGGGTAGCGGCTG  
AAGCACTGCACGCCGTAGGTCAGGGTGGTCACGAGGGTGGGCCAGGGCACGGGC  
AGCTTGCCGGTGGTGCAGATGAACTTCAGGGTCAGCTTGCCGTAGGTGGCATCGC  
CCTCGCCCTCGCCGGACACGCTGAACTTGTGGCCGTTTACGTCGCCGTCCAGCTCG  
ACCAGGATGGGCACCACCCCGGTGAACAGCTCCTCGCCCTTGCTCACCATGACAG  
TACCATTGCCCGATTGGACCTGTTGGTCCGGAGACTTCACGAGGGTGAGATACCC  
CATGAAGTACAGGAAAACAACCACACCATGATGAAAGTCGTGACTGCTGGAGCCT  
CACGCGGAAGTACGAATGCAGAGCGAGTGCCTGCAGACGTACTCAAGGACGGAG  
GCTTGAGGACAACATCACCCAGAGAGGTCGCGAGTGCAGACACGCGTAGCTCTCG

GCGATGAGCACGGCGGGGCARAWGCCATCAGACTGATGATTTCKGCMCCCCTA  
GCTAGARGTGGTCTCGGSCGTCGGCACATATTTGCGAASACGGAAGAAATCMCTC  
GATRRTGATCAGCTAACATTCCGAGAAGGAGTMARSGCTGTTAAGGCCGTAAAGG  
TKRGRGACACKSSGATGCMT

*Part B – Titer: Plaque Assays*

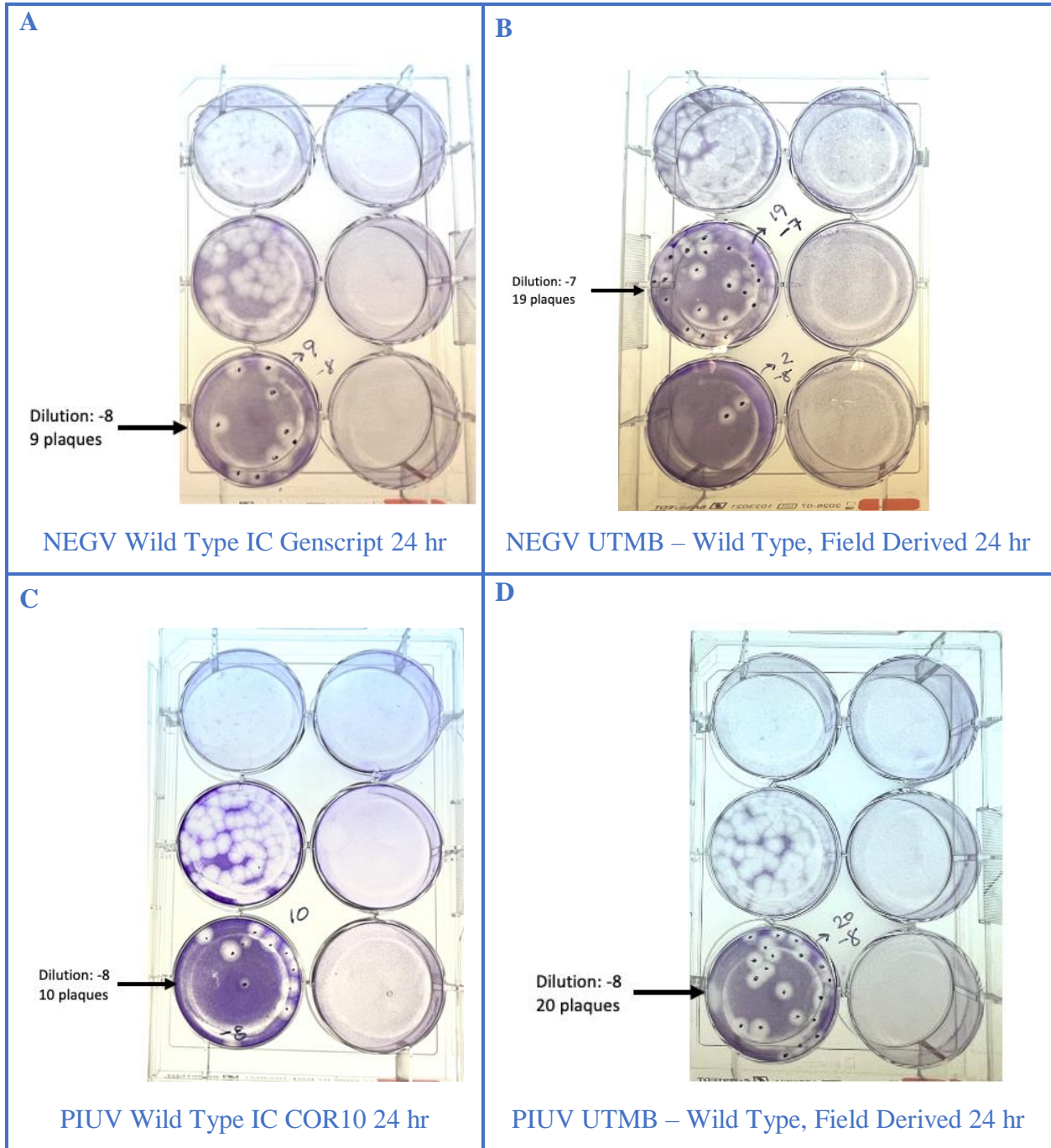


**Figure 25. Plaque assay using C6/36 cells to determine titers of NEG and PIUV wild type virus stocks.**

Image A shows 9 plaques formed at the -8 dilution for the NEGV infectious clone (IC), while image B shows 19 plaques at the -7 dilution for cells infected with the field derived NEG stock.

Image C shows 10 plaques formed at the -8 dilution for cells infected with the PIUV infectious clone (IC), while D shows 20 plaques at the same dilution for the field derived stock for PIUV.

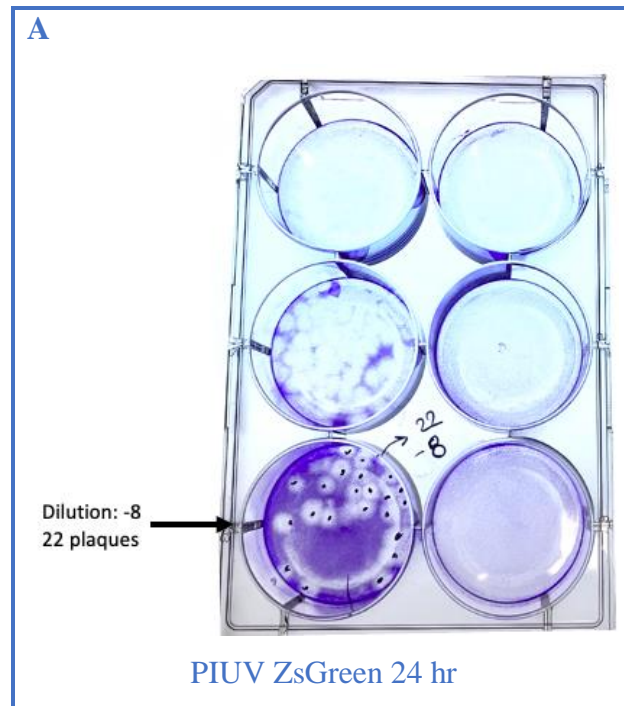


**Figure 26. Plaque assay using C6/36 cells to determine titers of PIUV ZsGreen.**

The image shows plaques formed at the -8 dilution when infecting cells with PIUV ZsGreen 24 hr, with a total of 22 plaques.

**Equation 1. Calculation used to determine titer from plaque assay experiments.**

$$\frac{PFU}{mL} = \frac{\text{Average number of plaques}}{(\text{dilution} \times \text{volume of inoculum})}$$

**Table 23. Raw data used to calculate titers for all Negevirus stocks.**

<b>Virus Name</b>	<b>Dilution</b>	<b>Plaque Total</b>	<b>Morphology</b>	<b>Dilution</b>	<b>Fluorescent Plaques</b>	<b>Titer (PFU/mL)</b>	<b>Fluorescent Titer (PFU/mL)</b>
PIUV WT 24hr	1.0x10 <sup>-8</sup>	10	large	-		6.67x10 <sup>9</sup>	N/A
PIUV UTMB 24hr	1.0x10 <sup>-8</sup>	20	large	-		1.33x10 <sup>10</sup>	N/A
PIUV ORF3 mScarlet 72 hr	1.0x10 <sup>-8</sup>	27	3 large : 24 small	1.0x10 <sup>-6</sup> : 16		1.80x10 <sup>10</sup>	1.1x10 <sup>8</sup>
PIUV ORF3 mScarlet 48 hr	1.0x10 <sup>-6</sup>	77	13 large : 64 small	1.0x10 <sup>-6</sup> : 12		5.13x10 <sup>8</sup>	8.0x10 <sup>7</sup>
PIUV ORF3 ZsGreen 24 hr	1.0x10 <sup>-8</sup>	22	large	0		1.47x10 <sup>10</sup>	0
NEGV WT 24 hr	1.0x10 <sup>-8</sup>	9	large	-		6.00x10 <sup>9</sup>	N/A
NEGV UTMB 24 hr	1.0x10 <sup>-7</sup>	19	large	-		1.27x10 <sup>9</sup>	N/A
NEGV ORF1 GFP 24 hr	1.0x10 <sup>-6</sup>	22	large	0		1.47x10 <sup>8</sup>	0
LORETO WT 24 hr	1.0x10 <sup>-7</sup>	8	large	-		5.33x10 <sup>8</sup>	N/A
NEGV ORF3 GFP 24 hr	1.0x10 <sup>-6</sup>	12	large	1.0x10 <sup>-5</sup> : 4		8.00x10 <sup>7</sup>	2.7x10 <sup>6</sup>
NEGV ORF3 GFP 48 hr	1.0x10 <sup>-6</sup>	27	large	1.0x10 <sup>-6</sup> : 18		1.80x10 <sup>8</sup>	1.2x10 <sup>8</sup>
NEGV ORF3 GFP 2A 24 hr	1.0x10 <sup>-6</sup>	8	large	0		5.33x10 <sup>7</sup>	0

*Part C – Growth Curve Raw Data*

**Table 24. Raw data used to calculate titers for Negevirus using C7/10 cells for the 48hpi sample of growth curves.**

Virus Stock Name	Replicate			Dilution	PFU/mL	Fluorescent Replicate			dilution	PFU/mL
	1	2	3			1	2	3		
PIUV WT 24hr	14	18	19	1.0x10 <sup>-7</sup>	1.1x10 <sup>9</sup>	-	-	-	-	-
PIUV UTMB 24hr	18	19	22	1.0x10 <sup>-8</sup>	1.3x10 <sup>10</sup>	-	-	-	-	-
PIUV ORF3 mScarlet 72 hr	42	38	35	1.0x10 <sup>-7</sup>	2.6x10 <sup>9</sup>	18	16	20	1.0x10 <sup>-7</sup>	1.2x10 <sup>9</sup>
NEGV WT 24 hr	12	16	15	1.0x10 <sup>-7</sup>	9.6x10 <sup>8</sup>	-	-	-	-	-
NEGV UTMB 24 hr	27	28	25	1.0x10 <sup>-7</sup>	1.8x10 <sup>9</sup>	-	-	-	-	-
LORETO WT 24 hr	24	25	24	1.0x10 <sup>-6</sup>	1.6x10 <sup>8</sup>	-	-	-	-	-
NEGV ORF3 GFP 48 hr	3	6	5	1.0x10 <sup>-7</sup>	3.1x10 <sup>8</sup>	1	4	3	1.0x10 <sup>-7</sup>	1.8x10 <sup>8</sup>

